MECHANISMS OF METHAMPHETAMINE-INDUCED DOPAMINE TERMINAL DEGENERATION

by

Danielle M. Friend

A dissertation submitted to the faculty of
The University of Utah
in partial fulfillment of the requirements for the degree of

Doctor of Philosophy

Department of Neuroscience

The University of Utah

August 2013

The University of Utah Graduate School

STATEMENT OF DISSERTATION APPROVAL

The dissertation of Danielle M. Friend

has been approved by the following supervisory committee members:

Kristen Keefe	, Chair	5.24.13 Date Approved
Karen Wilcox	, Member	5.24.13 Date Approved
Annette Fleckenstein	, Member	5.24.13 Date Approved
Matthew Wachowiak	, Member	5.24.13 Date Approved
Robert Fujinami	, Member	5.24.13 Date Approved

and by Kristen Keefe , Chair of

the Department of Neuroscience

and by Donna M. White, Interim Dean of The Graduate School.

ABSTRACT

Although it is well known that METH damages the dopamine (DA) system, the mechanisms underlying such toxicity have not been elucidated. Previous work indicates that animals with partial DA loss from prior exposure to METH are resistant to further decreases in DA when reexposed to METH 30 days later. This experimental paradigm results in four treatment groups based on postnatal day (PND)60:PND90 treatment (Saline:Saline, METH:Saline, Saline:METH, METH:METH) and allows for examination of factors associated with METH toxicity in animals matched for METH exposure, but differentiated with respect to acute METH neurotoxicity. We used this paradigm to examine factors implicated in METH-induced neurotoxicity. First, we investigated the possible contribution of nitric oxide (NO) by examining nitric oxide synthase (NOS) expression, activity, and protein nitration. We found that acute METH administration increased NO production; however, METH did not change expression of endothelial NOS or result in induction of inducible NOS. The number of cells positive for neuronal (nNOS) mRNA or the amount of nNOS mRNA per cell also did not change. However, NOS activity was increased acutely after METH exposure, suggesting that increased NO production after METH exposure arises from NOS activity and most likely, nNOS. Furthermore, animals resistant to METH-induced DA depletions show equivalent degrees of NO production, suggesting that NO alone is not sufficient to induce METH-induced neurotoxicity. Using the same paradigm, we then examined glial reactivity using glial-

fibrillary acidic protein (GFAP; astrocytes) and CD11b (Microglia), as well as markers of proliferation (BrdU and Ki67) immunohistochemistry. Animals experiencing acute toxicity (Saline:METH) showed activated microglia and astocytes, whereas those resistant to toxicity (METH:METH) did not show activated microglia. Furthermore, animals experiencing acute toxicity (Saline:METH) also showed increased proliferation compared to all other groups and a large proportion of proliferating cells were microglia with a smaller proportion being astrocytes. Interestingly, GFAP expression remained elevated in animals exposed to METH at PND60 (METH:Saline), and was not further elevated in resistant animals (METH:METH). These data suggest that astrocytes remain reactive up to 30 days post-METH exposure and that astrocyte reactivity does not reflect acute METH-induced neurotoxicity whereas microglial reactivity parallels acute METH-induced neurotoxicity.

To my parents Charles and Colleen Friend,

For your never-ending love and support,

And for your encouragement to always accomplish greater things

TABLE OF CONTENTS

LIST OF FIGURES

Figure Page

LIST OF ABBREVIATIONS

5-Bromo-2'-deoxyuridine; BrdU

+3,3'-diaminobenzidine; DAB

1-methyl-4-phenyl-1,2,3,6-tetrahydropyridine; MPTP

Adenosine triphosphate; ATP

Analysis of variance; ANOVA

Blood brain barrier; BBB

Central nervous system; CNS

Chondroitin sulfate proteoglycan; NG2

Cyclooxygenase-2; COX-2

Dopamine; DA

Dopamine Transporter; DAT

Endothelial nitric oxide synthase; eNOS

Glial fibrillary acidic protein; GFAP

Glutamate; GLU

Hepatic encephalopathy; HE

Human immunodeficiency virus; HIV

Inducible nitric oxide synthase; iNOS

Interlukin; IL

Intraperitoneal; i.p.

Major immunohistocompatibility complex; MHC

Methamphetamine; METH

Multivariate ANOVA; MANOVA

Neuronal nitric oxide synthase; nNOS

Nitric oxide; NO

Nitric oxide synthase; NOS

N-methyl-$_D$-aspartate; NMDA

Phosphate-buffered saline; PBS

Post-natal day; PND

Sodium chloride/0.015M sodium citrate buffer; SSC

Subcutaneous; s.c.

Tyrosine Hydroxylase; TH

Vesicular monoamine transporter; VMAT

ACKNOWLEDGEMENTS

More work then I could have ever imagined has gone into the design, execution, analysis, and eventual writing of the experiments detailed in this dissertation. And, it would not have been possible without the help of so many people. First, I would like to thank Dr. Kristen Keefe not only for her support and guidance during the completion of this scientific work but also for her advice regarding career development. Her persistent mentorship has clearly shaped me into the scientist that I am today and I consider myself lucky to have worked with her. I would also like to thank Dr. Ashley Fricks-Gleason as well as Dr. Jong Son. Dr. Fricks-Gleason and Dr. Son have also served as mentors to me during my graduate career, both constantly willing to read manuscripts, answer scientific questions, or help with experiments. I would also like to thank the other members of the Keefe Lab first for their scientific conversations but also for their friendship. Finally, I would also like to thank my family and Michael Economo for their encouragement throughout the completion of my graduate degree. Thank you for the phone calls, pep-talks, and the visits. Thank you for your love. Lastly, I would like to thank Utah. Thank you for the beautiful snowy ski days, the early morning sunrise hikes, the backpacking trips, and canyoneering. My time in Utah was more than I ever could have imagined.

CHAPTER 1

INTRODUCTION

1.1 Methamphetamine use and neurotoxicity

1.1.1 Current rates of methamphetamine use and abuse

Methamphetamine (METH) abuse continues to be a significant public health concern in the United States. According to the National Survey on Drug Use and Health, approximately 12 million Americans report using METH at least once in their lifetime (SAMHSA/OSM, 2011). Furthermore, the Arrestee Drug Abuse Monitoring program indicates high levels of abuse of METH in the western United States in particular, with as many as 20-30% of arrestees testing positive for METH, and 20-25% of arrestees reporting METH use in the 30 days prior to arrest (ADAMII, 2012). New evidence also indicates that individuals with a history of METH abuse have an increased risk for developing Parkinson's Disease years later, compared to both healthy controls and individuals with a history of cocaine use (Callaghan et al., 2010; Callaghan et al., 2012). Thus, abuse of amphetamines, and METH in particular, continues to be a significant public health concern and will continue to be a significant burden to society for years to come.

1.1.2 Methamphetamine exposure results in dopamine system damage and cognitive and behavioral deficits

Although acutely methamphetamine increases extracellular concentrations of dopamine (DA) (O'Dell et al., 1991; O'Dell et al., 1993), exposure to high doses or repeated administration results in long-lasting brain changes, including damage to the DA system. Initial investigation into METH-induced neurotoxicity in humans showed reduced levels of DA, tyrosine hydroxylase (TH), and dopamine transporter (DAT) in the

caudate- putamen, and nucleus accumbens in post mortem tissue from human METH abusers (Wilson et al., 1996). More recent studies using positron emission tomography (PET) with radiolabelled ligands have confirmed these findings, demonstrating decreased DAT binding in the prefrontal cortex, orbitofrontal cortex, amygdala, caudate-putamen, and nucleus accumbens and decreased vesicular monoamine transporter (VMAT) in the caudate-putamen of abstinent METH abusers (Sekine et al., 2001; Volkow et al., 2001a; Volkow et al., 2001b; Johanson et al., 2006; McCann et al., 2008). Furthermore, these DA lesions are associated with cognitive and behavioral deficits in human METH abusers (Simon et al., 2000; Volkow et al., 2001b; McCann et al., 2008), together suggesting that METH exposure results in long-lasting DA system damage in human METH abusers and that this damage may be related to the cognitive and behavioral deficits in these individuals.

Animal models have been developed to study METH-induced neurotoxicity in humans and to elucidated mechanisms contributing to such neurotoxicity. "Binge" exposure to METH, in which rodents are given multiple high doses of the drug in a single day to mimic binge administration seen in human abusers, results in monoamine depletions in rodents that are similar to those observed in humans. The effects of such regimens in rodents include reduced DA tissue content (Kogan et al., 1976; Wagner et al., 1980), DAT binding (Guilarte et al., 2003), TH (Kogan et al., 1976), and VMAT binding in striatum (Guilarte et al., 2003). Furthermore, similar to human METH abusers, METH-induced DA depletions in animals are associated with cognitive and behavioral deficits (Chapman et al., 2001; Daberkow et al., 2005; Son et al., 2011; Pastuzyn et al., 2012). Overall, these data clearly indicate that exposure to high doses of METH results

in persistent damage to the DA system in human METH abusers and that it is possible to model both the neurotoxic, as well as the cognitive and behavioral effects using rodents.

1.2 Mechanisms implicated in methamphetamine-induced neurotoxicity

The molecular underpinnings of METH-induced neurotoxicity have not been clearly elucidated; however, several factors have been suggested to play an important role in such neurotoxicity. These factors include increased extracellular and cytosolic DA (O'Dell et al., 1991; Gross et al., 2011b), increased extracellular glutamate (GLU)(e.g., Nash and Yamamoto, 1992; Stephans and Yamamoto, 1994; Gross et al., 2011a), the production of reactive oxygen (e.g., Wagner et al., 1986; Fukami et al., 2004) and nitrogen species (e.g., Itzhak and Ali, 1996; Ali and Itzhak, 1998; Imam et al., 1999), activation of glial cells (e.g., LaVoie et al., 2004; Thomas and Kuhn, 2005a), and hyperthermia (e.g., Ali et al., 1994). In this dissertation we will focus on the role of extracellular DA and GLU, the production of nitric oxide, and the activation of glial cells in the context of METH-induced DA nerve terminal degeneration in striatum.

1.2.1 Dopamine in methamphetamine-induced neurotoxicity

Acutely, METH increases extracellular monoamine concentrations in the brain, including DA (O'Dell et al., 1991; O'Dell et al., 1993) and the effects of METH on the DA system in particular have been suggested to play a detrimental role to DA nerve terminals in striatum (Broening et al., 2005; Gross et al., 2011b; Ares-Santos et al., 2012). This increased extracellular DA has been suggested to damage DA nerve terminals via activation of D1-type DA receptors. For instance, systemic co-

administration of a DA receptor antagonist with METH (Broening et al., 2005) protects against METH-induced neurotoxicity. Further, intrastriatal delivery of a D1 DA receptor antagonist during METH exposure mitigates METH-induced DA depletions (Gross et al., 2011b), although this treatment also reduced METH-induced hyperthermia, which is known to be critical for the neurotoxicity (Ali et al., 1995). Likewise, genetic deletion of the D1 DA receptor renders animals protected against METH-induced neurotoxicity, and this protection is not solely dependent upon loss of METH-induced hyperthermia (Ares-Santos et al., 2012). Taken together, these data strongly suggest that DA release and activation of D1-type DA receptors during METH exposure contribute to METH-induced neurotoxicity.

Although the data reviewed above implicate D1 DA receptor activation in METH-induced neurotoxicity, debate exists regarding whether D1 DA receptor activation contributes to DA terminal degeneration, as D1 DA receptors are located postsynaptic to DA nerve terminals on medium spiny neurons in striatum, rather than on the DA nerve terminals (Levey et al., 1993). One mechanism through which this pathway has been suggested to result in damage to DA terminals is through altered basal ganglia output, ultimately leading to excessive corticostriatal excitation and GLU-mediated excitotoxicity to DA nerve terminals (Mark et al., 2004). This mechanism will be discussed in greater detail in the coming sections of this dissertation.

Increased cytosolic DA has also been suggested to play an important role in DA nerve terminal degeneration. METH has been shown to alter VMAT function (Brown et al., 2000; Riddle et al., 2002) and expression (Eyerman and Yamamoto, 2005). This in turn may increase concentrations of cytosolic DA in DA nerve terminals. In fact, animals

with a VMAT gene deletion show higher cytosolic DA concentrations after METH administration compared to their wild-type counterparts (Larsen et al., 2002), emphasizing the significance of VMAT function in regulating cytosolic DA. This DA can then be oxidized, resulting in production of the highly reactive DA quinone (Tse et al., 1976). DA quinones are increased following METH exposure (LaVoie and Hastings, 1999) and can alter protein function, including the DAT (Berman et al., 1996) and TH (Kuhn et al., 1999). DA quinones also can cause microglia activation *in vitro* (Kuhn et al., 2006). Along these lines, decreasing DA synthesis prior to METH exposure results in protection against METH-induced DA depletions (Albers and Sonsalla, 1995; Thomas et al., 2008b). Therefore, in addition to METH increasing extracellular DA and resulting in DA receptor activation and neurotoxicity, METH-induced cytosolic DA elevations also play an important role in METH-induced neurotoxicity.

1.2.2 Glutamate in methamphetamine-induced neurotoxicity

Similar to DA, extracellular GLU concentrations are also increased following exposure to a neurotoxic regimen of METH (Nash and Yamamoto, 1992; Stephans and Yamamoto, 1994) and may contribute to neurotoxicity. Several lines of evidence suggest that METH increases extracellular GLU secondarily to METH-induced DA release and that this GLU contributes to METH-induced DA terminal degeneration via an excitotoxic mechanism. First, on a circuitry level, the striatum receives the majority of glutamatergic input from corticostriatal neurons (Gerfen, 1989; Bellomo et al., 1998), and corticostriatal activity can be regulated by nigrothalamic and thalamocortical projections. That is, γ-aminobutyric acid (GABA) release from striatonigral neurons activates GABA-A

receptors in the substantia nigra pars reticulata (SNpr) to decrease nigrothalamic neuron firing (Deniau and Chevalier, 1985; Nicholson et al., 1995; Timmerman and Westerink, 1997). In turn, activity of glutamatergic thalamocortical and corticostriatal projections is increased (Deniau and Chevalier, 1985; Kaneko and Mizuno, 1988). In fact, work from Yamamoto and colleagues has shown that METH-induced striatal GLU release is associated with GABA release in the SNpr and decreased GABA release in the thalamus (Mark et al., 2004). Furthermore, GABA-A receptor antagonism in the SNpr increased METH-induced GABA release in the thalamus, as well as METH-induced GLU release and DA nerve terminal degeneration in the striatum (Mark et al., 2004). Together, these findings suggest that striatonigral neuron activation is important for METH-induced GLU release in striatum via activation of basal ganglia circuitry.

The second line of evidence implicating GLU in METH-induced neurotoxicity is that administration of a "binge" regimen of METH causes increased extracellular GLU concentrations in striatum (Nash and Yamamoto, 1992; Stephans and Yamamoto, 1994) as measured using *in vivo* microdialysis. In addition, immunohistochemical staining for GLU in both striatal and cortical nerve terminals is reduced 12 hours after METH administration, consistent with high levels of GLU release during METH exposure (Burrows and Meshul, 1997). Together these data provide significant evidence that METH increases extracellular GLU in striatum via release from corticostriatal projections.

The third line of evidence consists of studies using pharmacological manipulations of the GLU system, which also strongly support a role of GLU in METH-induced neurotoxicity to DA nerve terminals. N-methyl-D-aspartate (NMDA)-type GLU

receptor antagonists co-administered with METH protect against DA nerve terminal degeneration (Sonsalla et al., 1989; Finnegan and Taraska, 1996), although this effect may be dependent upon attenuation of METH-induced hyperthermia (Ali et al., 1994). Furthermore, antagonism of type-5 metabotropic GLU receptors attenuated METH-induced DA depletions, independent of effects on METH-induced hyperthermia (Battaglia et al., 2002), clearly demonstrating that the protection observed resulted from inhibition of GLU receptor activation, rather than disruption of METH-induced hyperthermia. Moreover, recent work has also shown that epidural application of an NMDA receptor antagonist to the cortex reduces both METH-induced c-*fos* gene expression and DA nerve terminal degeneration in striatum (Gross et al., 2011a). Thus, taken together, these data suggest that METH increases GLU release in striatum via the activation of striatonigral GABAergic transmission, which then inhibits nigrothalamic GABA release and disinhibits glutamatergic thalamocortical afferents. This disinhibition of thalamocortical neurons increases GLU release in the cortex, thus activating corticostriatal neurons, ultimately resulting in increased extracellular striatal GLU and METH-induced DA terminal degeneration.

Although altered basal ganglia output has been suggested to influence GLU release during METH exposure as well as the resulting neurotoxicity, it is conceivable that other mechanisms may underlie increased concentrations of extracellular GLU and thus, toxicity. For instance, liver toxicity and elevations of peripheral ammonia have also recently been suggested to contribute to increased striatal GLU associated with METH-induced neurotoxicity (Halpin and Yamamoto, 2012). How this alternative mechanism interfaces with the circuit-level mechanisms driving striatal GLU release in response to

METH and the relative contributions of these different sources of GLU to METH-induced DA terminal degeneration deserves further exploration.

The activation of downstream cascades by GLU has previously been implicated in DA nerve terminal degeneration. For example, exposure of rats to a neurotoxic regimen of METH is associated with spectrin proteolysis (Staszewski and Yamamoto, 2006; Tata and Yamamoto, 2008). Activation of NMDA-type GLU receptors in particular results in activation of calpain, a $Ca2^{+}$-dependent protease (Suzuki et al., 1987; del Cerro et al., 1994). Once activated, calpain degrades the cytoskeletal membrane protein spectrin (Harris and Morrow, 1988). This particular pathway has been implicated in several other neurodegenerative processes including excitotoxicity associated with traumatic brain injury, ischemia and hyperthermia (Morimoto et al., 1997; Pike et al., 1998; Buki et al., 1999). In addition to the activation of calpain, GLU has also been suggested to result in METH-induced neurotoxicity though an increase in nitric oxide (NO) production (Itzhak and Ali, 1996; Itzhak et al., 1998; Deng and Cadet, 1999; Imam et al., 1999; Itzhak et al., 1999; Imam et al., 2000; Itzhak et al., 2000a; Anderson and Itzhak, 2006). Although it is conceivable that several other intracellular events subsequent to the activation of NMDA-type GLU receptors may influence METH-induced neurotoxicity, the overall goal of this dissertation was to explore the role of NO production in DA nerve terminal degeneration.

1.2.3 The role of nitric oxide in methamphetamine-induced neurotoxicity

Nitric oxide is a gaseous neuromodulator implicated in various physiological processes including neuroplasticity (Wang et al., 2005; Serulle et al., 2007), neurovascular coupling (Faraci and Breese, 1993), and neuronal excitability (Centonze et

al., 2001; West and Grace, 2004). However, NO has also been implicated in neuronal damage (Louin et al., 2006; Mohammadi et al., 2012) and various central nervous system (CNS) diseases including Alzheimer's disease (Sultana et al., 2006), Parkinson's disease (Hunot et al., 1996), and multiple sclerosis (Bo et al., 1994), suggesting that in addition to playing a role in normal CNS functions, NO may also play a role in neurodegeneration.

Nitric oxide is synthesized by a family of proteins termed nitric oxide synathase (NOS), of which there are three distinct isoforms. The two constitutively expressed, Ca^{2+}-dependent isoforms are neuronal nitric oxide synthase (nNOS or NOS-I) and endothelial nitric oxide synthase (eNOS or NOS-III) (Bredt and Snyder, 1990; Forstermann et al., 1991). These two isoforms are basally expressed in their respective cell types under normal conditions. In the brain, nNOS is predominantly expressed by neurons (Bredt et al., 1990; Bredt and Snyder, 1990), although some data suggest possible astrocytic expression of nNOS as well (Arbones et al., 1996). Importantly, in striatum, nNOS is expressed by a subpopulation of interneurons that co-express GABA, somatostatin, and neuropeptide Y (Kawaguchi et al., 1995; Figueredo-Cardenas et al., 1996). Endothelial nitric oxide synthase is expressed predominantly by endothelial cells (Seidel et al., 1997; Stanarius et al., 1997), although neuronal expression in hippocampus (Dinerman et al., 1994; O'Dell et al., 1994) and astrocytic expression (Lin et al., 2007a) have also been described. The third isoform, inducible nitric oxide synthase (iNOS or NOS-II), is not basally expressed under normal conditions, but rather is transcriptionally induced and activated in a Ca^{2+}-independent manner (Yui et al., 1991) during inflammatory reactions via a cytokine-mediated cascade (Lowenstein et al., 1993; Xie et al., 1993; Lin and Murphy, 1997; Park et al., 1997). Inducible nitric oxide synthase is

expressed mainly by astrocytes, microglia, and macrophages throughout the brain (Endoh et al., 1994; Liu et al., 1996). Therefore, although all three isoforms convert the precursor L-arginine to NO and L-citrulline, each isoform arises from different a gene product (Janssens et al., 1992; Geller et al., 1993; Hall et al., 1994) and unique expression pattern.

Under normal conditions, NO plays a role in normal physiological processes; however, over-production of NO may result in CNS damage. For example, under normal conditions, NO is known to bind soluble guanylate cyclase (sGC) resulting in activation of the enzyme, cyclic guanosine monophosphate (cGMP) production, and activation of cellular events downstream of cGMP (Stone and Marletta, 1996). However, NO has also been heavily implicated in several CNS injuries and neurodegenerative diseases. In particular, NO can interact with superoxide (0_2^-) to form peroxynitrite ($ONOO^-$) (Beckman et al., 1990), a potent oxidant (Radi et al., 1991). Peroxynitrite, in turn, can interact with various cellular targets, resulting in protein nitration, lipid peroxidation (Rubbo et al., 1994), and DNA damage (Salgo et al., 1995; Yermilov et al., 1995; Yermilov et al., 1996). More specifically, peroxynitrite can interrupt cellular respiration by inhibiting components of the mitochondrial electron transport chain, including complexes I and III (Radi et al., 1994; Clementi et al., 1998; Riobo et al., 2001). In addition, NO can also directly nitrate proteins, resulting in protein/enzyme malfunction (Konorev et al., 1998; Blanchard-Fillion et al., 2001). Thus while it is clear that NO is an important mediator of normal physiological processes, NO can also be detrimental to cellular function, and overproduction of NO can thus contribute to cellular injury.

To date, several studies have described increased NO production following METH exposure using various indices. For example, detection of nitrated proteins, an indirect measure of peroxynitrite formation, is increased in striatum following METH exposure (Imam et al., 1999; Imam et al., 2000; Anderson and Itzhak, 2006; Wang et al., 2008; Friend et al., 2013). Our lab has also shown an increase in NADPH diaphorase histochemical staining (Friend et al., 2013), a measure of NOS activity (Dawson et al., 1991; Hope et al., 1991), following exposure to a neurotoxic regimen of METH. Furthermore, the co-administration of peroxynitrite decomposition catalysts or NOS inhibitors is reported to result in decreased NO production following METH exposure (Imam et al., 1999; Imam et al., 2000). Thus, it is apparent that METH results in NO production.

1.2.3.1 Source of nitric oxide following methamphetamine exposure

Given that NO production is increased in METH-induced neurotoxicity and data suggest roles for NO and peroxynitrite in neurodegeneration, several studies have attempted to identify which isoform of NOS contributes to the METH-induced NO production. One study examined nNOS and iNOS expression in striatum and found that nNOS protein, as well as the number of cells positive for NADPH-diaphorase histochemical staining, were increased following METH exposure (Deng and Cadet, 1999). However, since this study was published, our lab and others have examined nNOS expression via immunohistochemistry (Wang and Angulo, 2011) or *in situ* hybridization (Friend et al., 2013) and have failed to see any change in the amount of nNOS expression at either the mRNA or protein level. Additionally, we also examined

the number of cells with histochemical staining for NADPH diaphorase—a stain produced by the enzymatic activity of NOS (Hope et al., 1991)—and again, we did not observe a METH-induced change in the number of cells positively stained. It is possible that the discrepancy between the studies reflect a mouse *vs.* rat difference, as differences in nNOS expression have been observed between species and strains of animals within a species (Blackshaw et al., 2003). Furthermore, it is generally accepted that nNOS is constitutively expressed and that NO production via nNOS arises as a consequence of Ca^{2+}-calmodulin and Ca^{2+} influx through NMDA receptors (Bredt and Snyder, 1990; Sattler et al., 1999). In fact, although we have not observed changes in the numbers of cells expressing nNOS mRNA or the number of cells positive for NADPH diaphorase histochemical staining, we did observe an increase in total NADPH diaphorase histochemical staining (*i.e.,* percent of the total imaged field with signal; (Friend et al., 2013; Chapter 2). These data suggest that METH increases NO production via activation of constitutively expressed nNOS rather than a change in its expression.

Inducible nitric oxide synthase expression has also been examined following a neurotoxic regimen of METH, and no induction of iNOS protein was observed (Deng and Cadet, 1999). However, Deng and Cadet examined iNOS expression at 1hr, 24hr, and 1 week following exposure to a neurotoxic regimen of METH—time points at which glial cells, the cell types in which induction of iNOS mRNA expression typically occurs (Gibson et al., 2005), may not be fully reactive (LaVoie et al., 2004). Therefore, we examined iNOS mRNA expression in animals 1hr and also 48hr following a neurotoxic regimen of METH, as glial reactivity is maximal at 48hr after exposure to a neurotoxic regimen of METH (LaVoie et al., 2004). Consistent with the data from Deng and Cadet

(Deng and Cadet, 1999), we also failed to see any induction of iNOS mRNA (Friend et al., 2013). Thus, because iNOS must be transcriptionally induced in order to produce NO (Lowenstein et al., 1993; Xie et al., 1993), these data suggest that NO is not produced via iNOS after exposure to a neurotoxic regimen of METH.

Finally, our lab is the first to have examined eNOS mRNA expression following a neurotoxic regimen of METH. As was the case for iNOS, we did not observe any change in eNOS expression in animals sacrificed 1 or 48hr after exposure to the neurotoxic regimen (Friend et al., 2013). However, given that eNOS is also constitutively expressed, there remains the possibility that eNOS may contribute, at least in part to METH-induced NO production. In this regard, our data show that when we limit our analysis of NOS activity to the nNOS expressing interneurons in striatum by excluding blood vessels from the NADPH diaphorase histochemical staining, we still observe an increase in NOS activity, suggesting that eNOS expressing endothelial cells are not contributing to METH-induced increases in NOS activation. Taken together, these data suggest that nNOS, rather than eNOS, is the source of NO production in response to METH. However, a better general understanding of how the constitutively expressed NOS isoforms are regulated will lead to a more definitive answer regarding the particular isoforms responsible for METH-induced NO production. For instance, studies examining NO in the context of long-term potentiating in the hippocampus have demonstrated compensatory interactions between nNOS and eNOS. These data show that LTP is disrupted only if both nNOS and eNOS are eliminated (Son et al., 1996), suggesting that in the absence of one isoform of NOS the other may suffice in generating the NO necessary for LTP to occur. If a similar scenario exists in the context of METH-induced

neurotoxicity, then it is conceivable that either isoform may contribute to METH-induced increases in NO.

1.2.3.2 Nitric oxide in methamphetamine-induced neurotoxicity

Several attempts have been made to elucidate the role of NO in METH-induce DA nerve terminal degeneration by using either pharmacological or genetic manipulations. Unfortunately, these studies have been inconclusive. For example, the co-administration of peroxynitrite decomposition catalysts with METH protects against METH-induced DA depletions (Imam et al., 1999). Further, studies using genetic manipulations have shown that METH-induced DA depletions are blocked in mice with deletion of nNOS (Itzhak et al., 1998; Itzhak et al., 2000b) and partially attenuated in mice with deletion of iNOS (Itzhak et al., 1999; Itzhak et al., 2000b), suggesting a role for NO and its downstream mediator, peroxynitrite, in METH-induced neurotoxicity. However, although the use of peroxynitrite decomposition catalysts or the use of nNOS and iNOS knockout mice afforded protection against the neurotoxic effects of METH, these manipulations also mitigated METH-induced hyperthermia (Itzhak et al., 1998; Imam et al., 1999; Itzhak et al., 1999). METH-induced hyperthermia is tightly associated with METH-induced monoamine toxicity (Ali et al., 1994). In fact, simply cooling animals during METH exposure protects animals against METH-induced toxicity (Ali et al., 1994). Therefore it is difficult to determine whether the protection observed following these manipulations of the NOS system resulted in the protection against METH-induced DA depletions or whether the protection arose from the mitigation of METH-induced hyperthermia. Finally, while some studies suggest protection against METH-induced DA

depletions when NOS inhibitors are co-administered (Di Monte et al., 1996; Itzhak and Ali, 1996; Ali and Itzhak, 1998; Itzhak et al., 2000a), others suggest that the neuroprotective effects of NOS inhibitors also result from mitigation of METH-induced hyperthermia (Taraska and Finnegan, 1997; Callahan and Ricaurte, 1998). Therefore, the work using pharmacological inhibition of NOS in the context of METH-induced neurotoxicity remains inconclusive. Conducting these studies while carefully controlling for METH-induced hyperthermia (*i.e.,* placing knockout animals in an environment with increased ambient temperature to maintain METH-induced hyperthermia) should lead to more conclusive results in this regard. Additionally, studies using knockdown approaches particularly in specific cell types (e.g*.,* shRNA driven by cell type specific promoters such as SST) should more clearly elucidate not only the NOS isoform contributing to increased NO during exposure to METH, but also the particular cell population involved.

Adding further debate to the role of NO in METH-induced neurotoxicity are studies that use other manipulations in attempts to clarify the role in METH-induced neurotoxicity. For example, ablation of nNOS-expressing interneurons in striatum did not protect against METH-induced TH or DAT depletions (Zhu et al., 2006; Fricks-Gleason and Keefe, 2013); however, there was incomplete mitigation of METH-induced NO production in such preparations (Fricks-Gleason and Keefe, 2013) raising questions as to whether the NO could be produced by constitutively expressed eNOS or by diffusion away from residual nNOS-containing interneurons.

An alternative conclusion for the results of these studies is that NO is not sufficient for METH-induced neurotoxicity. In this regard, our lab examined this issue in

animals resistant to the acute neurotoxic consequences of METH exposure. In this model, animals were initially treated with METH or saline on PND60 and then allowed to recover for 30 days. At PND90, the rats are treated again with either METH or saline, resulting in four treatment groups based on PND60:PND90 treatment (Saline:Saline, Saline:METH, METH:Saline, and METH:METH). Under this paradigm, we and others have found that animals with partial DA loss induced by a neurotoxic regimen of METH (METH:METH) fail to exhibit further decreases in striatal DA when reexposed to METH at PND90 (Thomas and Kuhn, 2005a; Hanson et al., 2009). This paradigm allowed us to compare changes in NOS enzyme activity and protein nitration in animals experiencing acute toxicity when exposed to METH at PND90 (*i.e.,* the saline:METH group) compared to animals not experiencing acute toxicity when exposed to METH at PND90 (*i.e.,* the METH:METH group)(Friend et al., 2013). We found that both protein nitration and NOS activity were increased in all animals exposed to METH at PND90 (*i.e.,* Saline:METH and METH:METH). Thus, NO was produced regardless of whether an animal was experiencing acute toxicity or not. These data, combined with data showing that METH exposure results in DA terminal damage in several brain regions (*i.e.* amygdala, hippocampus, and cortex) that do not exhibit changes in protein nitration (Anderson and Itzhak, 2006), indicate a significant dissociation between indices of NO production and acute DA neuron toxicity, suggesting that generation of NO is not sufficient and may not be necessary for METH-induced DA toxicity.

Although NO does not appear to be sufficient for METH-induced DA nerve terminal degeneration, it may be necessary when toxicity does occur, as NO may act together with other factors under those conditions to contribute to the toxicity. For

example, both DA and GLU regulate NO production via nNOS-expressing interneurons in striatum. In this regard, nNOS-expressing interneurons in striatum express NMDA-type GLU receptors (Gracy and Pickel, 1997), and intrastriatal infusion of NMDA receptor agonists (Iravani et al., 1998; Rossetti and Crespi, 2004) or application *in vitro* (Garthwaite et al., 1988; Bredt and Snyder, 1989) increases NO production. The striatum in particular receives extensive glutamatergic inputs from cortex (Gerfen, 1989; Bellomo et al., 1998), and stimulation of corticostriatal afferents, both *in vitro* and *in vivo*, increases the production of NO via an nNOS-dependent mechanism (Kawaguchi, 1993; Sammut et al., 2007). In addition to expressing NMDA-type GLU receptors, nNOS-expressing neurons also express D1-type (D1 and D5) DA receptors (Le Moine et al., 1991; Rivera et al., 2002; Centonze et al., 2003). D1-type DA receptor stimulation induces the production of NO (Le Moine et al., 1991; Sammut et al., 2006) and increases NADPH diaphorase staining in striatum (Morris et al., 1997; Hoque et al., 2010). Finally, NMDA and D1 DA receptor activation work together to increase NO production in striatum (Park and West, 2009). Therefore, these data, combined with studies demonstrating significant increases in both GLU (Nash and Yamamoto, 1992; Mark et al., 2004) and dopamine (O'Dell et al., 1991; Nash and Yamamoto, 1992; O'Dell et al., 1993) during and following exposure to a neurotoxic regimen of METH, suggest that NO produced by nNOS during METH exposure may simply be a readout of NMDA and DA receptor stimulation rather than a contributor to the neurotoxic process. Studies using specific manipulations of NMDA or DA receptors and then examining NO production during METH exposure would more specifically answer this question.

In summary, our recent data strongly indicate that METH-induced NO production results from an increase in activity of nNOS in striatum. Importantly, we also show that NO production is increased in animals exposed to METH whether or not animals are experiencing METH-induced neurotoxicity. Together, these data indicate that although METH increases NO production via nNOS, the NO produced is not sufficient for the induction of METH-induced DA terminal degeneration.

1.2.4 Microglia and astrocytes in methamphetamine-induced neurotoxicity

Neuroinflammation is a defense mechanism orchestrated by the CNS to protect against infection, injury, and disease. Most often, neuroinflammation initiates beneficial processes that resolve; however, under certain circumstances the neuroinflammatory response may persist, resulting in chronic neuroinflammation that can contribute to CNS pathologies. Both astrocytes and microglia play an important role in coordinating this neuroinflammatory response.

Paralleling the DA system damage observed in human METH abusers is the presence of reactive microglia and increased density of astrocytes (Kitamura et al., 2010). Unfortunately, studies examining glial reactivity in human METH abusers are few, and a significant limitation to these studies is that glial reactivity is examined in post mortem tissue (Kitamura et al., 2010). Therefore the ability to examine long-term changes in glial reactivity in these individuals is limited. However, the development of radiotracers for activated microglia for performing PET studies confirms that microglia take on an activated phenotype in the brains of human METH abusers (Sekine et al., 2008). In

addition to the observation that METH abuse causes activation of glial cells in human abusers, there is strong evidence indicating that amphetamine abuse has a high rate of comorbidity among individuals infected with human immunodeficiency virus (HIV) (Harris et al., 1993; Crofts et al., 1994). Importantly, synergistic effects of HIV and METH have now been documented, including increased dopaminergic system damage (Maragos et al., 2002) and enhanced glial responses (Kaul and Lipton, 1999; Zhao et al., 2001) and cytokine production (Shah et al., 2012a; Shah et al., 2012b). Together, these data clearly demonstrate that METH exposure results in reactive glial cells and that reactive glia may contribute to METH-induced neurotoxicity.

Similar to observations in human METH abusers, studies using animal models have provided evidence that METH exposure results in activated microglia and astrocytes (e.g., O'Callaghan and Miller, 1994; Cappon et al., 1997; Guilarte et al., 2003; LaVoie et al., 2004). Studies carefully examining these cells at several time points after a neurotoxic regimen of METH suggest that astrocytes increase expression of glial fibrillary acidic protein (GFAP; indicator of activated astrocytes) and that the increase is apparent approximately 1 day post treatment and remains elevated compared to controls for long periods of time (21-32 days)(O'Callaghan and Miller, 1994; Friend and Keefe, 2013) post treatment. Similarly, markers for microglia are elevated by approximately 1 day (LaVoie et al., 2004) post METH exposure and remain elevated for approximately 7 days (Thomas et al., 2004) post treatment. These data indicate that rodent models of METH-induced neurotoxicity mimic glial responses observed in human METH abusers and that glial responses in the rodent model begin shortly after METH exposure.

Although the reactivity of these cells types has been well documented, elucidating the role that both microglia and astrocytes play in METH-induced neurotoxicity is a much more difficult task. Several groups have attempted to understand the functional role of these cells in METH-induced neurotoxicity and thus elucidate whether they represent a cause or consequence of DA terminal degeneration associated with METH exposure. This review will summarize these findings as well as indicate areas of the field that warrant further investigation.

1.2.4.1 Microglia

Depending upon the particular CNS environment, microglia can dramatically change their morphology as well as their function. Under normal circumstances in the healthy brain, microglia can be observed in a "resting" state identified by a small cell body and ramified morphology (Kreutzberg, 1996). Although termed "resting," under these conditions microglia are constantly surveying the environment with highly motile processes (Nimmerjahn et al., 2005). In response to brain injury, inflammatory signals, or disease, microglia take on an "activated" phenotype characterized by dramatic changes in morphology, including an amoeboid shape with larger cell body (Kreutzberg, 1996). In this activated state, microglia also up-regulate surface molecules, including major histocompatibility complex (MHC), as well as cytokine and chemokine receptors (McKimmie and Fazakerley, 2005; Cho et al., 2006). On the one hand, microglial activation can provide beneficial support for neuronal survival, for example by clearing cellular debris (Beyer et al., 2000; Simard and Rivest, 2007). On the other hand, activated microglia can also cause significant neuronal damage via production of the

superoxide anion (Colton and Gilbert, 1987), nitric oxide (NO)(Moss and Bates, 2001), and inflammatory cytokines (Sawada et al., 1989). Therefore depending upon the particular circumstances, microglia morphology and function can change, and these changes may serve neuroprotective or neurotoxic functions.

Although attempts have been made to determine the mediators of microgliosis in the context of METH-induced neurotoxicity, the exact cascade is not yet fully understood. Classical mechanisms of microglial activation point to proinflammatory cytokines, chemokines, and toll-like receptor stimulation (For review see Hanisch, 2002). Previous work suggests that the expression of several proinflammatory cytokines and chemokines are upregulated following METH administration, including TNFα, interleukin (IL)1-β, IL-6, and IL-8 (Sriram et al., 2006; Goncalves et al., 2008; Tocharus et al., 2010; Shah et al., 2012b). Therefore, in the context of METH-induced neurotoxicity, microglial reactivity following METH exposure may be initiated via a pro-inflammatory cascade.

Alternatively, other signals may be responsible for microglia activation in the context of METH-induced neurotoxicity. For example, METH-induced changes in striatal neurotransmitter systems may function as an initiator of microglia reactivity. Microglia express receptors for GABA (Kuhn et al., 2004), GLU (Noda et al., 2000), DA (Farber et al., 2005), and acetylcholine (Chang and Liu, 2000). In particular, GLU receptor antagonism has been shown to decrease (Thomas and Kuhn, 2005c), whereas GLU receptor activation increases, microglia activation (Kaindl et al., 2012). Given the significant increases in extracellular GLU during and following METH exposure (Nash and Yamamoto, 1992; Stephans and Yamamoto, 1994), GLU-mediated microglia

activation remains an interesting possibility. Likewise, DA-mediated microglia activation appears to be a provocative possibility. For instance, inhibiting DA synthesis prior to METH exposure decreases microglial activation, whereas increased cytosolic DA increases microglial activation (Thomas et al., 2008b). The influence of DA on microglial activation may depend upon DA quinone formation, as METH exposure results in the formation of DA quinones (LaVoie and Hastings, 1999), and DA quinones alone can stimulate microglial activation *in vitro* (Kuhn et al., 2006). Additionally, microglial activation has also been shown to be stimulated via adenosine triphosphate (ATP). Microglia express receptors for ATP (Walz et al., 1993; Langosch et al., 1994), and ATP stimulation of purinergic receptors expressed by microglia increases cytokine production and regulates chemotaxis (Hide et al., 2000; Honda et al., 2001; Shigemoto-Mogami et al., 2001; Davalos et al., 2005). Additionally, under conditions of neuronal injury, such as hypoxia, ischemia, traumatic brain injury, and epilepsy, extracellular ATP is increased (For review see Franke et al., 2006). Although changes in extracellular ATP in the context of METH exposure have not been explored, given the significant amount of damage that occurs to DA nerve terminals, ATP release seems a likely possibility. Taken together, these data suggest critical roles for GLU, DA, and ATP neurotransmission in microglial activation in response to METH exposure; however, it is important to consider that many of the manipulations used to query the role of those systems in glial activation also mitigate the neurotoxic effects of METH. Therefore loss of glial activation may reflect the loss of toxicity to which glia are reacting, rather than a blockade of glial activation that is then causal in the METH-induced neurotoxicity. Furthermore, whether the above mentioned signals (GLU, DA, ATP) initiate a cytokine

cascade that stimulates microglial activation or whether these signals (GLU, DA, ATP) directly activate microglia has yet to be determined. Studies determining the exact mechanisms resulting in stimulation of resting microglia to their activated counterparts will lead to more specific ways in which microglial activation can be modulated in the context of METH-induced neurotoxicity and possibly provide insight to guide the development of beneficial therapeutic interventions.

In the context of METH-induced toxicity, there is a tight association between microglial activation and the neurotoxicity that occurs. For example, reactive microglia can be found in regions of the brain that undergo METH-induced DA nerve terminal degeneration, but not in regions that do not (Guilarte et al., 2003; Thomas et al., 2004). Additionally, animals with partial DA loss resulting from prior exposure to METH are resistant to further decreases in striatal DA when reexposed to METH 7 or 30 days later, and such resistant animals also do not show an activated microglial phenotype (Thomas and Kuhn, 2005a; Friend and Keefe, 2013). Together these studies strongly support an association between microglial activation and METH-induced degeneration; however, given the nature of these studies it remains unclear whether microglial activation is a cause or consequence of METH-induced neurotoxicity.

Two studies have attempted to elucidate whether microglial activation is a cause or consequence of METH-induced neurotoxicity by examining whether microglial activation occurs before DA nerve terminal injury is apparent. As mentioned above, microglial activation is detectable approximately 1 day after METH exposure. In one study, this change to a reactive microglial phenotype was reported to precede DA terminal degeneration (LaVoie et al., 2004), suggesting that microglia become activated

before degeneration occurs and that they could therefore contribute to the toxicity. However, another study has reported that the appearance of microglial activation occurred only after degeneration of TH fibers began (Bowyer et al., 2008), suggesting the converse—that degeneration occurs prior to changes in microglial activation and that glial activation may therefore be a consequence of METH-induced neurotoxicity. Thus, although it is clear that microglia become activated within hours of METH exposure, the appearance of microglial activation in relation to initial signs of DA terminal degeneration is still under debate.

Our ability to determine whether microglial activation is a cause or consequence of METH-induced neurotoxicity may be clarified with specific pharmacological or genetic inhibition of microglial activation. In this regard, antiinflammatory pretreatment prevented microglial activation following METH exposure, but did not result in protection against DA depletions (Sriram et al., 2006; Boger et al., 2009). Likewise, pretreatment of animals with free radical scavengers prior to METH exposure resulted in protection from METH-induced neurotoxicity, but not microglial activation (Kawasaki et al., 2006). Collectively, these data suggest that microglial activation can be separated from METH-induced neurotoxicity and thus may not be causal in METH-induced neurotoxicity.

In summary, whether reactive microglia are a cause or consequence of METH-induced neurotoxicity remains under debate. As mentioned above, our data strongly indicate that microglia reactivity, as measured using CD11b immunohistochemistry, parallels METH-induced neurotoxicity. In this work we found that reactive microglia phenotypes were only observed in animals exposed to METH and experiencing acute

toxicity, but not in those exposed to METH and not experiencing acute toxicity (Friend and Keefe, 2013). Likewise, we also show that microglial proliferation occurs to a much higher degree in animals experiencing toxicity compared to those that are not (Chapter 3). Other studies have shown similar associations between reactive microglia and METH-induced neurotoxicity (e.g., LaVoie et al., 2004; Thomas and Kuhn, 2005a). Conversely, work of other groups has suggested that microglia and indices of METH-induced DA terminal degeneration can be separated, suggesting that microglia do not play a causal role in METH-induced neurotoxicity (e.g. Sriram et al., 2006; Bowyer et al., 2008; Boger et al., 2009). Future studies using specific genetic manipulations to inhibit microglia activation will lead to more definitive answers regarding reactive microglia in this regard.

1.2.4.2 Astrocytes

Similar to microglia, when astocytes become reactive, both the morphology and functions of the cells change. Nonreactive astrocytes are characterized by finely branched processes, with each astrocyte occupying a nonoverlapping domain (Bushong et al., 2002). As astrocytes become activated, they upregulate expression of GFAP and other astrocytic markers (S100β and vimentin) (Sofroniew, 2009). In addition, their cell bodies and process become much thicker, and the processes begin to overlap (Sofroniew, 2009). As mentioned above, detectable increases in GFAP expression are apparent approximately 1 day after exposure to neurotoxic regimens of METH (O'Callaghan and Miller, 1994), and GFAP expression remains elevated compared to controls for long periods of time (O'Callaghan and Miller, 1994; Friend and Keefe, 2013). Similar to microglia, although astrocytes become activated following a neurotoxic regimen of

METH, whether these cells are a cause or consequence of METH-induced neurotoxicity is unknown.

As is the case for microglia, multiple signaling molecules activate astrocytes depending upon the specific context. For example, various cytokines (For review see John et al., 2003) and toll-like receptor stimulation (Farina et al., 2005; Park et al., 2006) have all been shown to activate astrocytes. In addition, neurotransmitters such as GLU (Lalo et al., 2006) and ATP (Neary et al., 2003) have also been implicated in activation of astrocytes in other CNS contexts. As argued above for microglial activation, identifying the specific signals that initiate astrocyte activation in the context of METH-induced DA neurotoxicity should provide novel insights into the function of astrocytes in this context.

To date, the effects of manipulations of astrocyte activation on METH-induced neurotoxicity have not been examined, and therefore it is unclear whether activated astrocytes, as for microglia, are a cause or consequence of METH-induced neurotoxicity. As mentioned above, astrocytic GFAP expression remains elevated 3-5 weeks after exposure to a neurotoxic regimen of METH (O'Callaghan and Miller, 1994; Friend and Keefe, 2013), suggesting that astrocytes become reactive and stay reactive long after METH-induced DA terminal degeneration occurs. Furthermore, a dissociation between increased levels of GFAP and DA terminal degeneration following METH exposure has been observed. For example, increased GFAP expression occurred simultaneously with indications of DA terminal damage in older rodents (PND60 and PND80), but, increased GFAP expression occurred in the absence of DA terminal degeneration in younger animals (PND40) (Pu and Vorhees, 1993), suggesting that astrocyte activation is not sufficient for METH-induced neurotoxicity. Additionally, animals with partial DA loss

from prior exposure to METH that are resistant to further decreases in striatal DA when reexposed to METH 30 days later show levels of GFAP expression similar to animals exposed to METH at PND90 and experiencing acute toxicity (Friend and Keefe, 2013). These findings further suggest a possible dissociation between reactive astrocytosis, as reflected in elevated GFAP expression, and acute METH-induced DA terminal injury. However, we should note that in animals experiencing acute toxicity when treated with METH at PND90 there is an increase in GFAP staining over baseline, whereas in animals resistant to acute toxicity at PND90, there is no increase in GFAP over the relevant baseline (which is elevated due to prior METH exposure at PND60). These findings, therefore, can be interpreted in a different light—that is, that there is *de novo* astrocyte activation only in animals experiencing acute toxicity. These different interpretations beg the same question asked above in the section on microglial activation of whether the marker being examined, in this case GFAP immunohistochemical staining, is a definitive measure of astrocyte reactivity. Overall, however, when taken together the studies reported to date suggest that activation of astrocytes alone are not sufficient to cause METH-induced DA terminal degeneration. Future studies using specific genetic manipulations to inhibit astrocyte activation should lead to more definitive answers regarding reactive microglia in this regard. The following section will discuss possible ways in which glia may contribute to or play a protective role in METH-induced neurotoxicity.

1.2.4.1 Mechanisms by which glia may contribute to or mitigate methamphetamine-induced neurotoxicity

As mentioned above, microglia and astrocytes are known to release several factors, including superoxide (Colton and Gilbert, 1987), NO (Moss and Bates, 2001), and various cytokines (Sawada et al., 1989) that may play an important causal role in CNS damage. Oxidative damage in particular has been suggested to play a significant role in METH-induced neurotoxicity. For example, markers of lipid oxidation (Fitzmaurice et al., 2006; Huang et al., 2013) and changes in antioxidant systems have been observed following a neurotoxic regimen of METH (Giovanni et al., 1995; Fleckenstein et al., 1997; Yamamoto and Zhu, 1998; Mirecki et al., 2004; Granado et al., 2011). Furthermore, animals to whom free radical scavengers and antioxidants are co-administered with METH are protected from METH-induced DA terminal degeneration (Wagner et al., 1986; Fukami et al., 2004). Therefore it could be possible that glial cells contribute to toxicity via production of reactive oxygen species.

Interestingly, astrocytes also can protect neurons against oxidative stress via several antioxidant mechanisms (Makar et al., 1994; Shih et al., 2003), including glutathione (GSH) production (Raps et al., 1989). In fact, treating animals with N-acetyl-L-cysteine, a glutathione precursor, prior to METH exposure protects animals against METH-induced DA terminal degeneration (Fukami et al., 2004). Recent work has also demonstrated that metallothioneins (MT) can scavenge DA quinones (Miyazaki et al., 2007). Astrocytes express certain isoforms of MTS to a greater degree than do neurons, and astrocytes up-regulate expression of these isoforms in response to CNS injury (Chung et al., 2004). Also, DA quinones increase expression of MTs in astrocytes and

astrocyte-derived MTs protect neurons from DA quinone toxicity (Miyazaki et al., 2011). Taken together, these data suggest that astrocytes may serve a protective function for neurons against oxidative stress in METH-induced neurotoxicity. Given the data mentioned above regarding the possible role for glial in contributing to oxidative stress as well as a possible role for astroytes in mitigating reactive oxygen species related damage, studies manipulating the ability of astrocytes and microglia to specifically contribute to or mitigate reactive oxygen species in the context of METH-induced neurotoxicity is needed.

In addition to reactive oxygen species, NO and $ONOO^-$ have been heavily implicated in METH-induced neurotoxicity (as reviewed above), and several groups have conducted studies in attempts to determine if glial-expressed inducible nitric oxide synthase (iNOS) plays a significant role in NO production following METH exposure. For example, animals with a depletion of the iNOS gene are protected against METH-induced neurotoxicity (Itzhak et al., 1999; Itzhak et al., 2000b). However, as already discussed above, a significant caveat to these studies is that METH-induced hyperthermia is disrupted in these animals (Itzhak et al., 1999), and METH-induced hyperthermia is tightly associated with the toxicity (Ali et al., 1994). Therefore it is unclear whether the protection observed resulted from the mitigation of METH-induced iNOS expression or METH-induced hyperthermia. Furthermore, because iNOS must be transcriptionally induced to produce NO (Lowenstein et al., 1993; Xie et al., 1993), and we (Friend et al., 2013) and others (Deng and Cadet, 1999) have failed to observe any induction of iNOS after METH exposure, the data suggest that METH-induced NO production does not result from the iNOS isoform (as discussed above). Under some conditions astrocytes

have been reported to express nNOS (Arbones et al., 1996). However, following METH exposure, there is no change in the number of cells expressing nNOS (Wang and Angulo, 2011; Friend et al., 2013). It is thus unlikely that astrocytes are contributing to METH-induced NO production via nNOS or iNOS. Altogether these data suggest that glia do not contribute to METH-induced DA terminal degeneration via an NO mechanism.

Microglia and astrocytes also have the ability to release both pro and anti-inflammatory cytokines, and over production of proinflammatory cytokines can result in chronic inflammation (Hanisch, 2002; Min et al., 2006; Brambilla et al., 2009). Recent work examining changes in gene expression in microglia in response to DA quinone exposure *in vitro* shows a robust increase in several proinflammatory mediators (Kuhn et al., 2006). Interestingly, central administration of proinflammatory mediators or lipopolysaccharide (Lin et al., 2007b; Hozumi et al., 2008) prior to or following METH administration attenuates METH-induced DA terminal degeneration, possibly suggesting that a "primed" neuroinflammatory response may serve a protective function. Therefore, work determining the particular pro- or antiinflammatory mediators released by microglia and astrocytes at different time points during and following METH exposure should shed additional light on the role of these cells in chronic neuroinflammation. A better understanding of the specific conditions under which astrocytes and microglia coordinate either pro- or antiinflammatory processes in the context of METH-induced neurotoxicity may point toward therapeutic targets for attenuating METH-induced neurotoxicity.

One inflammatory mediator that has been implicated in METH-induced neurotoxicity is cyclooxygenase-2 (COX-2). COX-2 expression is increased within just a few hours of exposure to a neurotoxic regimen of METH (Kita et al., 2000; Thomas and

Kuhn, 2005b; Zhang et al., 2007). The COX enzyme is a major inflammatory mediator and is the rate-limiting enzyme in the synthesis of prostaglandins, with the COX-2 isoform, in particular, being transcriptionally induced in neurons and glia in response to inflammatory stimuli (Smith et al., 2000; For review see Consilvio et al., 2004; Zhang et al., 2007). COX-2 and the downstream synthesis of prostaglandins are believed to play an important role in regulating neuroinflammation (Aid and Bosetti, 2011). Importantly, deletion of the COX-2 gene renders animals partially protected against METH-induced DA depletions (Thomas and Kuhn, 2005b). However, COX-2 inhibitor co-administration during METH exposure does not afford similar protection (Thomas and Kuhn, 2005b; Zhang et al., 2007), and thus the possible role for glial-derived COX-2 in METH-induced neurotoxicity is unclear and deserves further study.

In addition to release of factors that may contribute to or mitigate METH-induced DA terminal degeneration, microglia also have significant phagocytic capability. In this regard, microglia may contribute to METH-induced neurotoxicity *via* phagocytosis of DA nerve terminals (*i.e.,* prior to their degeneration). There is a growing amount of evidence suggesting phagocytosis-induced neuronal damage, particularly of cells that may have otherwise been viable (Neher et al., 2011; Fricker et al., 2012). Conversely, microglial activation may provide beneficial support for neuronal survival, by clearing cellular debris (Beyer et al., 2000; Simard and Rivest, 2007). To date, no one has examined whether microglia-mediate phagocytosis of DA terminals occurs early in response to METH exposure. Therefore, a more comprehensive understanding of microglia-mediated phagocytosis, the signals initiating this process, and whether such phagocytosis occurs following METH exposure are clearly needed and should provide

novel insight into the potential causal versus protective roles of microglia in METH-induced neurotoxicity

As reviewed above, extracellular GLU has also been heavily linked to METH-induced damage to the DA nerve terminals in striatum (Battaglia et al., 2002; Mark et al., 2004). Astrocytes are important regulators of extracellular GLU (Rothstein et al., 1996) via activity of excitatory amino acid transporter-1 (EAAT-1/GLAST) and 2 (EAAT2/GLT-1) (Chaudhry et al., 1995; Kondo et al., 1995; Lehre et al., 1995). To our knowledge, only one study has examined and shown an increase in GLT-1 expression in response to repeated METH exposure, and that was to a low dose (Nishino et al., 1996). Therefore regulation of extracellular GLU via EAAT1 and 2 deserves further investigation in the context of METH-induced neurotoxicity. In addition to EAAT 1 and 2, astrocytes also express the cystine/glutamate antiporter, and activity of this transporter has been shown to decrease GLU release following exposure to other psychostimulants (Baker et al., 2003). To our knowledge activity of the cystine/glutamate exchange has not been examined in the context of METH-induced neurotoxicity. Given the significant implication of high extracellular GLU concentrations in METH-induced neurotoxicity, studies examining astrocyte-mediated GLU regulation may provide novel therapeutic targets.

Although astrocyte mediated GLU regulation may function as a protective mechanism against METH-induced neurotoxicity, it also is conceivable that disruption of astrocyte-regulated GLU during METH exposure could contribute to the neurotoxicity. For example, in addition to regulating extracellular GLU concentrations via uptake mechanisms, astrocytes have the ability to release GLU. Furthermore, astrocyte-

mediated GLU release has been demonstrated in response to inflammatory stimuli, including increased tumor necrosis factor α (TNFα)(Rossi et al., 2005). Stimulation of CXCR4 receptors expressed by astrocytes via TNFα increases GLU release and produces excitotoxic consequences in hippocampal cultures (Bezzi et al., 2001). Importantly, TNFα is increased following METH exposure (Sriram et al., 2006; Goncalves et al., 2008), and animals with a depletion of the TNFα receptor gene are protected against 1-methyl-4-phenyl-1,2,3,6-tetrahydropyridine(MPTP)-induced neurotoxicity (Sriram et al., 2006). Additionally, recent work from Yamamoto and colleagues has suggested that increased extracellular GLU may be derived from the periphery secondarily to liver damage and hepatic encephalopathy (HE) may contribute to METH-induced neurotoxicity (Halpin and Yamamoto, 2012). Ammonia can decrease expression of astrocytic GLU transporters (Chan and Butterworth, 1999; Chan et al., 2000) and cause astrocyte-mediated Glu release (Gorg et al., 2010), thus ultimately increasing extracellular GLU and possibly resulting in excitotoxicity. Clearly, more in depth investigations into the regulation of extracellular GLU by astrocytes will provide novel insights into extracellular GLU implicated in METH neurotoxicity.

Finally, disruption of the blood brain barrier (BBB) following METH exposure has also been documented (Bowyer and Ali, 2006; Kiyatkin et al., 2007; Bowyer et al., 2008, and others). The mechanisms underlying this disruption of the BBB during and after METH exposure have not been fully elucidated; however, astrocytes are known to play a key role in the maintenance of BBB function. For example, ablation of astrocytes after CNS injury prevents BBB repair and allows for CNS edema (Bush et al., 1999).

Therefore further investigation into astocyte regulation of BBB function in METH-induced neurotoxicity could provide a beneficial therapeutic target.

While it is clear that both astrocytes and microglia become “reactive” in response to METH-induced neurotoxicity, our understanding of the role of these cells in such toxicity is far from complete. One important issue that complicates the examination of glial cells in METH-induced neurotoxicity is the reference to “activated” glia without acknowledging that the activation of these cells is a heterogenous process. In this regard, recent work has now shown that subtypes of astrocytes derived from different regions of the CNS serve distinct CNS functions (Stadlin et al., 1998; Lau et al., 2000; Yeh et al., 2009). Therefore, simply using markers, such as GFAP, as indicators of reactive gliosis limits our understanding of the particular function of these cells in different contexts. Similarly, our understanding of glial activation is still limited and our classification of “activated” glia may thus be incomplete, in that changes of glial function may occur prior to gross morphological changes. For instance, in the context of METH exposure, recent work has shown changes in astrocyte Ca^{2+} signaling within minutes of METH exposure in vitro (Granado et al., 2011), suggesting that changes in astrocyte function in response to METH occur long before observable changes in GFAP expression. In this regard, as mentioned above, we and others have shown that GFAP remains elevated compared to controls in animals exposed to METH 21 or 32 days prior (O'Callaghan and Miller, 1994; Friend and Keefe, 2013). However, the degree to which these astrocytes are all equally "reactive" and performing the same functions as the astrocytes with GFAP expression immediately after exposure to a neurotoxic regimen of METH is unknown. Re-

evaluating ways in which we classify glia as "activated" may result in a better understanding of the function of these cells in METH-induced neurotoxicity.

Finally, another important issue in studying activation of glia in the context of METH-induced neurotoxicity is that pharmacological manipulations to inhibit inflammatory responses or neurotransmitter signaling are relatively nonspecific. Therefore, the ability to determine whether particular cell types or signaling molecules are involved in METH-induced neurotoxicity is difficult. As mentioned above, many manipulations that prevent glial activation also prevent DA nerve terminal degeneration. It is unclear whether glial reactivity is inhibited due to mitigation of METH-induced DA terminal degeneration or because of direct inhibition of glial activation. Therefore, the use of transgenic models allowing for conditional ablation of reactive glia or similar genetic manipulations of signaling cascades that may lead to glial activation in this context will allow for more specific manipulations of these cells in METH-induced neurotoxicity. For example, the recent use of fractalkine receptor knockout mice demonstrated that this receptor is not involved in microglia activation following METH exposure (Thomas et al., 2008a). Similarly, genetic manipulations of astrocyte activation is now possible and could lead to significant insights into the role of these cells in METH-induced neurotoxicity (Liedtke et al., 1998; Wilhelmsson et al., 2004; Okada et al., 2006; Herrmann et al., 2008; Li et al., 2008). Thus, identifying the particular signals that activate glial cells and then manipulating such activation should lead to significant advances in our understanding of glial cells in METH-induced DA nerve terminal degeneration.

1.3 References

ADAMII (2012) Arrestee Drug Abuse Monitoring Program: 2011 Annual Report.

Aid S and Bosetti F (2011) Targeting cyclooxygenases-1 and -2 in neuroinflammation: Therapeutic implications. *Biochimie* **93**:46-51.

Albers DS and Sonsalla PK (1995) Methamphetamine-induced hyperthermia and dopaminergic neurotoxicity in mice: pharmacological profile of protective and nonprotective agents. *J Pharmacol Exp Ther* **275**:1104-1114.

Ali SF and Itzhak Y (1998) Effects of 7-nitroindazole, an NOS inhibitor on methamphetamine-induced dopaminergic and serotonergic neurotoxicity in mice. *Ann N Y Acad Sci* **844**:122-130.

Ali SF, Newport GD, Holson RR, Slikker W, Jr. and Bowyer JF (1994) Low environmental temperatures or pharmacologic agents that produce hypothermia decrease methamphetamine neurotoxicity in mice. *Brain Res* **658**:33-38.

Ali SF, Newport RR, Holson W, Slikker W, Jr. and Bowyer JF (1995) Low environmental temperatures or pharmacologic agents that produce hyperthermia decrease methamphetamine neurotoxicity in mice. *Ann N Y Acad Sci* **765**:338.

Anderson KL and Itzhak Y (2006) Methamphetamine-induced selective dopaminergic neurotoxicity is accompanied by an increase in striatal nitrate in the mouse. *Ann N Y Acad Sci* **1074**:225-233.

Arbones ML, Ribera J, Agullo L, Baltrons MA, Casanovas A, Riveros-Moreno V and Garcia A (1996) Characteristics of nitric oxide synthase type I of rat cerebellar astrocytes. *Glia* **18**:224-232.

Ares-Santos S, Granado N, Oliva I, O'Shea E, Martin ED, Colado MI and Moratalla R (2012) Dopamine D(1) receptor deletion strongly reduces neurotoxic effects of methamphetamine. *Neurobiol Dis* **45**:810-820.

Baker DA, McFarland K, Lake RW, Shen H, Tang XC, Toda S and Kalivas PW (2003) Neuroadaptations in cystine-glutamate exchange underlie cocaine relapse. *Nat Neurosci* **6**:743-749.

Battaglia G, Fornai F, Busceti CL, Aloisi G, Cerrito F, De Blasi A, Melchiorri D and Nicoletti F (2002) Selective blockade of mGlu5 metabotropic glutamate receptors is protective against methamphetamine neurotoxicity. *J Neurosci* **22**:2135-2141.

Beckman JS, Beckman TW, Chen J, Marshall PA and Freeman BA (1990) Apparent hydroxyl radical production by peroxynitrite: implications for endothelial injury from nitric oxide and superoxide. *Proc Natl Acad Sci U S A* **87**:1620-1624.

Bellomo M, Giuffrida R, Palmeri A and Sapienza S (1998) Excitatory amino acids as neurotransmitters of corticostriatal projections: immunocytochemical evidence in the rat. *Arch Ital Biol* **136**:215-223.

Berman SB, Zigmond MJ and Hastings TG (1996) Modification of dopamine transporter function: effect of reactive oxygen species and dopamine. *J Neurochem* **67**:593-600.

Beyer M, Gimsa U, Eyupoglu IY, Hailer NP and Nitsch R (2000) Phagocytosis of neuronal or glial debris by microglial cells: upregulation of MHC class II expression and multinuclear giant cell formation in vitro. *Glia* **31**:262-266.

Bezzi P, Domercq M, Brambilla L, Galli R, Schols D, De Clercq E, Vescovi A, Bagetta G, Kollias G, Meldolesi J and Volterra A (2001) CXCR4-activated astrocyte glutamate release via TNFalpha: amplification by microglia triggers neurotoxicity. *Nat Neurosci* **4**:702-710.

Blackshaw S, Eliasson MJ, Sawa A, Watkins CC, Krug D, Gupta A, Arai T, Ferrante RJ and Snyder SH (2003) Species, strain and developmental variations in hippocampal neuronal and endothelial nitric oxide synthase clarify discrepancies in nitric oxide-dependent synaptic plasticity. *Neuroscience* **119**:979-990.

Blanchard-Fillion B, Souza JM, Friel T, Jiang GC, Vrana K, Sharov V, Barron L, Schoneich C, Quijano C, Alvarez B, Radi R, Przedborski S, Fernando GS, Horwitz J and Ischiropoulos H (2001) Nitration and inactivation of tyrosine hydroxylase by peroxynitrite. *J Biol Chem* **276**:46017-46023.

Bo L, Dawson TM, Wesselingh S, Mork S, Choi S, Kong PA, Hanley D and Trapp BD (1994) Induction of nitric oxide synthase in demyelinating regions of multiple sclerosis brains. *Ann Neurol* **36**:778-786.

Boger HA, Middaugh LD, Granholm AC and McGinty JF (2009) Minocycline restores striatal tyrosine hydroxylase in GDNF heterozygous mice but not in methamphetamine-treated mice. *Neurobiol Dis* **33**:459-466.

Bowyer JF and Ali S (2006) High doses of methamphetamine that cause disruption of the blood-brain barrier in limbic regions produce extensive neuronal degeneration in mouse hippocampus. *Synapse* **60**:521-532.

Bowyer JF, Robinson B, Ali S and Schmued LC (2008) Neurotoxic-related changes in tyrosine hydroxylase, microglia, myelin, and the blood-brain barrier in the caudate-putamen from acute methamphetamine exposure. *Synapse* **62**:193-204.

Brambilla R, Persaud T, Hu X, Karmally S, Shestopalov VI, Dvoriantchikova G, Ivanov D, Nathanson L, Barnum SR and Bethea JR (2009) Transgenic inhibition of astroglial NF-kappa B improves functional outcome in experimental autoimmune encephalomyelitis by suppressing chronic central nervous system inflammation. *J Immunol* **182**:2628-2640.

Bredt DS, Hwang PM and Snyder SH (1990) Localization of nitric oxide synthase indicating a neural role for nitric oxide. *Nature* **347**:768-770.

Bredt DS and Snyder SH (1989) Nitric oxide mediates glutamate-linked enhancement of cGMP levels in the cerebellum. *Proc Natl Acad Sci U S A* **86**:9030-9033.

Bredt DS and Snyder SH (1990) Isolation of nitric oxide synthetase, a calmodulin-requiring enzyme. *Proc Natl Acad Sci U S A* **87**:682-685.

Broening HW, Morford LL and Vorhees CV (2005) Interactions of dopamine D1 and D2 receptor antagonists with D-methamphetamine-induced hyperthermia and striatal dopamine and serotonin reductions. *Synapse* **56**:84-93.

Brown JM, Hanson GR and Fleckenstein AE (2000) Methamphetamine rapidly decreases vesicular dopamine uptake. *J Neurochem* **74**:2221-2223.

Buki A, Siman R, Trojanowski JQ and Povlishock JT (1999) The role of calpain-mediated spectrin proteolysis in traumatically induced axonal injury. *J Neuropathol Exp Neurol* **58**:365-375.

Burrows KB and Meshul CK (1997) Methamphetamine alters presynaptic glutamate immunoreactivity in the caudate nucleus and motor cortex. *Synapse* **27**:133-144.

Bush TG, Puvanachandra N, Horner CH, Polito A, Ostenfeld T, Svendsen CN, Mucke L, Johnson MH and Sofroniew MV (1999) Leukocyte infiltration, neuronal degeneration, and neurite outgrowth after ablation of scar-forming, reactive astrocytes in adult transgenic mice. *Neuron* **23**:297-308.

Bushong EA, Martone ME, Jones YZ and Ellisman MH (2002) Protoplasmic astrocytes in CA1 stratum radiatum occupy separate anatomical domains. *J Neurosci* **22**:183-192.

Callaghan RC, Cunningham JK, Sajeev G and Kish SJ (2010) Incidence of Parkinson's disease among hospital patients with methamphetamine-use disorders. *Mov Disord* **25**:2333-2339.

Callaghan RC, Cunningham JK, Sykes J and Kish SJ (2012) Increased risk of Parkinson's disease in individuals hospitalized with conditions related to the use of methamphetamine or other amphetamine-type drugs. *Drug Alcohol Depend* **120**:35-40.

Callahan BT and Ricaurte GA (1998) Effect of 7-nitroindazole on body temperature and methamphetamine-induced dopamine toxicity. *Neuroreport* **9**:2691-2695.

Cappon GD, Morford LL and Vorhees CV (1997) Ontogeny of methamphetamine-induced neurotoxicity and associated hyperthermic response. *Brain Res Dev Brain Res* **103**:155-162.

Centonze D, Grande C, Saulle E, Martin AB, Gubellini P, Pavon N, Pisani A, Bernardi G, Moratalla R and Calabresi P (2003) Distinct roles of D1 and D5 dopamine receptors in motor activity and striatal synaptic plasticity. *J Neurosci* **23**:8506-8512.

Centonze D, Pisani A, Bonsi P, Giacomini P, Bernardi G and Calabresi P (2001) Stimulation of nitric oxide-cGMP pathway excites striatal cholinergic interneurons via protein kinase G activation. *J Neurosci* **21**:1393-1400.

Chan H and Butterworth RF (1999) Evidence for an astrocytic glutamate transporter deficit in hepatic encephalopathy. *Neurochem Res* **24**:1397-1401.

Chan H, Hazell AS, Desjardins P and Butterworth RF (2000) Effects of ammonia on glutamate transporter (GLAST) protein and mRNA in cultured rat cortical astrocytes. *Neurochem Int* **37**:243-248.

Chang JY and Liu LZ (2000) Catecholamines inhibit microglial nitric oxide production. *Brain Res Bull* **52**:525-530.

Chapman DE, Hanson GR, Kesner RP and Keefe KA (2001) Long-term changes in basal ganglia function after a neurotoxic regimen of methamphetamine. *J Pharmacol Exp Ther* **296**:520-527.

Chaudhry FA, Lehre KP, van Lookeren Campagne M, Ottersen OP, Danbolt NC and Storm-Mathisen J (1995) Glutamate transporters in glial plasma membranes: highly differentiated localizations revealed by quantitative ultrastructural immunocytochemistry. *Neuron* **15**:711-720.

Cho BP, Song DY, Sugama S, Shin DH, Shimizu Y, Kim SS, Kim YS and Joh TH (2006) Pathological dynamics of activated microglia following medial forebrain bundle transection. *Glia* **53**:92-102.

Chung RS, Adlard PA, Dittmann J, Vickers JC, Chuah MI and West AK (2004) Neuron-glia communication: metallothionein expression is specifically up-regulated by astrocytes in response to neuronal injury. *J Neurochem* **88**:454-461.

Clementi E, Brown GC, Feelisch M and Moncada S (1998) Persistent inhibition of cell respiration by nitric oxide: crucial role of S-nitrosylation of mitochondrial complex I and protective action of glutathione. *Proc Natl Acad Sci U S A* **95**:7631-7636.

Colton CA and Gilbert DL (1987) Production of superoxide anions by a CNS macrophage, the microglia. *FEBS Lett* **223**:284-288.

Consilvio C, Vincent AM and Feldman EL (2004) Neuroinflammation, COX-2, and ALS--a dual role? *Exp Neurol* **187**:1-10.

Crofts N, Hopper JL, Milner R, Breschkin AM, Bowden DS and Locarnini SA (1994) Blood-borne virus infections among Australian injecting drug users: implications for spread of HIV. *Eur J Epidemiol* **10**:687-694.

Daberkow DP, Kesner RP and Keefe KA (2005) Relation between methamphetamine-induced monoamine depletions in the striatum and sequential motor learning. *Pharmacol Biochem Behav* **81**:198-204.

Davalos D, Grutzendler J, Yang G, Kim JV, Zuo Y, Jung S, Littman DR, Dustin ML and Gan WB (2005) ATP mediates rapid microglial response to local brain injury in vivo. *Nat Neurosci* **8**:752-758.

Dawson TM, Bredt DS, Fotuhi M, Hwang PM and Snyder SH (1991) Nitric oxide synthase and neuronal NADPH diaphorase are identical in brain and peripheral tissues. *Proc Natl Acad Sci U S A* **88**:7797-7801.

del Cerro S, Arai A, Kessler M, Bahr BA, Vanderklish P, Rivera S and Lynch G (1994) Stimulation of NMDA receptors activates calpain in cultured hippocampal slices. *Neurosci Lett* **167**:149-152.

Deng X and Cadet JL (1999) Methamphetamine administration causes overexpression of nNOS in the mouse striatum. *Brain Res* **851**:254-257.

Deniau JM and Chevalier G (1985) Disinhibition as a basic process in the expression of striatal functions. II. The striato-nigral influence on thalamocortical cells of the ventromedial thalamic nucleus. *Brain Res* **334**:227-233.

Di Monte DA, Royland JE, Jakowec MW and Langston JW (1996) Role of nitric oxide in methamphetamine neurotoxicity: protection by 7-nitroindazole, an inhibitor of neuronal nitric oxide synthase. *J Neurochem* **67**:2443-2450.

Dinerman JL, Dawson TM, Schell MJ, Snowman A and Snyder SH (1994) Endothelial nitric oxide synthase localized to hippocampal pyramidal cells: implications for synaptic plasticity. *Proc Natl Acad Sci U S A* **91**:4214-4218.

Endoh M, Maiese K and Wagner J (1994) Expression of the inducible form of nitric oxide synthase by reactive astrocytes after transient global ischemia. *Brain Res* **651**:92-100.

Eyerman DJ and Yamamoto BK (2005) Lobeline attenuates methamphetamine-induced changes in vesicular monoamine transporter 2 immunoreactivity and monoamine depletions in the striatum. *J Pharmacol Exp Ther* **312**:160-169.

Faraci FM and Breese KR (1993) Nitric oxide mediates vasodilatation in response to activation of N-methyl-D-aspartate receptors in brain. *Circ Res* **72**:476-480.

Farber K, Pannasch U and Kettenmann H (2005) Dopamine and noradrenaline control distinct functions in rodent microglial cells. *Mol Cell Neurosci* **29**:128-138.

Farina C, Krumbholz M, Giese T, Hartmann G, Aloisi F and Meinl E (2005) Preferential expression and function of Toll-like receptor 3 in human astrocytes. *J Neuroimmunol* **159**:12-19.

Figueredo-Cardenas G, Morello M, Sancesario G, Bernardi G and Reiner A (1996) Colocalization of somatostatin, neuropeptide Y, neuronal nitric oxide synthase and NADPH-diaphorase in striatal interneurons in rats. *Brain Res* **735**:317-324.

Finnegan KT and Taraska T (1996) Effects of glutamate antagonists on methamphetamine and 3,4-methylenedioxymethamphetamine-induced striatal dopamine release in vivo. *J Neurochem* **66**:1949-1958.

Fitzmaurice PS, Tong J, Yazdanpanah M, Liu PP, Kalasinsky KS and Kish SJ (2006) Levels of 4-hydroxynonenal and malondialdehyde are increased in brain of human chronic users of methamphetamine. *J Pharmacol Exp Ther* **319**:703-709.

Fleckenstein AE, Metzger RR, Beyeler ML, Gibb JW and Hanson GR (1997) Oxygen radicals diminish dopamine transporter function in rat striatum. *Eur J Pharmacol* **334**:111-114.

Forstermann U, Pollock JS, Schmidt HH, Heller M and Murad F (1991) Calmodulin-dependent endothelium-derived relaxing factor/nitric oxide synthase activity is present in the particulate and cytosolic fractions of bovine aortic endothelial cells. *Proc Natl Acad Sci U S A* **88**:1788-1792.

Franke H, Krugel U and Illes P (2006) P2 receptors and neuronal injury. *Pflugers Arch* **452**:622-644.

Fricker M, Neher JJ, Zhao JW, Thery C, Tolkovsky AM and Brown GC (2012) MFG-E8 mediates primary phagocytosis of viable neurons during neuroinflammation. *J Neurosci* **32**:2657-2666.

Fricks-Gleason AN and Keefe KA (2013) Evaluating the Role of Neuronal Nitric Oxide Synthase-Containing Striatal Interneurons in Methamphetamine-Induced Dopamine Neurotoxicity. *Neurotox Res*.

Friend DM and Keefe KA (2013) Glial Reactivity in Resistance to Methamphetamine-Induced Neurotoxicity. *J Neurochem*.

Friend DM, Son JH, Keefe KA and Fricks-Gleason AN (2013) Expression and activity of nitric oxide synthase isoforms in methamphetamine-induced striatal dopamine toxicity. *J Pharmacol Exp Ther* **344**:511-521.

Fukami G, Hashimoto K, Koike K, Okamura N, Shimizu E and Iyo M (2004) Effect of antioxidant N-acetyl-L-cysteine on behavioral changes and neurotoxicity in rats after administration of methamphetamine. *Brain Res* **1016**:90-95.

Garthwaite J, Charles SL and Chess-Williams R (1988) Endothelium-derived relaxing factor release on activation of NMDA receptors suggests role as intercellular messenger in the brain. *Nature* **336**:385-388.

Geller DA, Lowenstein CJ, Shapiro RA, Nussler AK, Di Silvio M, Wang SC, Nakayama DK, Simmons RL, Snyder SH and Billiar TR (1993) Molecular cloning and expression of inducible nitric oxide synthase from human hepatocytes. *Proc Natl Acad Sci U S A* **90**:3491-3495.

Gerfen CR (1989) The neostriatal mosaic: striatal patch-matrix organization is related to cortical lamination. *Science* **246**:385-388.

Gibson CL, Coughlan TC and Murphy SP (2005) Glial nitric oxide and ischemia. *Glia* **50**:417-426.

Giovanni A, Liang LP, Hastings TG and Zigmond MJ (1995) Estimating hydroxyl radical content in rat brain using systemic and intraventricular salicylate: impact of methamphetamine. *J Neurochem* **64**:1819-1825.

Goncalves J, Martins T, Ferreira R, Milhazes N, Borges F, Ribeiro CF, Malva JO, Macedo TR and Silva AP (2008) Methamphetamine-induced early increase of IL-6 and TNF-alpha mRNA expression in the mouse brain. *Ann N Y Acad Sci* **1139**:103-111.

Gorg B, Morwinsky A, Keitel V, Qvartskhava N, Schror K and Haussinger D (2010) Ammonia triggers exocytotic release of L-glutamate from cultured rat astrocytes. *Glia* **58**:691-705.

Gracy KN and Pickel VM (1997) Ultrastructural localization and comparative distribution of nitric oxide synthase and N-methyl-D-aspartate receptors in the shell of the rat nucleus accumbens. *Brain Res* **747**:259-272.

Granado N, Lastres-Becker I, Ares-Santos S, Oliva I, Martin E, Cuadrado A and Moratalla R (2011) Nrf2 deficiency potentiates methamphetamine-induced dopaminergic axonal damage and gliosis in the striatum. *Glia* **59**:1850-1863.

Gross NB, Duncker PC and Marshall JF (2011a) Cortical ionotropic glutamate receptor antagonism protects against methamphetamine-induced striatal neurotoxicity. *Neuroscience* **199**:272-283.

Gross NB, Duncker PC and Marshall JF (2011b) Striatal dopamine D1 and D2 receptors: Widespread influences on methamphetamine-induced dopamine and serotonin neurotoxicity. *Synapse* **65**:1144-1155.

Guilarte TR, Nihei MK, McGlothan JL and Howard AS (2003) Methamphetamine-induced deficits of brain monoaminergic neuronal markers: distal axotomy or neuronal plasticity. *Neuroscience* **122**:499-513.

Hall AV, Antoniou H, Wang Y, Cheung AH, Arbus AM, Olson SL, Lu WC, Kau CL and Marsden PA (1994) Structural organization of the human neuronal nitric oxide synthase gene (NOS1). *J Biol Chem* **269**:33082-33090.

Halpin LE and Yamamoto BK (2012) Peripheral ammonia as a mediator of methamphetamine neurotoxicity. *J Neurosci* **32**:13155-13163.

Hanisch UK (2002) Microglia as a source and target of cytokines. *Glia* **40**:140-155.

Hanson JE, Birdsall E, Seferian KS, Crosby MA, Keefe KA, Gibb JW, Hanson GR and Fleckenstein AE (2009) Methamphetamine-induced dopaminergic deficits and refractoriness to subsequent treatment. *Eur J Pharmacol* **607**:68-73.

Harris AS and Morrow JS (1988) Proteolytic processing of human brain alpha spectrin (fodrin): identification of a hypersensitive site. *J Neurosci* **8**:2640-2651.

Harris NV, Thiede H, McGough JP and Gordon D (1993) Risk factors for HIV infection among injection drug users: results of blinded surveys in drug treatment centers, King County, Washington 1988-1991. *J Acquir Immune Defic Syndr* **6**:1275-1282.

Herrmann JE, Imura T, Song B, Qi J, Ao Y, Nguyen TK, Korsak RA, Takeda K, Akira S and Sofroniew MV (2008) STAT3 is a critical regulator of astrogliosis and scar formation after spinal cord injury. *J Neurosci* **28**:7231-7243.

Hide I, Tanaka M, Inoue A, Nakajima K, Kohsaka S, Inoue K and Nakata Y (2000) Extracellular ATP triggers tumor necrosis factor-alpha release from rat microglia. *J Neurochem* **75**:965-972.

Honda S, Sasaki Y, Ohsawa K, Imai Y, Nakamura Y, Inoue K and Kohsaka S (2001) Extracellular ATP or ADP induce chemotaxis of cultured microglia through Gi/o-coupled P2Y receptors. *J Neurosci* **21**:1975-1982.

Hope BT, Michael GJ, Knigge KM and Vincent SR (1991) Neuronal NADPH diaphorase is a nitric oxide synthase. *Proc Natl Acad Sci U S A* **88**:2811-2814.

Hoque KE, Indorkar RP, Sammut S and West AR (2010) Impact of dopamine-glutamate interactions on striatal neuronal nitric oxide synthase activity. *Psychopharmacology (Berl)* **207**:571-581.

Hozumi H, Asanuma M, Miyazaki I, Fukuoka S, Kikkawa Y, Kimoto N, Kitamura Y, Sendo T, Kita T and Gomita Y (2008) Protective effects of interferon-gamma against methamphetamine-induced neurotoxicity. *Toxicol Lett* **177**:123-129.

Huang MC, Lin SK, Chen CH, Pan CH, Lee CH and Liu HC (2013) Oxidative stress status in recently abstinent methamphetamine abusers. *Psychiatry Clin Neurosci* **67**:92-100.

Hunot S, Boissiere F, Faucheux B, Brugg B, Mouatt-Prigent A, Agid Y and Hirsch EC (1996) Nitric oxide synthase and neuronal vulnerability in Parkinson's disease. *Neuroscience* **72**:355-363.

Imam SZ, Crow JP, Newport GD, Islam F, Slikker W, Jr. and Ali SF (1999) Methamphetamine generates peroxynitrite and produces dopaminergic neurotoxicity in mice: protective effects of peroxynitrite decomposition catalyst. *Brain Res* **837**:15-21.

Imam SZ, Islam F, Itzhak Y, Slikker W, Jr. and Ali SF (2000) Prevention of dopaminergic neurotoxicity by targeting nitric oxide and peroxynitrite: implications for the prevention of methamphetamine-induced neurotoxic damage. *Ann N Y Acad Sci* **914**:157-171.

Iravani MM, Millar J and Kruk ZL (1998) Differential release of dopamine by nitric oxide in subregions of rat caudate putamen slices. *J Neurochem* **71**:1969-1977.

Itzhak Y and Ali SF (1996) The neuronal nitric oxide synthase inhibitor, 7-nitroindazole, protects against methamphetamine-induced neurotoxicity in vivo. *J Neurochem* **67**:1770-1773.

Itzhak Y, Gandia C, Huang PL and Ali SF (1998) Resistance of neuronal nitric oxide synthase-deficient mice to methamphetamine-induced dopaminergic neurotoxicity. *J Pharmacol Exp Ther* **284**:1040-1047.

Itzhak Y, Martin JL and Ail SF (2000a) nNOS inhibitors attenuate methamphetamine-induced dopaminergic neurotoxicity but not hyperthermia in mice. *Neuroreport* **11**:2943-2946.

Itzhak Y, Martin JL and Ali SF (1999) Methamphetamine- and 1-methyl-4-phenyl- 1,2,3, 6-tetrahydropyridine-induced dopaminergic neurotoxicity in inducible nitric oxide synthase-deficient mice. *Synapse* **34**:305-312.

Itzhak Y, Martin JL and Ali SF (2000b) Comparison between the role of the neuronal and inducible nitric oxide synthase in methamphetamine-induced neurotoxicity and sensitization. *Ann N Y Acad Sci* **914**:104-111.

Janssens SP, Shimouchi A, Quertermous T, Bloch DB and Bloch KD (1992) Cloning and expression of a cDNA encoding human endothelium-derived relaxing factor/nitric oxide synthase. *J Biol Chem* **267**:14519-14522.

Johanson CE, Frey KA, Lundahl LH, Keenan P, Lockhart N, Roll J, Galloway GP, Koeppe RA, Kilbourn MR, Robbins T and Schuster CR (2006) Cognitive function and nigrostriatal markers in abstinent methamphetamine abusers. *Psychopharmacology (Berl)* **185**:327-338.

John GR, Lee SC and Brosnan CF (2003) Cytokines: powerful regulators of glial cell activation. *Neuroscientist* **9**:10-22.

Kaindl AM, Degos V, Peineau S, Gouadon E, Chhor V, Loron G, Le Charpentier T, Josserand J, Ali C, Vivien D, Collingridge GL, Lombet A, Issa L, Rene F, Loeffler JP, Kavelaars A, Verney C, Mantz J and Gressens P (2012) Activation of microglial N-methyl-D-aspartate receptors triggers inflammation and neuronal cell death in the developing and mature brain. *Ann Neurol* **72**:536-549.

Kaneko T and Mizuno N (1988) Immunohistochemical study of glutaminase-containing neurons in the cerebral cortex and thalamus of the rat. *J Comp Neurol* **267**:590-602.

Kaul M and Lipton SA (1999) Chemokines and activated macrophages in HIV gp120-induced neuronal apoptosis. *Proc Natl Acad Sci U S A* **96**:8212-8216.

Kawaguchi Y (1993) Physiological, morphological, and histochemical characterization of three classes of interneurons in rat neostriatum. *J Neurosci* **13**:4908-4923.

Kawaguchi Y, Wilson CJ, Augood SJ and Emson PC (1995) Striatal interneurones: chemical, physiological and morphological characterization. *Trends Neurosci* **18**:527-535.

Kawasaki T, Ishihara K, Ago Y, Nakamura S, Itoh S, Baba A and Matsuda T (2006) Protective effect of the radical scavenger edaravone against methamphetamine-induced dopaminergic neurotoxicity in mouse striatum. *Eur J Pharmacol* **542**:92-99.

Kita T, Shimada K, Mastunari Y, Wagner GC, Kubo K and Nakashima T (2000) Methamphetamine-induced striatal dopamine neurotoxicity and cyclooxygenase-2 protein expression in BALB/c mice. *Neuropharmacology* **39**:399-406.

Kitamura O, Takeichi T, Wang EL, Tokunaga I, Ishigami A and Kubo S (2010) Microglial and astrocytic changes in the striatum of methamphetamine abusers. *Leg Med (Tokyo)* **12**:57-62.

Kiyatkin EA, Brown PL and Sharma HS (2007) Brain edema and breakdown of the blood-brain barrier during methamphetamine intoxication: critical role of brain hyperthermia. *Eur J Neurosci* **26**:1242-1253.

Kogan FJ, Nichols WK and Gibb JW (1976) Influence of methamphetamine on nigral and striatal tyrosine hydroxylase activity and on striatal dopamine levels. *Eur J Pharmacol* **36**:363-371.

Kondo K, Hashimoto H, Kitanaka J, Sawada M, Suzumura A, Marunouchi T and Baba A (1995) Expression of glutamate transporters in cultured glial cells. *Neurosci Lett* **188**:140-142.

Konorev EA, Hogg N and Kalyanaraman B (1998) Rapid and irreversible inhibition of creatine kinase by peroxynitrite. *FEBS Lett* **427**:171-174.

Kreutzberg GW (1996) Microglia: a sensor for pathological events in the CNS. *Trends Neurosci* **19**:312-318.

Kuhn DM, Arthur RE, Jr., Thomas DM and Elferink LA (1999) Tyrosine hydroxylase is inactivated by catechol-quinones and converted to a redox-cycling quinoprotein: possible relevance to Parkinson's disease. *J Neurochem* **73**:1309-1317.

Kuhn DM, Francescutti-Verbeem DM and Thomas DM (2006) Dopamine quinones activate microglia and induce a neurotoxic gene expression profile: relationship to methamphetamine-induced nerve ending damage. *Ann N Y Acad Sci* **1074**:31-41.

Kuhn SA, van Landeghem FK, Zacharias R, Farber K, Rappert A, Pavlovic S, Hoffmann A, Nolte C and Kettenmann H (2004) Microglia express GABA(B) receptors to modulate interleukin release. *Mol Cell Neurosci* **25**:312-322.

Lalo U, Pankratov Y, Kirchhoff F, North RA and Verkhratsky A (2006) NMDA receptors mediate neuron-to-glia signaling in mouse cortical astrocytes. *J Neurosci* **26**:2673-2683.

Langosch JM, Gebicke-Haerter PJ, Norenberg W and Illes P (1994) Characterization and transduction mechanisms of purinoceptors in activated rat microglia. *Br J Pharmacol* **113**:29-34.

Larsen KE, Fon EA, Hastings TG, Edwards RH and Sulzer D (2002) Methamphetamine-induced degeneration of dopaminergic neurons involves autophagy and upregulation of dopamine synthesis. *J Neurosci* **22**:8951-8960.

Lau JW, Senok S and Stadlin A (2000) Methamphetamine-induced oxidative stress in cultured mouse astrocytes. *Ann N Y Acad Sci* **914**:146-156.

LaVoie MJ, Card JP and Hastings TG (2004) Microglial activation precedes dopamine terminal pathology in methamphetamine-induced neurotoxicity. *Exp Neurol* **187**:47-57.

LaVoie MJ and Hastings TG (1999) Dopamine quinone formation and protein modification associated with the striatal neurotoxicity of methamphetamine: evidence against a role for extracellular dopamine. *J Neurosci* **19**:1484-1491.

Le Moine C, Normand E and Bloch B (1991) Phenotypical characterization of the rat striatal neurons expressing the D1 dopamine receptor gene. *Proc Natl Acad Sci U S A* **88**:4205-4209.

Lehre KP, Levy LM, Ottersen OP, Storm-Mathisen J and Danbolt NC (1995) Differential expression of two glial glutamate transporters in the rat brain: quantitative and immunocytochemical observations. *J Neurosci* **15**:1835-1853.

Levey AI, Hersch SM, Rye DB, Sunahara RK, Niznik HB, Kitt CA, Price DL, Maggio R, Brann MR and Ciliax BJ (1993) Localization of D1 and D2 dopamine receptors in brain with subtype-specific antibodies. *Proc Natl Acad Sci U S A* **90**:8861-8865.

Li L, Lundkvist A, Andersson D, Wilhelmsson U, Nagai N, Pardo AC, Nodin C, Stahlberg A, Aprico K, Larsson K, Yabe T, Moons L, Fotheringham A, Davies I, Carmeliet P, Schwartz JP, Pekna M, Kubista M, Blomstrand F, Maragakis N, Nilsson M and Pekny M (2008) Protective role of reactive astrocytes in brain ischemia. *J Cereb Blood Flow Metab* **28**:468-481.

Liedtke W, Edelmann W, Chiu FC, Kucherlapati R and Raine CS (1998) Experimental autoimmune encephalomyelitis in mice lacking glial fibrillary acidic protein is characterized by a more severe clinical course and an infiltrative central nervous system lesion. *Am J Pathol* **152**:251-259.

Lin HL and Murphy S (1997) Regulation of astrocyte nitric oxide synthase type II expression by ATP and glutamate involves loss of transcription factor binding to DNA. *J Neurochem* **69**:612-616.

Lin LH, Taktakishvili O and Talman WT (2007a) Identification and localization of cell types that express endothelial and neuronal nitric oxide synthase in the rat nucleus tractus solitarii. *Brain Res* **1171**:42-51.

Lin YC, Kuo YM, Liao PC, Cherng CG, Su SW and Yu L (2007b) Attenuation of methamphetamine-induced nigrostriatal dopaminergic neurotoxicity in mice by lipopolysaccharide pretreatment. *Chin J Physiol* **50**:51-56.

Liu J, Zhao ML, Brosnan CF and Lee SC (1996) Expression of type II nitric oxide synthase in primary human astrocytes and microglia: role of IL-1beta and IL-1 receptor antagonist. *J Immunol* **157**:3569-3576.

Louin G, Marchand-Verrecchia C, Palmier B, Plotkine M and Jafarian-Tehrani M (2006) Selective inhibition of inducible nitric oxide synthase reduces neurological deficit but not cerebral edema following traumatic brain injury. *Neuropharmacology* **50**:182-190.

Lowenstein CJ, Alley EW, Raval P, Snowman AM, Snyder SH, Russell SW and Murphy WJ (1993) Macrophage nitric oxide synthase gene: two upstream regions mediate induction by interferon gamma and lipopolysaccharide. *Proc Natl Acad Sci U S A* **90**:9730-9734.

Makar TK, Nedergaard M, Preuss A, Gelbard AS, Perumal AS and Cooper AJ (1994) Vitamin E, ascorbate, glutathione, glutathione disulfide, and enzymes of glutathione metabolism in cultures of chick astrocytes and neurons: evidence that astrocytes play an important role in antioxidative processes in the brain. *J Neurochem* **62**:45-53.

Maragos WF, Young KL, Turchan JT, Guseva M, Pauly JR, Nath A and Cass WA (2002) Human immunodeficiency virus-1 Tat protein and methamphetamine interact synergistically to impair striatal dopaminergic function. *J Neurochem* **83**:955-963.

Mark KA, Soghomonian JJ and Yamamoto BK (2004) High-dose methamphetamine acutely activates the striatonigral pathway to increase striatal glutamate and mediate long-term dopamine toxicity. *J Neurosci* **24**:11449-11456.

McCann UD, Kuwabara H, Kumar A, Palermo M, Abbey R, Brasic J, Ye W, Alexander M, Dannals RF, Wong DF and Ricaurte GA (2008) Persistent cognitive and dopamine transporter deficits in abstinent methamphetamine users. *Synapse* **62**:91-100.

McKimmie CS and Fazakerley JK (2005) In response to pathogens, glial cells dynamically and differentially regulate Toll-like receptor gene expression. *J Neuroimmunol* **169**:116-125.

Min KJ, Yang MS, Kim SU, Jou I and Joe EH (2006) Astrocytes induce hemeoxygenase-1 expression in microglia: a feasible mechanism for preventing excessive brain inflammation. *J Neurosci* **26**:1880-1887.

Mirecki A, Fitzmaurice P, Ang L, Kalasinsky KS, Peretti FJ, Aiken SS, Wickham DJ, Sherwin A, Nobrega JN, Forman HJ and Kish SJ (2004) Brain antioxidant systems in human methamphetamine users. *J Neurochem* **89**:1396-1408.

Miyazaki I, Asanuma M, Hozumi H, Miyoshi K and Sogawa N (2007) Protective effects of metallothionein against dopamine quinone-induced dopaminergic neurotoxicity. *FEBS Lett* **581**:5003-5008.

Miyazaki I, Asanuma M, Kikkawa Y, Takeshima M, Murakami S, Miyoshi K, Sogawa N and Kita T (2011) Astrocyte-derived metallothionein protects dopaminergic neurons from dopamine quinone toxicity. *Glia* **59**:435-451.

Mohammadi MT, Shid-Moosavi SM and Dehghani GA (2012) Contribution of nitric oxide synthase (NOS) in blood-brain barrier disruption during acute focal cerebral ischemia in normal rat. *Pathophysiology* **19**:13-20.

Morimoto T, Ginsberg MD, Dietrich WD and Zhao W (1997) Hyperthermia enhances spectrin breakdown in transient focal cerebral ischemia. *Brain Res* **746**:43-51.

Morris BJ, Simpson CS, Mundell S, Maceachern K, Johnston HM and Nolan AM (1997) Dynamic changes in NADPH-diaphorase staining reflect activity of nitric oxide synthase: evidence for a dopaminergic regulation of striatal nitric oxide release. *Neuropharmacology* **36**:1589-1599.

Moss DW and Bates TE (2001) Activation of murine microglial cell lines by lipopolysaccharide and interferon-gamma causes NO-mediated decreases in mitochondrial and cellular function. *Eur J Neurosci* **13**:529-538.

Nash JF and Yamamoto BK (1992) Methamphetamine neurotoxicity and striatal glutamate release: comparison to 3,4-methylenedioxymethamphetamine. *Brain Res* **581**:237-243.

Neary JT, Kang Y, Willoughby KA and Ellis EF (2003) Activation of extracellular signal-regulated kinase by stretch-induced injury in astrocytes involves extracellular ATP and P2 purinergic receptors. *J Neurosci* **23**:2348-2356.

Neher JJ, Neniskyte U, Zhao JW, Bal-Price A, Tolkovsky AM and Brown GC (2011) Inhibition of microglial phagocytosis is sufficient to prevent inflammatory neuronal death. *J Immunol* **186**:4973-4983.

Nicholson LF, Faull RL, Waldvogel HJ and Dragunow M (1995) GABA and GABAA receptor changes in the substantia nigra of the rat following quinolinic acid lesions in the striatum closely resemble Huntington's disease. *Neuroscience* **66**:507-521.

Nimmerjahn A, Kirchhoff F and Helmchen F (2005) Resting microglial cells are highly dynamic surveillants of brain parenchyma in vivo. *Science* **308**:1314-1318.

Nishino N, Shirai Y, Kajimoto Y, Kitamura N, Yamamoto H, Yang CQ and Shirakawa O (1996) Increased glutamate transporter (GLT-1) immunoreactivity in the rat striatum after repeated intermittent administration of methamphetamine. *Ann N Y Acad Sci* **801**:310-314.

Noda M, Nakanishi H, Nabekura J and Akaike N (2000) AMPA-kainate subtypes of glutamate receptor in rat cerebral microglia. *J Neurosci* **20**:251-258.

O'Callaghan JP and Miller DB (1994) Neurotoxicity profiles of substituted amphetamines in the C57BL/6J mouse. *J Pharmacol Exp Ther* **270**:741-751.

O'Dell SJ, Weihmuller FB and Marshall JF (1991) Multiple methamphetamine injections induce marked increases in extracellular striatal dopamine which correlate with subsequent neurotoxicity. *Brain Res* **564**:256-260.

O'Dell SJ, Weihmuller FB and Marshall JF (1993) Methamphetamine-induced dopamine overflow and injury to striatal dopamine terminals: attenuation by dopamine D1 or D2 antagonists. *J Neurochem* **60**:1792-1799.

O'Dell TJ, Huang PL, Dawson TM, Dinerman JL, Snyder SH, Kandel ER and Fishman MC (1994) Endothelial NOS and the blockade of LTP by NOS inhibitors in mice lacking neuronal NOS. *Science* **265**:542-546.

Okada S, Nakamura M, Katoh H, Miyao T, Shimazaki T, Ishii K, Yamane J, Yoshimura A, Iwamoto Y, Toyama Y and Okano H (2006) Conditional ablation of Stat3 or Socs3 discloses a dual role for reactive astrocytes after spinal cord injury. *Nat Med* **12**:829-834.

Park C, Lee S, Cho IH, Lee HK, Kim D, Choi SY, Oh SB, Park K, Kim JS and Lee SJ (2006) TLR3-mediated signal induces proinflammatory cytokine and chemokine gene expression in astrocytes: differential signaling mechanisms of TLR3-induced IP-10 and IL-8 gene expression. *Glia* **53**:248-256.

Park DJ and West AR (2009) Regulation of striatal nitric oxide synthesis by local dopamine and glutamate interactions. *J Neurochem* **111**:1457-1465.

Park SK, Lin HL and Murphy S (1997) Nitric oxide regulates nitric oxide synthase-2 gene expression by inhibiting NF-kappaB binding to DNA. *Biochem J* **322 (Pt 2)**:609-613.

Pastuzyn ED, Chapman DE, Wilcox KS and Keefe KA (2012) Altered learning and Arc-regulated consolidation of learning in striatum by methamphetamine-induced neurotoxicity. *Neuropsychopharmacology* **37**:885-895.

Pike BR, Zhao X, Newcomb JK, Posmantur RM, Wang KK and Hayes RL (1998) Regional calpain and caspase-3 proteolysis of alpha-spectrin after traumatic brain injury. *Neuroreport* **9**:2437-2442.

Pu C and Vorhees CV (1993) Developmental dissociation of methamphetamine-induced depletion of dopaminergic terminals and astrocyte reaction in rat striatum. *Brain Res Dev Brain Res* **72**:325-328.

Radi R, Beckman JS, Bush KM and Freeman BA (1991) Peroxynitrite-induced membrane lipid peroxidation: the cytotoxic potential of superoxide and nitric oxide. *Arch Biochem Biophys* **288**:481-487.

Radi R, Rodriguez M, Castro L and Telleri R (1994) Inhibition of mitochondrial electron transport by peroxynitrite. *Arch Biochem Biophys* **308**:89-95.

Raps SP, Lai JC, Hertz L and Cooper AJ (1989) Glutathione is present in high concentrations in cultured astrocytes but not in cultured neurons. *Brain Res* **493**:398-401.

Riddle EL, Topham MK, Haycock JW, Hanson GR and Fleckenstein AE (2002) Differential trafficking of the vesicular monoamine transporter-2 by methamphetamine and cocaine. *Eur J Pharmacol* **449**:71-74.

Riobo NA, Clementi E, Melani M, Boveris A, Cadenas E, Moncada S and Poderoso JJ (2001) Nitric oxide inhibits mitochondrial NADH:ubiquinone reductase activity through peroxynitrite formation. *Biochem J* **359**:139-145.

Rivera A, Alberti I, Martin AB, Narvaez JA, de la Calle A and Moratalla R (2002) Molecular phenotype of rat striatal neurons expressing the dopamine D5 receptor subtype. *Eur J Neurosci* **16**:2049-2058.

Rossetti ZL and Crespi F (2004) Inhibition of nitric oxide release in vivo by ethanol. *Alcohol Clin Exp Res* **28**:1746-1751.

Rossi D, Brambilla L, Valori CF, Crugnola A, Giaccone G, Capobianco R, Mangieri M, Kingston AE, Bloc A, Bezzi P and Volterra A (2005) Defective tumor necrosis factor-alpha-dependent control of astrocyte glutamate release in a transgenic mouse model of Alzheimer disease. *J Biol Chem* **280**:42088-42096.

Rubbo H, Radi R, Trujillo M, Telleri R, Kalyanaraman B, Barnes S, Kirk M and Freeman BA (1994) Nitric oxide regulation of superoxide and peroxynitrite-dependent lipid peroxidation. Formation of novel nitrogen-containing oxidized lipid derivatives. *J Biol Chem* **269**:26066-26075.

Salgo MG, Bermudez E, Squadrito GL and Pryor WA (1995) Peroxynitrite causes DNA damage and oxidation of thiols in rat thymocytes [corrected]. *Arch Biochem Biophys* **322**:500-505.

SAMHSA/OSM (2011) Results from the 2010 National Survey on Drug Use and Health.

Sammut S, Dec A, Mitchell D, Linardakis J, Ortiguela M and West AR (2006) Phasic dopaminergic transmission increases NO efflux in the rat dorsal striatum via a neuronal NOS and a dopamine D(1/5) receptor-dependent mechanism. *Neuropsychopharmacology* **31**:493-505.

Sammut S, Park DJ and West AR (2007) Frontal cortical afferents facilitate striatal nitric oxide transmission in vivo via a NMDA receptor and neuronal NOS-dependent mechanism. *J Neurochem* **103**:1145-1156.

Sattler R, Xiong Z, Lu WY, Hafner M, MacDonald JF and Tymianski M (1999) Specific coupling of NMDA receptor activation to nitric oxide neurotoxicity by PSD-95 protein. *Science* **284**:1845-1848.

Sawada M, Kondo N, Suzumura A and Marunouchi T (1989) Production of tumor necrosis factor-alpha by microglia and astrocytes in culture. *Brain Res* **491**:394-397.

Seidel B, Stanarius A and Wolf G (1997) Differential expression of neuronal and endothelial nitric oxide synthase in blood vessels of the rat brain. *Neurosci Lett* **239**:109-112.

Sekine Y, Iyo M, Ouchi Y, Matsunaga T, Tsukada H, Okada H, Yoshikawa E, Futatsubashi M, Takei N and Mori N (2001) Methamphetamine-related psychiatric symptoms and reduced brain dopamine transporters studied with PET. *Am J Psychiatry* **158**:1206-1214.

Sekine Y, Ouchi Y, Sugihara G, Takei N, Yoshikawa E, Nakamura K, Iwata Y, Tsuchiya KJ, Suda S, Suzuki K, Kawai M, Takebayashi K, Yamamoto S, Matsuzaki H,

Ueki T, Mori N, Gold MS and Cadet JL (2008) Methamphetamine causes microglial activation in the brains of human abusers. *J Neurosci* **28**:5756-5761.

Serulle Y, Zhang S, Ninan I, Puzzo D, McCarthy M, Khatri L, Arancio O and Ziff EB (2007) A GluR1-cGKII interaction regulates AMPA receptor trafficking. *Neuron* **56**:670-688.

Shah A, Silverstein PS, Kumar S, Singh DP and Kumar A (2012a) Synergistic Cooperation between Methamphetamine and HIV-1 gsp120 through the P13K/Akt Pathway Induces IL-6 but not IL-8 Expression in Astrocytes. *PLoS One* **7**:e52060.

Shah A, Silverstein PS, Singh DP and Kumar A (2012b) Involvement of metabotropic glutamate receptor 5, AKT/PI3K signaling and NF-kappaB pathway in methamphetamine-mediated increase in IL-6 and IL-8 expression in astrocytes. *J Neuroinflammation* **9**:52.

Shigemoto-Mogami Y, Koizumi S, Tsuda M, Ohsawa K, Kohsaka S and Inoue K (2001) Mechanisms underlying extracellular ATP-evoked interleukin-6 release in mouse microglial cell line, MG-5. *J Neurochem* **78**:1339-1349.

Shih AY, Johnson DA, Wong G, Kraft AD, Jiang L, Erb H, Johnson JA and Murphy TH (2003) Coordinate regulation of glutathione biosynthesis and release by Nrf2-expressing glia potently protects neurons from oxidative stress. *J Neurosci* **23**:3394-3406.

Simard AR and Rivest S (2007) Neuroprotective effects of resident microglia following acute brain injury. *J Comp Neurol* **504**:716-729.

Simon SL, Domier C, Carnell J, Brethen P, Rawson R and Ling W (2000) Cognitive impairment in individuals currently using methamphetamine. *Am J Addict* **9**:222-231.

Smith WL, DeWitt DL and Garavito RM (2000) Cyclooxygenases: structural, cellular, and molecular biology. *Annu Rev Biochem* **69**:145-182.

Sofroniew MV (2009) Molecular dissection of reactive astrogliosis and glial scar formation. *Trends Neurosci* **32**:638-647.

Son H, Hawkins RD, Martin K, Kiebler M, Huang PL, Fishman MC and Kandel ER (1996) Long-term potentiation is reduced in mice that are doubly mutant in endothelial and neuronal nitric oxide synthase. *Cell* **87**:1015-1023.

Son JH, Latimer C and Keefe KA (2011) Impaired formation of stimulus-response, but not action-outcome, associations in rats with methamphetamine-induced neurotoxicity. *Neuropsychopharmacology* **36**:2441-2451.

Sonsalla PK, Nicklas WJ and Heikkila RE (1989) Role for excitatory amino acids in methamphetamine-induced nigrostriatal dopaminergic toxicity. *Science* **243**:398-400.

Sriram K, Miller DB and O'Callaghan JP (2006) Minocycline attenuates microglial activation but fails to mitigate striatal dopaminergic neurotoxicity: role of tumor necrosis factor-alpha. *J Neurochem* **96**:706-718.

Stadlin A, Lau JW and Szeto YK (1998) A selective regional response of cultured astrocytes to methamphetamine. *Ann N Y Acad Sci* **844**:108-121.

Stanarius A, Topel I, Schulz S, Noack H and Wolf G (1997) Immunocytochemistry of endothelial nitric oxide synthase in the rat brain: a light and electron microscopical study using the tyramide signal amplification technique. *Acta Histochem* **99**:411-429.

Staszewski RD and Yamamoto BK (2006) Methamphetamine-induced spectrin proteolysis in the rat striatum. *J Neurochem* **96**:1267-1276.

Stephans SE and Yamamoto BK (1994) Methamphetamine-induced neurotoxicity: roles for glutamate and dopamine efflux. *Synapse* **17**:203-209.

Stone JR and Marletta MA (1996) Spectral and kinetic studies on the activation of soluble guanylate cyclase by nitric oxide. *Biochemistry* **35**:1093-1099.

Sultana R, Poon HF, Cai J, Pierce WM, Merchant M, Klein JB, Markesbery WR and Butterfield DA (2006) Identification of nitrated proteins in Alzheimer's disease brain using a redox proteomics approach. *Neurobiol Dis* **22**:76-87.

Suzuki K, Imajoh S, Emori Y, Kawasaki H, Minami Y and Ohno S (1987) Calcium-activated neutral protease and its endogenous inhibitor. Activation at the cell membrane and biological function. *FEBS Lett* **220**:271-277.

Taraska T and Finnegan KT (1997) Nitric oxide and the neurotoxic effects of methamphetamine and 3,4-methylenedioxymethamphetamine. *J Pharmacol Exp Ther* **280**:941-947.

Tata DA and Yamamoto BK (2008) Chronic stress enhances methamphetamine-induced extracellular glutamate and excitotoxicity in the rat striatum. *Synapse* **62**:325-336.

Thomas DM, Francescutti-Verbeem DM and Kuhn DM (2008a) Methamphetamine-induced neurotoxicity and microglial activation are not mediated by fractalkine receptor signaling. *J Neurochem* **106**:696-705.

Thomas DM, Francescutti-Verbeem DM and Kuhn DM (2008b) The newly synthesized pool of dopamine determines the severity of methamphetamine-induced neurotoxicity. *J Neurochem* **105**:605-616.

Thomas DM and Kuhn DM (2005a) Attenuated microglial activation mediates tolerance to the neurotoxic effects of methamphetamine. *J Neurochem* **92**:790-797.

Thomas DM and Kuhn DM (2005b) Cyclooxygenase-2 is an obligatory factor in methamphetamine-induced neurotoxicity. *J Pharmacol Exp Ther* **313**:870-876.

Thomas DM and Kuhn DM (2005c) MK-801 and dextromethorphan block microglial activation and protect against methamphetamine-induced neurotoxicity. *Brain Res* **1050**:190-198.

Thomas DM, Walker PD, Benjamins JA, Geddes TJ and Kuhn DM (2004) Methamphetamine neurotoxicity in dopamine nerve endings of the striatum is associated with microglial activation. *J Pharmacol Exp Ther* **311**:1-7.

Timmerman W and Westerink BH (1997) Electrical stimulation of the substantia nigra reticulata: detection of neuronal extracellular GABA in the ventromedial thalamus and its regulatory mechanism using microdialysis in awake rats. *Synapse* **26**:62-71.

Tocharus J, Khonthun C, Chongthammakun S and Govitrapong P (2010) Melatonin attenuates methamphetamine-induced overexpression of pro-inflammatory cytokines in microglial cell lines. *J Pineal Res* **48**:347-352.

Tse DC, McCreery RL and Adams RN (1976) Potential oxidative pathways of brain catecholamines. *J Med Chem* **19**:37-40.

Volkow ND, Chang L, Wang GJ, Fowler JS, Franceschi D, Sedler M, Gatley SJ, Miller E, Hitzemann R, Ding YS and Logan J (2001a) Loss of dopamine transporters in methamphetamine abusers recovers with protracted abstinence. *J Neurosci* **21**:9414-9418.

Volkow ND, Chang L, Wang GJ, Fowler JS, Leonido-Yee M, Franceschi D, Sedler MJ, Gatley SJ, Hitzemann R, Ding YS, Logan J, Wong C and Miller EN (2001b) Association of dopamine transporter reduction with psychomotor impairment in methamphetamine abusers. *Am J Psychiatry* **158**:377-382.

Wagner GC, Carelli RM and Jarvis MF (1986) Ascorbic acid reduces the dopamine depletion induced by methamphetamine and the 1-methyl-4-phenyl pyridinium ion. *Neuropharmacology* **25**:559-561.

Wagner GC, Ricaurte GA, Seiden LS, Schuster CR, Miller RJ and Westley J (1980) Long-lasting depletions of striatal dopamine and loss of dopamine uptake sites following repeated administration of methamphetamine. *Brain Res* **181**:151-160.

Walz W, Ilschner S, Ohlemeyer C, Banati R and Kettenmann H (1993) Extracellular ATP activates a cation conductance and a K+ conductance in cultured microglial cells from mouse brain. *J Neurosci* **13**:4403-4411.

Wang HG, Lu FM, Jin I, Udo H, Kandel ER, de Vente J, Walter U, Lohmann SM, Hawkins RD and Antonova I (2005) Presynaptic and postsynaptic roles of NO, cGK, and RhoA in long-lasting potentiation and aggregation of synaptic proteins. *Neuron* **45**:389-403.

Wang J and Angulo JA (2011) Synergism between methamphetamine and the neuropeptide substance P on the production of nitric oxide in the striatum of mice. *Brain Res* **1369**:131-139.

Wang J, Xu W, Ali SF and Angulo JA (2008) Connection between the striatal neurokinin-1 receptor and nitric oxide formation during methamphetamine exposure. *Ann N Y Acad Sci* **1139**:164-171.

West AR and Grace AA (2004) The nitric oxide-guanylyl cyclase signaling pathway modulates membrane activity States and electrophysiological properties of striatal medium spiny neurons recorded in vivo. *J Neurosci* **24**:1924-1935.

Wilhelmsson U, Li L, Pekna M, Berthold CH, Blom S, Eliasson C, Renner O, Bushong E, Ellisman M, Morgan TE and Pekny M (2004) Absence of glial fibrillary acidic protein and vimentin prevents hypertrophy of astrocytic processes and improves post-traumatic regeneration. *J Neurosci* **24**:5016-5021.

Wilson JM, Kalasinsky KS, Levey AI, Bergeron C, Reiber G, Anthony RM, Schmunk GA, Shannak K, Haycock JW and Kish SJ (1996) Striatal dopamine nerve terminal markers in human, chronic methamphetamine users. *Nat Med* **2**:699-703.

Xie QW, Whisnant R and Nathan C (1993) Promoter of the mouse gene encoding calcium-independent nitric oxide synthase confers inducibility by interferon gamma and bacterial lipopolysaccharide. *J Exp Med* **177**:1779-1784.

Yamamoto BK and Zhu W (1998) The effects of methamphetamine on the production of free radicals and oxidative stress. *J Pharmacol Exp Ther* **287**:107-114.

Yeh TH, Lee da Y, Gianino SM and Gutmann DH (2009) Microarray analyses reveal regional astrocyte heterogeneity with implications for neurofibromatosis type 1 (NF1)-regulated glial proliferation. *Glia* **57**:1239-1249.

Yermilov V, Rubio J and Ohshima H (1995) Formation of 8-nitroguanine in DNA treated with peroxynitrite in vitro and its rapid removal from DNA by depurination. *FEBS Lett* **376**:207-210.

Yermilov V, Yoshie Y, Rubio J and Ohshima H (1996) Effects of carbon dioxide/bicarbonate on induction of DNA single-strand breaks and formation of 8-nitroguanine, 8-oxoguanine and base-propenal mediated by peroxynitrite. *FEBS Lett* **399**:67-70.

Yui Y, Hattori R, Kosuga K, Eizawa H, Hiki K and Kawai C (1991) Purification of nitric oxide synthase from rat macrophages. *J Biol Chem* **266**:12544-12547.

Zhang X, Dong F, Mayer GE, Bruch DC, Ren J and Culver B (2007) Selective inhibition of cyclooxygenase-2 exacerbates methamphetamine-induced dopamine depletion in the striatum in rats. *Neuroscience* **150**:950-958.

Zhao ML, Kim MO, Morgello S and Lee SC (2001) Expression of inducible nitric oxide synthase, interleukin-1 and caspase-1 in HIV-1 encephalitis. *J Neuroimmunol* **115**:182-191.

Zhu JP, Xu W and Angulo JA (2006) Distinct mechanisms mediating methamphetamine-induced neuronal apoptosis and dopamine terminal damage share the neuropeptide substance p in the striatum of mice. *Ann N Y Acad Sci* **1074**:135-148.

CHAPTER 2

EXPRESSION AND ACTIVITY OF NITRIC OXIDE SYNTHASE ISOFROMS IN METHAMHETAMINE-INDUCED STRIATAL DOPAMINE TOXICITY

Reprinted with permission from The Journal of Pharmacology and Experimental Therapeutics

1521-0103/344/2/511–521$25.00
THE JOURNAL OF PHARMACOLOGY AND EXPERIMENTAL THERAPEUTICS

http://dx.doi.org/10.1124/jpet.112.199745
J Pharmacol Exp Ther 344:511–521, February 2013

JPET
PHARMACOLOGY AND EXPERIMENTAL THERAPEUTICS
aspet

Expression and Activity of Nitric Oxide Synthase Isoforms in Methamphetamine-Induced Striatal Dopamine Toxicity

Danielle M. Friend, Jong H. Son, Kristen A. Keefe, and Ashley N. Fricks-Gleason

Interdepartmental Program in Neuroscience (D.M.F., K.A.K.) and Department of Pharmacology and Toxicology (J.H.S., K.A.K., A.N.F.), University of Utah, Salt Lake City, Utah

Received September 7, 2012; accepted December 7, 2012

ABSTRACT

Nitric oxide is implicated in methamphetamine (METH)-induced neurotoxicity; however, the source of the nitric oxide has not been identified. Previous work has also revealed that animals with partial dopamine loss induced by a neurotoxic regimen of methamphetamine fail to exhibit further decreases in striatal dopamine when re-exposed to methamphetamine 7–30 days later. The current study examined nitric oxide synthase expression and activity and protein nitration in striata of animals administered saline or neurotoxic regimens of methamphetamine at postnatal days 60 and/or 90, resulting in four treatment groups: Saline:Saline, METH:Saline, Saline:METH, and METH:METH. Acute administration of methamphetamine on postnatal day 90 (Saline:METH and METH:METH) increased nitric oxide production, as evidenced by increased protein nitration. Methamphetamine did not, however, change the expression of endothelial or inducible isoforms of nitric oxide synthase, nor did it change the number of cells positive for neuronal nitric oxide synthase mRNA expression or the amount of neuronal nitric oxide synthase mRNA per cell. However, nitric oxide synthase activity in striatal interneurons was increased in the Saline:METH and METH:METH animals. These data suggest that increased nitric oxide production after a neurotoxic regimen of methamphetamine results from increased nitric oxide synthase activity, rather than an induction of mRNA, and that constitutively expressed neuronal nitric oxide synthase is the most likely source of nitric oxide after methamphetamine administration. Of interest, animals rendered resistant to further methamphetamine-induced dopamine depletions still show equivalent degrees of methamphetamine-induced nitric oxide production, suggesting that nitric oxide production alone in response to methamphetamine is not sufficient to induce acute neurotoxic injury.

Introduction

It is estimated that 60 million people worldwide have abused amphetamine-type psychostimulants, including methamphetamine (METH; Maxwell, 2005). METH abuse results in selective damage to central monoamine systems. In particular, repeated high-dose administration of METH results in persistent dopamine (DA) deficits in rodents, nonhuman primates, and humans. These DA deficits are manifested as decreases in DA concentration (Kogan et al., 1976; Wagner et al., 1980), DA transporter (DAT; Volkow et al., 2001; Guilarte et al., 2003) and vesicular monoamine transporter-2 levels (Guilarte et al., 2003), and tyrosine hydroxylase activity (Kogan et al., 1976), particularly in striatum. The exact mechanisms contributing to this phenomenon have yet to be fully elucidated; however, a number of factors occurring during or shortly after administration of a neurotoxic regimen of METH, including the production of nitric oxide (NO), have been implicated in this toxicity.

NO production is involved in a variety of normal physiologic process and various pathologic conditions. NO is produced by nitric oxide synthase (NOS), of which there are three isoforms: neuronal nitric oxide synthase (nNOS), inducible nitric oxide synthase (iNOS), and endothelial nitric oxide synthase (eNOS). The work of several groups has suggested an important role for NO in METH-induced monoamine system damage. First, NO can interact with oxygen to form peroxynitrite, a potent oxidant (Radi et al., 1991). Second, prior studies have suggested that nNOS protein (Deng and Cadet, 1999), nitrate (Anderson and Itzhak, 2006), and protein nitration—an indirect measure of peroxynitrite

This work was supported by the National Institutes of Health National Institute on Drug Abuse [Grants DA 013367 and DA 031523].

Portions of this work were previously presented at the following meetings: Friend DM, Keefe KA, Chen P (2009) nNOS & iNOS expression in resistance to methamphetamine neurotoxicity. *The Society for Neuroscience*; 2009 Oct 17-21; Chicago, IL. Friend DM, Fricks-Gleason AN, Chen P, Keefe KA (2010) Expression of NOS isoforms in methamphetamine-induced striatal dopamine toxicity. *International Basal Ganglia Society*; 2010 June 20-24; Long Branch, NJ. Friend DM, Fricks-Gleason AN, Chen P, Hanson GR, Keefe KA (2010) Expression of NOS isoforms in methamphetamine-induced striatal dopamine toxicity. *Translational Research in Methamphetamine Addiction*; 2010 Jul 19-21; Pray, MT. Friend DM, Fricks-Gleason AN, Keefe KA (2010) Expression of NOS isoforms in methamphetamine-induced striatal dopamine neurotoxicity. *The Society for Neuroscience*; 2010 Nov 13-17; San Diego, CA. Friend DM, Fricks-Gleason AN, Keefe, KA (2010) NOS isoform expression and activity in methamphetamine-induced striatal dopamine toxicity. *Gordon Research Conference on Catecholamines*; 2010 Aug 6-12; Lewiston, ME. Friend DM, Fricks-Gleason AN, Keefe, KA (2011) Nitric oxide synthase isoform expression and activity in methamphetamine-induced striatal neurotoxicity. *Winter Conference on Brain Research*; 2011 Jan 21-26; Snowbird, UT.

dx.doi.org/10.1124/jpet.112.199745.

ABBREVIATIONS: ANOVA, analysis of variance; DA, dopamine; DAT, dopamine transporter; eNOS, endothelial nitric oxide synthase; GLU, glutamate; iNOS, inducible nitric oxide synthase; MANOVA, multivariate ANOVA; METH, methamphetamine; NMDA, *N*-methyl-D-aspartate; NO, nitric oxide; NOS, nitric oxide synthase; nNOS, neuronal nitric oxide synthase; PBS, phosphate-buffered saline; PND, postnatal day.

production (Imam et al., 1999; Imam et al., 2000)—are increased in striatum after METH exposure. Third, coadministration of peroxynitrite decomposition catalysts prevents METH-induced DA depletions (Imam et al., 1999). Fourth, METH-induced DA depletions are blocked in mice with deletion of nNOS (Itzhak et al., 1998; Itzhak et al., 2000b) and partially attenuated in mice with deletion of iNOS (Itzhak et al., 1999; Itzhak et al., 2000b). However, the use of peroxynitrite decomposition catalysts and nNOS and iNOS knockout mice also mitigated METH-induced hyperthermia (Itzhak et al., 1998; Imam et al., 1999; Itzhak et al., 1999) known to be critical for METH-induced monoamine toxicity (Ali et al., 1994). In addition, studies using pharmacological inhibitors of NOS are similarly inconclusive. Some studies suggest protection against METH-induced DA depletions when NOS inhibitors are coadministered (Di Monte et al., 1996; Itzhak and Ali, 1996; Ali and Itzhak, 1998; Itzhak et al., 2000a), whereas others suggest that the neuroprotective effects of NOS inhibitors result from mitigation of METH-induced hyperthermia (Taraska and Finnegan, 1997; Callahan and Ricaurte, 1998). Adding to the debate on the role of NO production in METH-induced neurotoxicity are data demonstrating that the elimination of nNOS-expressing cells in striatum fails to protect against METH-induced tyrosine hydroxylase depletions (Zhu et al., 2006).

To further explore factors sufficient for METH-induced monoamine toxicity, we have used a model of resistance to this toxicity, in which animals are treated with a binge regimen of METH but do not show acute monoamine toxicity. That is, our laboratory and others have conducted studies in which animals are treated with a neurotoxic regimen of METH and are challenged seven or 30 days later with a second neurotoxic regimen of METH. The data from these studies show that animals with partial DA loss induced by an initial exposure to a neurotoxic regimen of METH fail to exhibit further DA, DAT, and vesicular monoamine transporter-2 depletions when exposed to the second neurotoxic regimen (Thomas and Kuhn, 2005; Hanson et al., 2009). The extent to which this resistance to subsequent METH-induced neurotoxicity is associated with decreased NO production is unknown. Thus, the purpose of the current study was to determine the source of NO after METH exposure and to examine whether animals rendered resistant to further METH-induced DA depletions have decreases in NO production.

Materials and Methods

Animals. Male Sprague-Dawley rats (Charles River Laboratories, Raleigh, NC) were housed in wire mesh cages in a temperature-controlled room on a 12:12-hour light/dark cycle with free access to food and water. All animal care and experimental procedures were in accordance with the *Guide for the Care and Use of Laboratory Animals* (8th Ed., National Research Council) and were approved by the Institutional Animal Care and Use Committee at the University of Utah.

METH Administration. On days of METH injections (postnatal days [PNDs] 60 and 90), rats were housed in groups of four in plastic tub cages (33 cm × 28 cm × 17 cm) with corncob bedding. Rats were given injections of (±)-METH•HCl (National Institutes of Health National Institute on Drug Abuse, Bethesda, MD; 10 mg/kg, free base, subcutaneous) or 0.9% saline (1 ml/kg, subcutaneous) at 2-hour intervals for a total of four injections. This METH dosing regimen has previously been shown to significantly reduce DA levels and tyrosine hydroxylase activity in the striatum (Kogan et al., 1976). To monitor METH-induced hyperthermia, rectal temperatures were recorded using a digital thermometer (BAT-12; Physitemp Instruments, Clifton, NJ). Temperatures were taken 30 minutes before the first injection of saline or METH and 1 hour after each injection thereafter. Animals whose core temperature exceeded 40.5°C were cooled by placement in a cool chamber until their core temperature decreased below 39°C. Eighteen hours after the last injection of METH or saline on PND60, animals were returned to their home cages and allowed to recover for 30 days. On PND90, animals were again housed in plastic tub cages as described above and injected with either saline or the neurotoxic regimen of METH, similar to PND60 treatments. This experimental protocol resulted in four treatment groups based on treatments on PND60 and PND90 (PND60:PND90): Saline:Saline, Saline:METH, METH:Saline, and METH:METH. Animals were sacrificed 1 hour or 48 hours after their last injection on PND90.

Tissue Preparation. Rats were sacrificed by exposure to carbon dioxide for 1 minute, followed by decapitation. To perform both in situ hybridization histochemistry for the NOS isoforms and histochemistry for NOS activity and immunohistochemistry for protein nitration, brains were rapidly removed and hemisected. One hemisphere was immediately frozen in 2-methylbutane chilled on dry ice and stored at −80°C. The other hemisphere was submerged in 4% formaldehyde with 0.9% sodium chloride for 24 hours at 4°C, then cryoprotected in 30% sucrose in 0.1 M phosphate-buffered saline (PBS) and stored at 4°C. The fresh-frozen hemispheres were cut into 12-μm thick sections on a cryostat (Cryocut 1800; Cambridge Instruments, Bayreuth, Germany). These striatal sections (Bregma: +1.6 mm to +0.2 mm) were thaw-mounted on slides and stored at −20°C. Slides from all animals to be used for a particular in situ hybridization histochemical analysis were then postfixed in 4% formaldehyde/0.9% sodium chloride, acetylated in 0.25% acetic anhydride in 0.1 M triethanolamine/0.9% sodium chloride (pH, 8), dehydrated in alcohol, delipidated in chloroform, and rehydrated in a descending series of alcohol concentrations. Slides were air-dried and stored at −20°C until further processing. The fixed hemispheres were cut into 30-μm thick sections on a freezing microtome (Microm, HM 440E). These sections of striatum (Bregma: +1.6 mm to +0.2 mm) were stored at 4°C in 1 mg/ml sodium azide in 0.1 M PBS.

DAT Autoradiography. DAT levels in striatum were determined by [^{125}I]RTI-55 (PerkinElmer, Waltham, MA) binding, as previously described (Pastuzyn et al., 2012). Slides were apposed to film (Biomax MR; Eastman Kodak, Rochester, NY) for 24 hours and developed. Film autoradiograms were analyzed using NIH ImageJ (http://imagej.nih.gov/ij/) to yield mean background-subtracted gray values in the dorsomedial and dorsolateral striatum. Two rostral and two middle striatal sections were analyzed per rat and averaged. Mean gray values were then converted to percentage of control (Saline:Saline).

Nitrotyrosine Immunohistochemistry. Tissue sections from the fixed hemispheres were processed for nitrotyrosine immunohistochemistry. The sections were washed in 0.1 M PBS, incubated for 10 minutes in 0.1 M PBS with 3% hydrogen peroxide to block endogenous peroxidases, and washed again in 0.1 M PBS. The tissue was blocked with 0.1 M PBS containing 10% normal horse serum for 1 hour, then incubated overnight at 4°C with 5% normal horse serum and anti-nitrotyrosine mouse monoclonal antibody (1:100, Abcam, ab78163). The following day, sections were washed in 0.1 M PBS and incubated for 1 hour at room temperature with 5% normal horse serum and biotinylated horse anti-mouse IgG (1:200, Vector Laboratories, Burlingame, CA; BA-2001). Sections were then rinsed and incubated with avidin-biotinylated peroxidase complex (ABC Elite kit; Vector, PK-6100) for 1 hour at room temperature. The reaction was terminated by rinsing sections three times in 0.1 M PBS. The tissue was then incubated in nickel-enhanced diaminobenzidine tetrahydrochloride (Ni-DAB, Vector, SK-4100) for 3–5 minutes, washed again in 0.1 M PBS, mounted onto slides, dried, dehydrated, and coverslipped.

Images were digitized and densitometric analysis was performed with ImageJ, yielding mean gray values. Two rostral and two middle

striatal sections were analyzed per rat, and the values were averaged. Mean gray values were then compared among treatment groups.

nNOS, iNOS, and eNOS In Situ Hybridization Histochemistry. Full-length rat nNOS and iNOS cDNAs were generously provided by Dr. Michael Marletta (University of California Berkeley). Polymerase chain reaction amplification with forward and reverse primers containing T7 and SP6 promoter sequences were used to amplify the nNOS and iNOS cDNAs (nNOS antisense: 5′-AATACGACTCACTATAGGGCAGTTCATCATGTTCCCCGAT-3′; nNOS sense: 5′-ATTTAGGTGACACTATAGATGGAAGAGAACACGTTTGGGGT-3′; iNOS antisense: 5′-TAATACGACTCACTATAGGGACAATCCACAACTCGCTCCAA-3′; and iNOS sense 5′-ATTTAGGTGACACTATAGGTTCAGCTACGCCTTCAACACCA-3′). Ribonucleotide probes were then synthesized from the amplified cDNAs using T7 (antisense) or SP6 (sense) RNA polymerases (Roche Applied Science, Indianapolis, IN) and [^{35}S]-UTP (PerkinElmer Life and Analytical Sciences, Boston, MA). Full-length, rat eNOS cDNA in a pCMV-Sport6 vector was purchased from Origene (RN200806; Rockville, MD), transformed into *Escherichia coli* cells for amplification, and extracted using a DNA extraction kit (Qiagen, Valencia, CA). eNOS cDNA was then linearized with NcoI and transcribed with T7 (sense) and SP6 (antisense) RNA polymerases and [^{33}P]-UTP. For all in situ hybridizations, probes were prepared and added to hybridization buffer to a final concentration of 1×10^6 cpm/μl, as previously described (Keefe and Gerfen, 1996). Hybridization buffer (100 μl) with probe was applied to each slide containing four brain sections, each slide was covered with a glass coverslip, and slides were hybridized overnight in humid chambers at 55°C. The following day, slides were washed four times in 2 × saline-sodium citrate (0.15 M sodium chloride with 0.015 M sodium citrate), treated with Ribonuclease-A (5 mg/ml; Roche Applied Science) in 2 × SSC for 15 minutes at room temperature, washed again in 2 × SSC, dried, and apposed to X-ray film (Biomax MR; Eastman Kodak) for approximately 1 week.

Film autoradiograms were digitized and analyzed using ImageJ. The images of sections from all groups in an experiment that were processed and hybridized together were captured and measured under constant lighting and camera conditions. nNOS mRNA expression, which was punctate because of its expression in striatal interneurons (Kawaguchi et al., 1995), was quantified by counting the number of cells labeled for nNOS mRNA. To this end, images were thresholded to include cell bodies of nNOS-positive cells. The mean signal density per labeled cell was also measured from the thresholded images. For iNOS and eNOS mRNA expression, both of which were more diffuse, the mean gray value of the dorsal striatum was measured, and the mean gray value of the corpus callosum overlying the striatum was subtracted for background correction. Two rostral and two middle striatal sections were analyzed per rat and averaged.

The specificity of our iNOS probe was confirmed by examining the induction of iNOS mRNA in the brain of an animal infected with Theiler's murine virus, because previous studies have demonstrated an induction of iNOS in these animals (Oleszak et al., 1997; Iwahashi et al., 1999). As shown in Fig. 1A, hybridization of a brain section from this animal with the antisense ribonucleotide against iNOS revealed iNOS induction in the area of the intrahemispheric injection of the virus. Alternatively, hybridization of an adjacent brain section from the same animal with the sense ribonucleotide probe did not yield any staining (Fig. 1B). We also evaluated the specificity of our eNOS ribonucleotide probe. As shown in Fig. 1C, hybridization with the antisense ribonucleotide probe revealed expression in the pyramidal cell layer of the hippocampus, consistent with prior reports (Dinerman et al., 1994; Vaid et al., 1996; Doyle and Slater, 1997). In addition, hybridization of an adjacent brain section with the sense ribonucleotide probe again yielded no signal (Fig. 1D). Finally, the specificity of the nNOS antisense ribonucleotide probe used was based on the correspondence between the staining obtained in the present study and previous findings from our laboratory and others that showed the distribution of the nNOS/somatostatin/neuropeptide Y-containing interneuron population in striatum (Uhl and Sasek, 1986; Rushlow et al., 1995; Horner et al., 2006). Thus, the antisense ribonucleotide probes generated for this study appear to specifically label NOS isoform mRNAs in the brain.

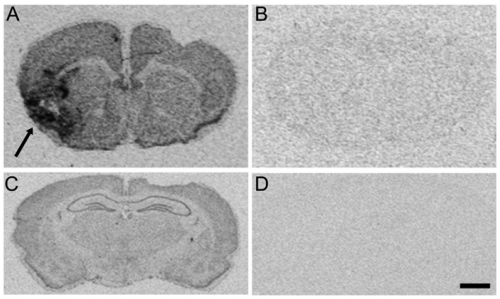

Fig. 1. Controls for iNOS and eNOS in situ hybridization histochemistry. (A) Positive control image of a striatal section from a mouse with Theiler's murine virus (TMV) infection in the brain (indicated by the arrow) showing detection of iNOS mRNA induction using the antisense ribonucleotide probe described in this article. (B) Negative control image showing a lack of signal in a brain section from the same TMV-infected mouse hybridized with the sense ribonucleotide probe. (C) Positive control image of a rat brain section at the level of the dorsal hippocampus hybridized with the antisense ribonucleotide probe against eNOS mRNA used in the present study. (D) Control image of a rat brain section at the level of the dorsal hippocampus hybridized with the sense ribonucleotide probe against eNOS mRNA used in the present study. Scale bar = 2 mm, applies to all panels.

NADPH Diaphorase Histochemical Staining. Tissue sections from the fixed hemispheres were processed for NADPH diaphorase histochemical staining to assess NOS activity (Hope et al., 1991). Tissue was washed in 0.1 M Tris-HCL (pH, 8.0), followed by preincubation in 0.1 M Tris-HCl containing 0.04% Tween-80 and 0.05% TritonX-100. The tissue was then incubated in Tris-HCl containing 0.8 mg/ml NADP, 0.16 mg/ml NBT, 0.04% Tween-80, 0.05% TritonX-100, 1 mM $MgCl_2$, and 15 mM malate for 2 hours at 37°C. Sections were then rinsed in 0.1 M Tris-HCL for 5 minutes, mounted onto slides, dried, and coverslipped. Digitized images of the NADPH diaphorase histochemical staining were captured under bright field conditions with a 40× objective with use of a Leica DM 4000B microscope. A 3 × 3 montage (0.63 mm^2) centered over dorsal striatum was captured from one hemisphere per section, resulting in four images per animal. The images were analyzed using ImageJ. Each image was thresholded such that the minimum threshold value in ImageJ was set to zero and the maximum threshold value was set to 16 points above the lowest edge of the threshold histogram. Blood vessels with NADPH diaphorase histochemical staining (indicative of eNOS activity) were excluded. The percentage area of the total remaining field with signal was measured and averaged across the four sections for each animal. This standardized image analysis allowed for the measurement of NADPH diaphorase-positive cell bodies and processes and excluded NADPH-diaphorase histochemical staining associated with endothelial cells. In addition, the number of cell bodies positive for NADPH diaphorase histochemical staining per image was recorded, averaged across the four sections for each animal, and then compared among treatment groups.

Statistical Analysis. All image analysis was conducted by an experimenter blinded to the treatment groups. Statistical analysis was performed using a two-factor analysis of variance [analysis of variance (ANOVA); PND60 treatment × PND90 treatment], followed by post hoc analysis via Student's *t* or Tukey HSD test, as appropriate. Statistical analysis of body temperature data was conducted using a multivariate ANOVA (MANOVA) with repeated measures (PND60 treatment × PND90 treatment × time), followed by post hoc analysis via *t* tests at individual time points to assess main effects of

treatments, as appropriate. No differences between dorsolateral and dorsomedial striatum were observed for the DAT binding, iNOS and eNOS mRNA expression, or nitrotyrosine staining; thus, values were averaged across these two regions for each striatal section.

Results

METH-Induced Hyperthermia in Rats Sacrificed 1 Hour After the Final Treatment on PND90. For the body temperature data collected during treatment of this cohort of animals on PND60 (Fig. 2A), MANOVA revealed a main effect of PND60 treatment ($F_{(1,33)}$=169.5, $P < 0.0001$) and time ($F_{(4,30)}$=49.5, $P < 0.0001$). There was also a significant PND60 treatment × time interaction ($F_{(4,30)}$=53.5, $P < 0.001$). Post hoc analysis revealed that the temperatures of animals receiving METH were significantly greater than those of controls at all four time points after the injections of METH began (60 minutes, t=16.3, $P < 0.0001$; 180 minutes, t=15.5, $P < 0.0001$; 300 minutes, t=9.4, $P < 0.0001$; 420 minutes, t=9.7, $P < 0.0001$), but were not different from controls at baseline (t=1.6, $P = 0.1$).

For the body temperature data collected during treatment of this cohort of animals on PND90 (Fig. 2B), MANOVA revealed a main effect of PND90 treatment ($F_{(1,31)}$=343.3, $P < 0.0001$), a main effect of time ($F_{(3,29)}$=33.9, $P < 0.0001$), and significant PND60 treatment × time ($F_{(3,29)}$=5.2, $P = 0.005$) and PND90 treatment × time ($F_{(3,29)}$=51.4, $P < 0.0001$) interactions. Post hoc analysis of the PND60 × time interaction revealed that, at baseline on PND90, the rats treated with METH at PND60 had statistically higher body temperatures than did rats treated with saline on PND60 (t=4.1, $P = 0.0002$). However, the body temperatures at the

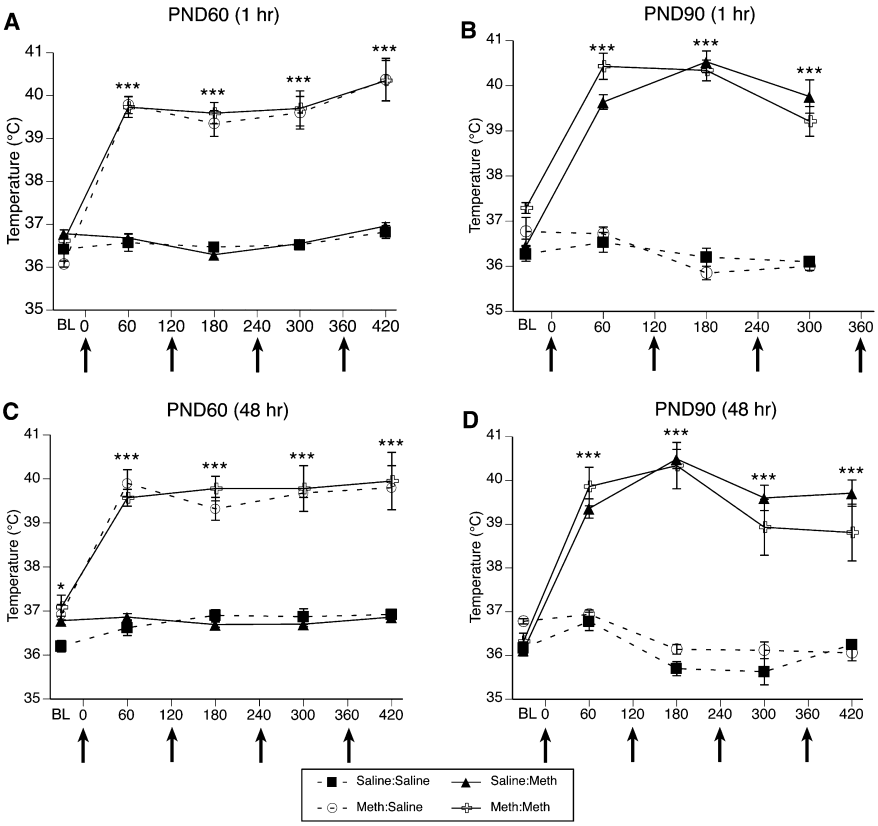

Fig. 2. Core body temperatures (mean ± S.E.M.; n = 5–12) of animals that received systemic injections of saline (4 × 1 mL/kg, subcutaneous at 2-hour intervals) or METH (4 × 10 mg/kg, subcutaneous at 2-hour intervals). Treatment group designations in the legend indicate PND60 treatment:PND90 treatment, resulting in the four treatment groups. Rectal temperatures were obtained 30 minutes before the first injection [baseline (BL)] and 1 hour after each subsequent injection. *X*-axis values represent minutes after the first injection, and arrows represent the time of each saline or METH injection. (A and C) Temperatures recorded during treatment on PND60 of animals sacrificed 1 hour (A) or 48 hours (C) after the last injection on PND90. (B and D) Temperatures recorded during treatment on PND90 of animals sacrificed 1 hour (B) or 48 hours (D) after the last injection on PND90. *$P < 0.05$; ***$P < 0.001$ indicate that groups receiving METH were significantly hyperthermic, relative to groups receiving saline.

other time points recorded on PND90 were not different between the rats treated with METH versus saline at PND60 (60 minutes, t=1.1, P = 0.3; 180 minutes, t=0.2, P = 0.8; 300 minutes, t=0.5, P = 0.6). Post hoc analysis of the PND90 treatment × time interaction again revealed that the temperatures of animals acutely receiving METH (i.e., PND90 treatment) were significantly higher than those of controls at all time points after the administration of METH began (60 minutes, t=12.3, $P < 0.0001$; 180 minutes, t=17.9, $P < 0.0001$; 300 minutes, t=9.7, $P < 0.0001$), but were not different from controls at baseline (t=1.7, P = 0.1). Of importance, there was no significant PND60 treatment × PND90 treatment interaction ($F_{(1,31)}$=0.3, P = 0.6) or PND60 treatment × PND90 treatment × time interactions ($F_{(3,29)}$=0.6, P = 0.6), indicating that the pretreatment on PND60 did not impact METH-induced hyperthermia on PND90.

METH-Induced Hyperthermia in Rats Sacrificed 48 Hours After the Final Treatment on PND90. For the body temperature data collected during treatment of this cohort of animals on PND60 (Fig. 2C), MANOVA revealed a main effect of PND60 treatment ($F_{(1,26)}$=213, $P < 0.0001$), a main effect of time ($F_{(4,23)}$=52.8, $P < 0.0001$), and a significant PND60 treatment × time interaction ($F_{(4,23)}$=33.8, $P < 0.0001$). Post hoc analysis revealed that the body temperatures of the rats given METH at PND60 were significantly greater than the temperatures of the controls at all time points (baseline, t=2.5, P = 0.02; 60 minutes, t=15.9, $P < 0.0001$; 180 minutes, t=14.2 $P < 0.0001$; 300 minutes, t=10.8, $P < 0.0001$; 420 minutes, t=8.1, $P < 0.0001$).

For the body temperature data collected during treatment of this cohort of animals on PND90 (Fig. 2D), MANOVA revealed a main effect of PND90 treatment ($F_{(1,24)}$=195.1, $P < 0.0001$), a main effect of time ($F_{(4,21)}$=35.7, $P < 0.0001$), and a significant PND90 treatment × time interaction ($F_{(4,21)}$=51.4, $P < 0.0001$). Post hoc analysis of the PND90 treatment × time interaction again revealed that the temperatures of animals acutely receiving METH (i.e., PND90 treatment) were significantly higher than those of controls at all time points after the administration of METH began (60 minutes, t=10.8, $P < 0.0001$; 180 minutes, t=16.9, $P < 0.0001$; 300 minutes, t=9.4, $P < 0.0001$; 420 minutes, t=9.1, $P < 0.0001$), but were not different from controls at baseline (t=1.2, P = 0.3). Of importance, there was no significant PND60 treatment × PND90 treatment interaction ($F_{(1,24)}$=1.7, P = 0.2), PND60 treatment × time ($F_{(4,21)}$=1.6, P = 0.2), or PND60 treatment × PND90 treatment × time interaction ($F_{(4,21)}$=1.3, P = 0.3), indicating again that the pretreatment on PND60 did not impact METH-induced hyperthermia on PND90.

METH-Induced DA Depletions. Administration of METH resulted in significant decreases in [^{125}I]RTI-55 binding to the DAT, compared with saline-treated controls (Fig. 3). In animals sacrificed 1 hour after the last injection on PND90 (Fig. 3A), a two-factor ANOVA revealed a main effect of PND60 treatment ($F_{(1,30)}$=42.1, $P < 0.0001$), with rats treated with METH at PND60 showing decreased DAT binding, compared with rats treated with saline. There was no significant main effect of PND90 treatment ($F_{(1,30)}$=79.3, P = 0.6) and no significant PND60 treatment × PND90 treatment interaction ($F_{(1,30)}$=0.1, P = 0.8). In the cohort of animals sacrificed 48 hours after the last injection on PND90 (Fig. 3, B and C), a two-factor ANOVA revealed a main effect of PND60 treatment ($F_{(1,23)}$=11.2, $P < 0.003$), a main effect of PND90 treatment ($F_{(1,23)}$=202.2, $P < 0.0001$), and a significant PND60 treatment × PND90 treatment interaction ($F_{(1,23)}$=78.9, $P < 0.0001$). Post hoc analysis of the interaction revealed that all treatment groups were significantly different from each other (Tukey's test, P values ≤ 0.005).

To assess whether the decrease in DAT autoradiographic labeling reflects METH-induced DA terminal degeneration, we examined, in another cohort of animals treated with the same neurotoxic regimen of METH, the relation between this measure and other indices of METH-induced DA depletion. [^{125}I]RTI-55 binding to the DAT correlates strongly with decreases in DA tissue content measured via high-performance liquid chromatography (n = 9; DM r^2=0.897, $P < 0.0001$, DL r^2=0.79, P = 0.0013). Thus, [^{125}I]RTI-55 binding to the DAT appears to reflect the degree of DA loss induced by the neurotoxic regimen of METH.

Effect of METH on Protein Nitration in Striatum. Consistent with prior reports in the literature implicating reactive nitrogen species in METH-induced neurotoxicity (Di Monte et al., 1996; Itzhak and Ali, 1996; Imam et al., 1999), in this study, treatment of rats with a neurotoxic regimen of METH resulted in a significant increase in protein nitration in the striata of rats sacrificed 1 hour after the final injection on PND90 (Fig. 4). A two-factor ANOVA revealed a significant main effect of PND90 treatment ($F_{(1,31)}$= 8.8, P = 0.006), but no main effect of PND60 treatment ($F_{(1,31)}$=0.1, P = 0.7) and no significant PND60 treatment × PND90 treatment interaction ($F_{(1,31)}$=0.3, P = 0.6). Thus, all rats receiving a neurotoxic regimen of METH on PND90 (i.e., Saline:METH and METH:METH groups), whether they experienced acute toxicity or not, showed equivalent increases in protein nitration in striatum.

Effect of METH on iNOS Expression in Striatum. Repeated high-dose administrations of METH did not result in an induction of iNOS mRNA expression either at 1 hour (Fig. 5A) or 48 hours (Fig. 5, B and C) after the last injection on PND90. A two-way ANOVA on iNOS expression in the striata of rats sacrificed 1 hour after the final injection on PND90 revealed no significant main effects of PND60 treatment ($F_{(1,30)}$=0.0002, P = 0.99) or PND90 treatment ($F_{(1,30)}$=0.3, P = 0.6) and no significant PND60 treatment × PND90 treatment interaction ($F_{(1,30)}$=0.0000, P = 0.99). Similarly, analysis of iNOS expression in the striata of animals sacrificed 48 hours after the last injection on PND90 showed no significant main effects of PND60 treatment ($F_{(1,23)}$=0.9, P = 0.3) or PND90 treatment ($F_{(1,23)}$=0.04, P = 0.8) and no significant PND60 treatment × PND90 treatment interaction ($F_{(1,23)}$=0.1, P = 0.7).

Effect of METH on eNOS Expression in Striatum. Administration of the neurotoxic regimen of METH did not alter eNOS mRNA expression in the striata of rats sacrificed either at 1 hour (Fig. 6A) or at 48 hours (Fig. 6, B and C) after the last administration of METH on PND90. That is, in the cohort of rats sacrificed at 1 hour after the last injection, there was no significant main effect of PND60 treatment ($F_{(1,31)}$=0.6, P = 0.5) or PND90 treatment ($F_{(1,31)}$=0.7, P = 0.4) and no significant PND60 treatment × PND90 treatment interaction ($F_{(1,31)}$=0.3, P = 0.6). Likewise, in the cohort of rats sacrificed 48 hours after the last injection, there was no significant main effect of PND60 treatment ($F_{(1,23)}$=1.3, P = 0.3) or PND90 treatment

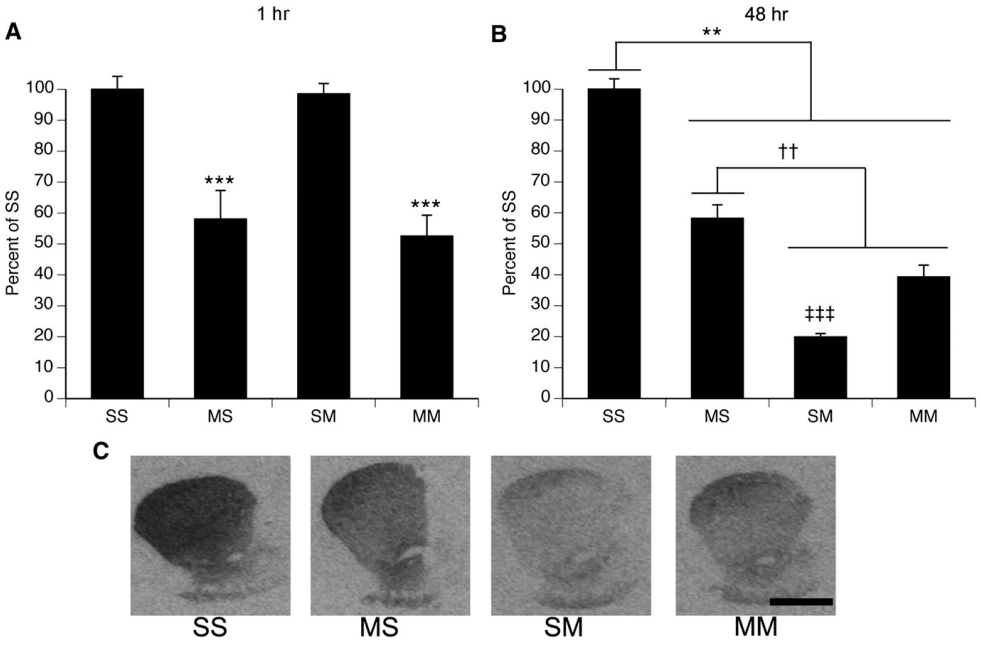

Fig. 3. Striatal DAT binding density after single or repeated exposure to a neurotoxic regimen of METH (mean ± S.E.M.; n = 5–12). Treatment group designations indicate PND60 treatment:PND90 treatment, resulting in the four treatment groups: Saline:Saline (SS), METH:Saline (MS), Saline:METH (SM), and METH:METH (MM). (A) Animals sacrificed 1 hour after the last injection on PND90. ***Main effect of PND60 treatment, $P < 0.001$. (B) Animals sacrificed 48 hours after the last injection on PND90. **SS group significantly different from all other groups, $P < 0.005$; ††MS group significantly different from all other groups; $P < 0.005$; ‡‡‡SM group significantly different from all other groups, $P < 0.005$. (C) Representative images of DAT autoradiography in animals sacrificed 48 hours after the last injection. Scale bar = 2 mm, applies to all images.

($F_{(1,23)}$=0.4, P = 0.6) and no significant PND60 treatment × PND90 treatment interaction ($F_{(1,23)}$=0.8, P = 0.4).

Effect of METH on nNOS Expression in Striatum. Repeated high-dose administrations of METH did not alter the number of cells expressing nNOS mRNA (Fig. 7A) or the mean density of nNOS mRNA signal per cell (Fig. 7B) in rats sacrificed either 1 hour or 48 hours after the last injection on PND90. That is, there was no main effect of PND60 treatment (1-hour survival cohort, $F_{(1,30)}$=0.4, P = 0.5; 48-hour survival cohort, $F_{(1,23)}$=0.3, P = 0.8), no main effect of PND90 treatment (1-hour survival cohort, $F_{(1,30)}$=0.1, P = 0.7; 48-hour survival cohort, $F_{(1,23)}$=0.0003, P = 0.99), and no significant PND60 treatment × PND90 treatment interaction (1-hour survival cohort, $F_{(1,30)}$=0.003, P = 0.96; 48-hour survival cohort, $F_{(1,23)}$=0.3, P = 0.6) on the number of nNOS-positive cells in each striatum . Likewise, there was no main effect of PND60 treatment (1-hour survival cohort, $F_{(1,30)}$=0.02, P = 0.9; 48-hour survival cohort, $F_{(1,23)}$=0.3, P = 0.6), no main effect of PND90 treatment (1-hour survival cohort, $F_{(1,30)}$=0.5, P = 0.5; 48-hour survival cohort, $F_{(1,23)}$=3.1, P = 0.09), and no significant PND60 treatment × PND90 treatment interaction (1-hour survival cohort, $F_{(1,30)}$=0.7, P = 0.4; 48-hour survival cohort, $F_{(1,23)}$=2.8, P = 0.1) on the mean density of nNOS mRNA staining per cell.

To further validate the nNOS mRNA results, we quantified the number of NADPH diaphorase-positive cells in the striata of animals sacrificed at 1 hour after the last injection. These data confirmed that the number of NADPH diaphorase-positive cells did not change after single or repeated exposure to a neurotoxic regimen of METH (unpublished data).

Effect of METH on NOS Activity in the Striatum. Because eNOS and nNOS are constitutively expressed, the enzymes increase their production of NO without observable changes in mRNA expression. Previous work has shown that the NADPH diaphorase histochemical staining allows for the quantification of nNOS activity in the striatum (Dawson et al., 1991; Hope et al., 1991; Morris et al., 1997). Therefore, we examined the effects of a neurotoxic regimen of METH on NOS activity, as reflected in NADPH diaphorase histochemical staining in striatum. Administration of the METH binge regimen on PND90 resulted in a significant increase in NADPH diaphorase histochemical staining in the striata of rats sacrificed 1 hour after the final injection on PND90 (Fig. 8). A two-factor ANOVA revealed a main effect of PND90 treatment ($F_{(1,28)}$=5.8, $P < 0.05$), but no main effect of PND60 treatment ($F_{(1,28)}$=0.06, P = 0.8) and no significant PND60 treatment × PND90 treatment interaction ($F_{(1,28)}$=0.9, P = 0.4). Thus, as was the case for protein nitration in striatum, NADPH diaphorase histochemical staining and, thus, nNOS

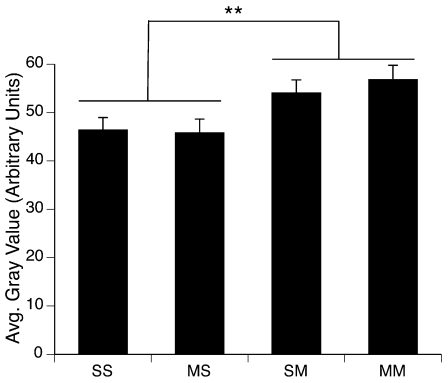

Fig. 4. Quantitative analysis of the effects of single or repeated METH exposure on protein nitration in the striata of animals sacrificed 1 hour after the last injection on PND90. Protein nitration data are expressed as average (avg.) gray values (mean ± S.E.M.; n = 6–12) obtained from densitometric analysis of immunohistochemically stained sections. Treatment group designations indicate PND60 treatment:PND90 treatment, resulting in the four treatment groups: Saline:Saline (SS), METH:Saline (MS), Saline:METH (SM), and METH:METH (MM). **Significant main effect of PND90 treatment, $P < 0.01$.

activity were increased in all rats receiving a neurotoxic regimen of METH on PND90, regardless of whether they experienced acute DA neuron toxicity (Saline:METH group) or not (METH:METH group).

Discussion

Recent data suggest that abuse of METH may contribute to increased incidence of Parkinsonism secondary to damage to striatal DA systems (Callaghan et al., 2012). Thus, delineating the necessary and sufficient factors involved in METH-induced damage to central DA systems is critical for advancing our ability to mitigate long-term consequences of METH use. Our laboratory and others have found that animals pretreated with a neurotoxic regimen of METH do not show further depletions of striatal DA when challenged with a subsequent neurotoxic regimen of METH (Thomas and Kuhn, 2005; Hanson et al., 2009). This paradigm thus affords a model in which animals can be matched for acute METH exposure, but differentiated with respect to acute DA neuron toxicity, to identify factors that are sufficient to induce striatal DA toxicity. Prior evidence has suggested that NO may be such a critical factor for METH-induced neurotoxicity (Di Monte et al., 1996; Itzhak and Ali, 1996; Deng and Cadet, 1999; Imam et al., 1999). Therefore, the purpose of this study was to determine whether NO production secondary to METH exposure is sufficient to induce striatal DA depletions and to determine the source of NO after METH exposure. The data reveal that production of NO, as reflected in protein nitration, is similar whether an animal is experiencing acute DA toxicity or not, suggesting that NO production is not sufficient to induce such toxicity. Furthermore, the data suggest that the NO likely arises from the constitutively expressed isoforms of NOS, most likely the nNOS-containing interneuron population in striatum.

The present results suggest that NO production in response to METH may not contribute to METH-induced DA neuron toxicity, because both rats experiencing acute toxicity to METH administration on PND90 and those resistant to it showed equivalent increases in protein nitration and NOS activity in striatum. As noted above, studies have implicated NO in METH-induced DA neuron toxicity on the basis of observations that inhibition of NOS blocks or attenuates such toxicity (Di Monte et al., 1996; Itzhak and Ali, 1996; Ali and Itzhak, 1998; Itzhak et al., 1998; Imam et al., 1999; Itzhak et al., 2000a; Itzhak et al., 2000b; Itzhak et al., 2004). However, there is controversy over whether this protection reflects a critical mechanistic role of NO in METH-induced DA neuron toxicity or whether it results from a disruption of METH-induced hyperthermia necessary for the toxicity (Taraska and Finnegan, 1997; Callahan and Ricaurte,

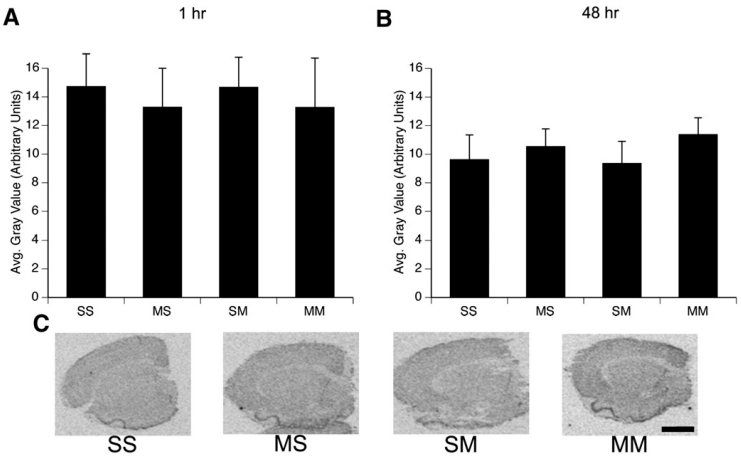

Fig. 5. Quantitative analysis of the effects of single or repeated METH exposure on iNOS mRNA expression in the striata of animals sacrificed 1 hour (A) or 48 hour (B) after the last injection on PND90. Treatment group designations indicate PND60 treatment:PND90 treatment, resulting in the four treatment groups: Saline:Saline (SS), METH:Saline (MS), Saline:METH (SM), and METH:METH (MM). Values are background-subtracted average (avg.) gray values (mean ± SEM; n = 5-12). No significant differences between treatment groups were observed. (C) Representative images of iNOS mRNA in situ hybridization histochemical staining in rats sacrificed 48 hour after the last injection on PND90. Scale bar = 2 mm, applies to all images.

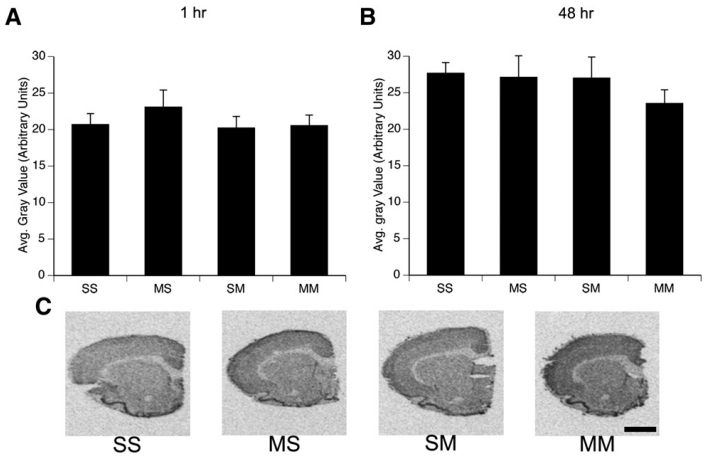

Fig. 6. Quantitative analysis of the effects of single or repeated METH exposure on eNOS mRNA expression in the striata of animals sacrificed 1 hour (A) or 48 hours (B) after the last injection on PND90. Treatment group designations indicate PND60 treatment:PND90 treatment, resulting in the four treatment groups: Saline:Saline (SS), METH:Saline (MS), Saline:METH (SM), and METH:METH (MM). Values are background-subtracted mean gray values (mean ± S.E.M.; n = 5–12). No significant differences between treatment groups were observed. (C) Representative images of eNOS mRNA in situ hybridization histochemical staining in rats sacrificed 48 hours after the last injection on PND90. Scale bar = 2 mm, applies to all images.

1998). The present findings of a dissociation between indices of NO production and acute DA neuron toxicity support the conclusion that the generation of NO is not sufficient for METH-induced DA toxicity.

Although the present data suggest that generation of NO is not sufficient for METH-induced DA terminal damage, we cannot rule out the possibility that NO is necessary for such toxicity when it occurs (e.g., in the Saline:METH group), because NO may act in concert with other factors under those conditions to contribute to the toxicity. For example, evidence suggests that NO regulates DA release in striatum (Zhu and Luo, 1992; West and Galloway, 1997; West et al., 2002), including METH-induced DA release (Bowyer et al., 1995; Inoue et al., 1996), which has been suggested to play an important role in damage to DA terminals (O'Dell et al., 1991; O'Dell et al., 1993; Gross et al., 2011). Thus, NO production during an initial exposure to a neurotoxic regimen of METH may increase DA overflow, and this DA overflow may result in the DA neuron toxicity. Under conditions in which DA overflow is reduced, such as in animals with prior METH-induced DA neuron toxicity (Hanson et al., 2009), such a role of NO might not be apparent. Clearly, studies with strict control over potential contributing factors allowing for systematic independent and coordinate manipulation of the factors will be necessary to fully understand the process by which METH induces DA neurotoxicity. Furthermore, we cannot exclude a role of NO in striatal-efferent neuron toxicity observed in some models of METH-induced neurotoxicity (Zhu et al., 2009).

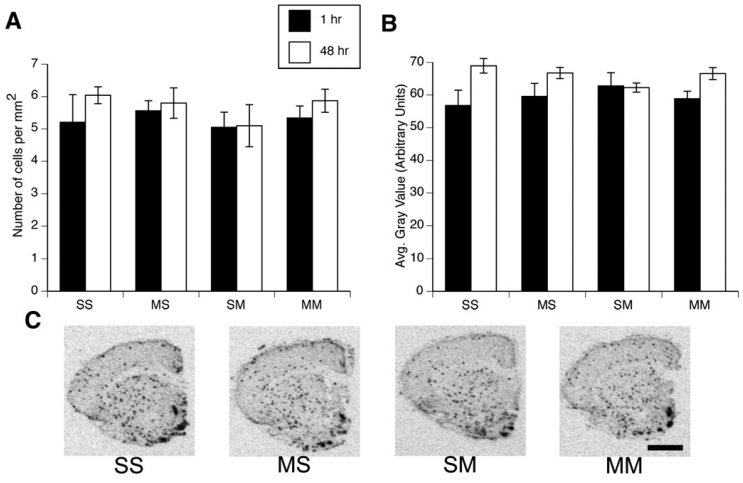

Fig. 7. Quantitative analysis of the effects of single or repeated METH exposure on nNOS mRNA expression in the striata of animals sacrificed 1 hour or 48 hours after the last injection on PND90. Treatment group designations indicate PND60 treatment:PND90 treatment, resulting in the four treatment groups: Saline:Saline (SS), METH:Saline (MS), Saline:METH (SM), and METH:METH (MM). Values are expressed as the mean number of cells expressing nNOS per square millimeter of the imaged striatal sections (A; mean ± S.E.M.; n = 4–12) and the mean density (i.e., average [avg.] gray value) of the nNOS signal per labeled cell (B) in the striatal sections analyzed. No significant differences among treatment groups were observed. (C) Representative images of nNOS mRNA in situ hybridization histochemical staining in rats sacrificed 48 hours after the last injection on PND90. Scale bar = 2 mm, applies to all images.

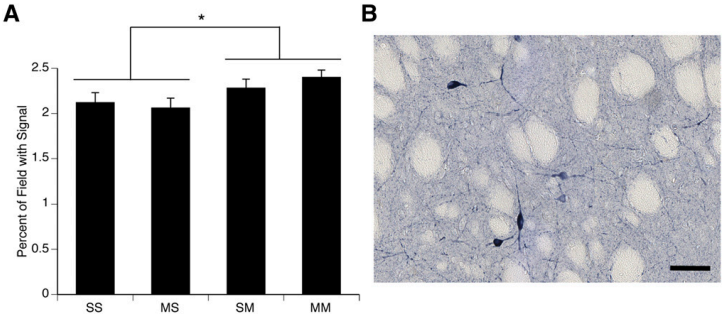

Fig. 8. (A) Quantitative analysis of the effects of single or repeated METH exposure on nNOS activity in the striata of animals sacrificed 1 hour after the last injection on PND90. Treatment group designations indicate PND60 treatment:PND90 treatment, resulting in the four treatment groups: Saline:Saline (SS), METH:Saline (MS), Saline:METH (SM), and METH:METH (MM). Data are expressed as the percentage area of the field with signal above threshold. *Significant main effect of PND90 treatment, $P < 0.05$. (B) Representative image of NADPH diaphorase histochemical staining in an SM animal sacrificed 1 hour after the last injection on PND90. Scale bar = 50μm.

Although the necessity of NO for METH-induced DA neurotoxicity remains in question, it is clear from the present findings that administration of a binge regimen of METH increases NO production. The data further suggest that METH-induced increases in NOS activity/NO production may largely arise secondary to activation of nNOS, which is found in striatal somatostatin/neuropeptide Y-positive interneurons (Kawaguchi et al., 1995). First, we found no induction of iNOS mRNA 1 or 48 hours after the last administration on PND90. These data are consistent with previous work (Deng and Cadet, 1999) showing that iNOS protein expression is not induced after a neurotoxic regimen of METH. However, in that study, iNOS protein was examined at 1 hour, 24 hours, and 1 week after exposure to METH, time points when glial cells may not be fully activated (LaVoie et al., 2004). Of importance, it is these cell types in which induction of iNOS mRNA expression typically occurs (Gibson et al., 2005). Therefore, we examined iNOS expression at 1 and 48 hours, because previous work has shown that glial reactivity peaks at 48 hours after a neurotoxic regimen of METH (LaVoie et al., 2004). Our data combined with the work of others (Deng and Cadet, 1999) strongly suggest that iNOS is not a likely source of NO after METH exposure.

Second, induction of eNOS and nNOS isoforms also does not appear to underlie the METH-induced increases in NO production. At both 1 and 48 hours after the last administration of METH on PND90, there were no changes in the numbers of cells expressing eNOS or nNOS mRNA. Likewise, there was no increase in the numbers of NADPH diaphorase-positive cells and no increase in eNOS immunohistochemical staining in sections from animals sacrificed 48 hours after the last injection (data not shown). A prior study in mice reported an increase in the number of cells expressing nNOS protein after a neurotoxic regimen of METH (Deng and Cadet, 1999), but others have not (Wang et al., 2008; Wang and Angulo, 2011). Differences in nNOS expression have been observed between species and strains of animals within a species (Blackshaw et al., 2003), suggesting that differences between our results and the prior report by Deng and Cadet may reflect a species difference. Our data thus suggest that induction of eNOS or nNOS expression by METH exposure is not contributing to METH-induced NO production in this rat model.

Taken together, the data suggest that activation of constitutively expressed NOS isoforms (i.e., eNOS or nNOS) is the likely basis for METH-induced NO production. This conclusion is based on the data showing increased NADPH diaphorase histochemical staining, which reflects NOS activity (Hope et al., 1991). We further restricted this assay to determination of nNOS activity in striatum by excluding stained vasculature from the images during the analysis and thresholding the images to include only cell bodies and processes of NADPH-positive cells. We found that animals acutely exposed to a neurotoxic regimen of METH on PND90 showed increased staining, suggesting increased nNOS activation by the binge regimen of METH. On the basis of these observations, we conclude that activation of nNOS is a major source of NO production in response to the binge regimen of METH. However, we cannot rule out a contribution of eNOS activation to METH-induced NO production and METH-induced protein nitration in striatum.

Activation of nNOS in striatal interneurons in the context of binge regimens of METH is not surprising, because of what is known about NO production in striatum and the cascade of events occurring during and after METH administration. First, activation of the *N*-methyl-D-aspartate (NMDA) subtype of glutamate (GLU) receptors initiates NO production via Ca-dependent activation of nNOS (Garthwaite et al., 1988; Bredt and Snyder, 1989). Furthermore, binge regimens of METH increase GLU efflux in striatum and activation of NMDA receptors (Nash and Yamamoto, 1992; Mark et al., 2004). Second, activation of DA D1 receptors increases NO efflux in striatum (Le Moine et al., 1991; Sammut et al., 2006) and NADPH diaphorase histochemical staining (Morris et al., 1997; Hoque et al., 2010), and striatal nNOS-containing interneurons express DA D1 family receptors (Le Moine et al., 1991). Furthermore, NMDA and DA D1 receptor activation work in concert to increase NO production (Park and West, 2009), and stimulation of either type of receptor or blockade of either type of receptor decreases NOS activity, as assessed via NADPH diaphorase histochemical staining (Morris et al., 1997). Together with data showing increased extracellular levels of both DA and GLU during and after METH exposure (O'Dell et al., 1991; Nash and Yamamoto, 1992; O'Dell et al., 1993), it seems to be likely that activation of nNOS in striatal interneurons is a major source of NO production after METH exposure.

In conclusion, the data presented here show that administration of a binge regimen of METH in rats increases protein nitration in striatum. The data further show that activation of

nNOS, as reflected in increased NADPH-diaphorase histochemical staining in cell bodies and processes of striatal interneurons, was apparent in rats acutely exposed to a binge regimen of METH, implicating nNOS as the likely source of METH-induced NO production. However, the data also show a dissociation between measures of NOS activity (NADPH diaphorase staining) and NO production (immunohistochemical staining of protein nitration) and METH-induced DA neurotoxicity, suggesting that NO production by a binge regimen of METH is not sufficient to induce acute DA neurotoxicity and that NO may not be a useful therapeutic target for prevention of acute METH-induced neurotoxicity in human METH abusers.

Acknowledgments

The authors thank Dr. Michael Marletta for the nNOS and iNOS cDNAs, and Dr. Steve O'Dell in Dr. John Marshall's laboratory for assistance with the DAT autoradiography assay.

Author Contributions

Participated in research design: Friend, Son, Fricks-Gleason, Keefe.

Conducted experiments: Friend, Son, Fricks-Gleason.

Performed data analysis: Friend, Son, Fricks-Gleason, Keefe.

Wrote or contributed to the writing of the manuscript: Friend, Son, Fricks-Gleason, Keefe.

References

Ali SF and Itzhak Y (1998) Effects of 7-nitroindazole, an NOS inhibitor on methamphetamine-induced dopaminergic and serotonergic neurotoxicity in mice. *Ann N Y Acad Sci* **844**:122–130.

Ali SF, Newport GD, Holson RR, Slikker W, Jr, and Bowyer JF (1994) Low environmental temperatures or pharmacologic agents that produce hypothermia decrease methamphetamine neurotoxicity in mice. *Brain Res* **658**:33–38.

Anderson KL and Itzhak Y (2006) Methamphetamine-induced selective dopaminergic neurotoxicity is accompanied by an increase in striatal nitrate in the mouse. *Ann N Y Acad Sci* **1074**:225–233.

Blackshaw S, Eliasson MJ, Sawa A, Watkins CC, Krug D, Gupta A, Arai T, Ferrante RJ, and Snyder SH (2003) Species, strain and developmental variations in hippocampal neuronal and endothelial nitric oxide synthase clarify discrepancies in nitric oxide-dependent synaptic plasticity. *Neuroscience* **119**:979–990.

Bowyer JF, Clausing P, Gough B, Slikker W, Jr, and Holson RR (1995) Nitric oxide regulation of methamphetamine-induced dopamine release in caudate/putamen. *Brain Res* **699**:62–70.

Bredt DS and Snyder SH (1989) Nitric oxide mediates glutamate-linked enhancement of cGMP levels in the cerebellum. *Proc Natl Acad Sci USA* **86**:9030–9033.

Callaghan RC, Cunningham JK, Sykes J, and Kish SJ (2012) Increased risk of Parkinson's disease in individuals hospitalized with conditions related to the use of methamphetamine or other amphetamine-type drugs. *Drug Alcohol Depend* **120**: 35–40.

Callahan BT and Ricaurte GA (1998) Effect of 7-nitroindazole on body temperature and methamphetamine-induced dopamine toxicity. *Neuroreport* **9**:2691–2695.

Dawson TM, Bredt DS, Fotuhi M, Hwang PM, and Snyder SH (1991) Nitric oxide synthase and neuronal NADPH diaphorase are identical in brain and peripheral tissues. *Proc Natl Acad Sci USA* **88**:7797–7801.

Deng X and Cadet JL (1999) Methamphetamine administration causes overexpression of nNOS in the mouse striatum. *Brain Res* **851**:254–257.

Di Monte DA, Royland JE, Jakowec MW, and Langston JW (1996) Role of nitric oxide in methamphetamine neurotoxicity: protection by 7-nitroindazole, an inhibitor of neuronal nitric oxide synthase. *J Neurochem* **67**:2443–2450.

Dinerman JL, Dawson TM, Schell MJ, Snowman A, and Snyder SH (1994) Endothelial nitric oxide synthase localized to hippocampal pyramidal cells: implications for synaptic plasticity. *Proc Natl Acad Sci USA* **91**:4214–4218.

Doyle CA and Slater P (1997) Localization of neuronal and endothelial nitric oxide synthase isoforms in human hippocampus. *Neuroscience* **76**:387–395.

Garthwaite J, Charles SL, and Chess-Williams R (1988) Endothelium-derived relaxing factor release on activation of NMDA receptors suggests role as intercellular messenger in the brain. *Nature* **336**:385–388.

Gibson CL, Coughlan TC, and Murphy SP (2005) Glial nitric oxide and ischemia. *Glia* **50**:417–426.

Gross NB, Duncker PC, and Marshall JF (2011) Striatal dopamine D1 and D2 receptors: widespread influences on methamphetamine-induced dopamine and serotonin neurotoxicity. *Synapse* **65**:1144–1155.

Guilarte TR, Nihei MK, McGlothan JL, and Howard AS (2003) Methamphetamine-induced deficits of brain monoaminergic neuronal markers: distal axotomy or neuronal plasticity. *Neuroscience* **122**:499–513.

Hanson JE, Birdsall E, Seferian KS, Crosby MA, Keefe KA, Gibb JW, Hanson GR, and Fleckenstein AE (2009) Methamphetamine-induced dopaminergic deficits and refractoriness to subsequent treatment. *Eur J Pharmacol* **607**:68–73.

Hope BT, Michael GJ, Knigge KM, and Vincent SR (1991) Neuronal NADPH diaphorase is a nitric oxide synthase. *Proc Natl Acad Sci USA* **88**:2811–2814.

Hoque KE, Indorkar RP, Sammut S, and West AR (2010) Impact of dopamine-glutamate interactions on striatal neuronal nitric oxide synthase activity. *Psychopharmacology (Berl)* **207**:571–581.

Horner KA, Westwood SC, Hanson GR, and Keefe KA (2006) Multiple high doses of methamphetamine increase the number of preproneuropeptide Y mRNA-expressing neurons in the striatum of rat via a dopamine D1 receptor-dependent mechanism. *J Pharmacol Exp Ther* **319**:414–421.

Imam SZ, Crow JP, Newport GD, Islam F, Slikker W, Jr, and Ali SF (1999) Methamphetamine generates peroxynitrite and produces dopaminergic neurotoxicity in mice: protective effects of peroxynitrite decomposition catalyst. *Brain Res* **837**: 15–21.

Imam SZ, Islam F, Itzhak Y, Slikker W, Jr, and Ali SF (2000) Prevention of dopaminergic neurotoxicity by targeting nitric oxide and peroxynitrite: implications for the prevention of methamphetamine-induced neurotoxic damage. *Ann N Y Acad Sci* **914**:157–171.

Inoue H, Arai I, Shibata S, and Watanabe S (1996) NG-nitro-L-arginine methyl ester attenuates the maintenance and expression of methamphetamine-induced behavioral sensitization and enhancement of striatal dopamine release. *J Pharmacol Exp Ther* **277**:1424–1430.

Itzhak Y and Ali SF (1996) The neuronal nitric oxide synthase inhibitor, 7-nitroindazole, protects against methamphetamine-induced neurotoxicity in vivo. *J Neurochem* **67**:1770–1773.

Itzhak Y, Anderson KL, and Ali SF (2004) Differential response of nNOS knockout mice to MDMA ("ecstasy")- and methamphetamine-induced psychomotor sensitization and neurotoxicity. *Ann N Y Acad Sci* **1025**:119–128.

Itzhak Y, Gandia C, Huang PL, and Ali SF (1998) Resistance of neuronal nitric oxide synthase-deficient mice to methamphetamine-induced dopaminergic neurotoxicity. *J Pharmacol Exp Ther* **284**:1040–1047.

Itzhak Y, Martin JL, and Ail SF (2000a) nNOS inhibitors attenuate methamphetamine-induced dopaminergic neurotoxicity but not hyperthermia in mice. *Neuroreport* **11**:2943–2946.

Itzhak Y, Martin JL, and Ali SF (1999) Methamphetamine- and 1-methyl-4-phenyl-1,2,3, 6-tetrahydropyridine-induced dopaminergic neurotoxicity in inducible nitric oxide synthase-deficient mice. *Synapse* **34**:305–312.

Itzhak Y, Martin JL, and Ali SF (2000b) Comparison between the role of the neuronal and inducible nitric oxide synthase in methamphetamine-induced neurotoxicity and sensitization. *Ann N Y Acad Sci* **914**:104–111.

Iwahashi T, Inoue A, Koh CS, Shin TK, and Kim BS (1999) Expression and potential role of inducible nitric oxide synthase in the central nervous system of Theiler's murine encephalomyelitis virus-induced demyelinating disease. *Cell Immunol* **194**: 186–193.

Kawaguchi Y, Wilson CJ, Augood SJ, and Emson PC (1995) Striatal interneurones: chemical, physiological and morphological characterization. *Trends Neurosci* **18**: 527–535.

Keefe KA and Gerfen CR (1996) D1 dopamine receptor-mediated induction of zif268 and c-fos in the dopamine-depleted striatum: differential regulation and independence from NMDA receptors. *J Comp Neurol* **367**:165–176.

Kogan FJ, Nichols WK, and Gibb JW (1976) Influence of methamphetamine on nigral and striatal tyrosine hydroxylase activity and on striatal dopamine levels. *Eur J Pharmacol* **36**:363–371.

LaVoie MJ, Card JP, and Hastings TG (2004) Microglial activation precedes dopamine terminal pathology in methamphetamine-induced neurotoxicity. *Exp Neurol* **187**:47–57.

Le Moine C, Normand E, and Bloch B (1991) Phenotypical characterization of the rat striatal neurons expressing the D1 dopamine receptor gene. *Proc Natl Acad Sci USA* **88**:4205–4209.

Mark KA, Soghomonian JJ, and Yamamoto BK (2004) High-dose methamphetamine acutely activates the striatonigral pathway to increase striatal glutamate and mediate long-term dopamine toxicity. *J Neurosci* **24**:11449–11456.

Maxwell JC (2005) Emerging research on methamphetamine. *Curr Opin Psychiatry* **18**:235–242.

Morris BJ, Simpson CS, Mundell S, Maceachern K, Johnston HM, and Nolan AM (1997) Dynamic changes in NADPH-diaphorase staining reflect activity of nitric oxide synthase: evidence for a dopaminergic regulation of striatal nitric oxide release. *Neuropharmacology* **36**:1589–1599.

Nash JF and Yamamoto BK (1992) Methamphetamine neurotoxicity and striatal glutamate release: comparison to 3,4-methylenedioxymethamphetamine. *Brain Res* **581**:237–243.

O'Dell SJ, Weihmuller FB, and Marshall JF (1991) Multiple methamphetamine injections induce marked increases in extracellular striatal dopamine which correlate with subsequent neurotoxicity. *Brain Res* **564**:256–260.

O'Dell SJ, Weihmuller FB, and Marshall JF (1993) Methamphetamine-induced dopamine overflow and injury to striatal dopamine terminals: attenuation by dopamine D1 or D2 antagonists. *J Neurochem* **60**:1792–1799.

Oleszak EL, Katsetos CD, Kuzmak J, and Varadhachary A (1997) Inducible nitric oxide synthase in Theiler's murine encephalomyelitis virus infection. *J Virol* **71**: 3228–3235.

Park DJ and West AR (2009) Regulation of striatal nitric oxide synthesis by local dopamine and glutamate interactions. *J Neurochem* **111**:1457–1465.

Pastuzyn ED, Chapman DE, Wilcox KS, and Keefe KA (2012) Altered learning and Arc-regulated consolidation of learning in striatum by methamphetamine-induced neurotoxicity. *Neuropsychopharmacology* **37**:885–895.

Radi R, Beckman JS, Bush KM, and Freeman BA (1991) Peroxynitrite-induced membrane lipid peroxidation: the cytotoxic potential of superoxide and nitric oxide. *Arch Biochem Biophys* **288**:481–487.

Rushlow W, Flumerfelt BA, and Naus CC (1995) Colocalization of somatostatin, neuropeptide Y, and NADPH-diaphorase in the caudate-putamen of the rat. *J Comp Neurol* **351**:499–508.

Sammut S, Dec A, Mitchell D, Linardakis J, Ortiguela M, and West AR (2006) Phasic dopaminergic transmission increases NO efflux in the rat dorsal striatum via

a neuronal NOS and a dopamine D(1/5) receptor-dependent mechanism. *Neuropsychopharmacology* **31**:493–505.
Taraska T and Finnegan KT (1997) Nitric oxide and the neurotoxic effects of methamphetamine and 3,4-methylenedioxymethamphetamine. *J Pharmacol Exp Ther* **280**:941–947.
Thomas DM and Kuhn DM (2005) Attenuated microglial activation mediates tolerance to the neurotoxic effects of methamphetamine. *J Neurochem* **92**:790–797.
Uhl GR and Sasek CA (1986) Somatostatin mRNA: regional variation in hybridization densities in individual neurons. *J Neurosci* **6**:3258–3264.
Vaid RR, Yee BK, Rawlins JN, and Totterdell S (1996) NADPH-diaphorase reactive pyramidal neurons in Ammon's horn and the subiculum of the rat hippocampal formation. *Brain Res* **733**:31–40.
Volkow ND, Chang L, Wang GJ, Fowler JS, Leonido-Yee M, Franceschi D, Sedler MJ, Gatley SJ, Hitzemann R, and Ding YS, et al. (2001) Association of dopamine transporter reduction with psychomotor impairment in methamphetamine abusers. *Am J Psychiatry* **158**:377–382.
Wagner GC, Ricaurte GA, Seiden LS, Schuster CR, Miller RJ, and Westley J (1980) Long-lasting depletions of striatal dopamine and loss of dopamine uptake sites following repeated administration of methamphetamine. *Brain Res* **181**: 151–160.
Wang J and Angulo JA (2011) Synergism between methamphetamine and the neuropeptide substance P on the production of nitric oxide in the striatum of mice. *Brain Res* **1369**:131–139.
Wang J, Xu W, Ali SF, and Angulo JA (2008) Connection between the striatal neurokinin-1 receptor and nitric oxide formation during methamphetamine exposure. *Ann N Y Acad Sci* **1139**:164–171.
West AR and Galloway MP (1997) Endogenous nitric oxide facilitates striatal dopamine and glutamate efflux in vivo: role of ionotropic glutamate receptor-dependent mechanisms. *Neuropharmacology* **36**:1571–1581.
West AR, Galloway MP, and Grace AA (2002) Regulation of striatal dopamine neurotransmission by nitric oxide: effector pathways and signaling mechanisms. *Synapse* **44**:227–245.
Zhu J, Xu W, Wang J, Ali SF, and Angulo JA (2009) The neurokinin-1 receptor modulates the methamphetamine-induced striatal apoptosis and nitric oxide formation in mice. *J Neurochem* **111**:656–668.
Zhu JP, Xu W, and Angulo JA (2006) Distinct mechanisms mediating methamphetamine-induced neuronal apoptosis and dopamine terminal damage share the neuropeptide substance p in the striatum of mice. *Ann N Y Acad Sci* **1074**:135–148.
Zhu XZ and Luo LG (1992) Effect of nitroprusside (nitric oxide) on endogenous dopamine release from rat striatal slices. *J Neurochem* **59**:932–935.

Address correspondence to: Ashley N. Fricks-Gleason, Department of Pharmacology and Toxicology, 30 S 2000 East, Room 112, Salt Lake City, UT 84112. E-mail: a.fricks@utah.edu

CHAPTER 3

GLIAL REACTIVITY IN RESISTANCE TO METHAMPHETAMINE-INDUCED NEUROTOXICITY

Reprinted with permission from The Journal of Neurochemistry

Journal of Neurochemistry JNC

JOURNAL OF NEUROCHEMISTRY | 2013 | 125 | 566–574 doi: 10.1111/jnc.12201

ORIGINAL ARTICLE

Glial reactivity in resistance to methamphetamine-induced neurotoxicity

Danielle M. Friend* and Kristen A. Keefe*,†

*Interdepartmental Program in Neuroscience, University of Utah, Salt Lake City, Utah, USA
†Department of Pharmacology and Toxicology, University of Utah, Salt Lake City, Utah, USA

Abstract

Neurotoxic regimens of methamphetamine (METH) result in reactive microglia and astrocytes in striatum. Prior data indicate that rats with partial dopamine (DA) loss resulting from prior exposure to METH are resistant to further decreases in striatal DA when re-exposed to METH 30 days later. Such resistant animals also do not show an activated microglia phenotype, suggesting a relation between microglial activation and METH-induced neurotoxicity. To date, the astrocyte response in such resistance has not been examined. Thus, this study examined glial-fibrillary acidic protein (GFAP) and CD11b protein expression in striata of animals administered saline or a neurotoxic regimen of METH on post-natal days 60 and/or 90 (Saline:Saline, Saline:METH, METH:Saline, METH:METH). Consistent with previous work, animals experiencing acute toxicity (Saline:METH) showed both activated microglia and astocytes, whereas those resistant to the acute toxicity (METH:METH) did not show activated microglia. Interestingly, GFAP expression remained elevated in rats exposed to METH at PND60 (METH:Saline), and was not elevated further in resistant rats treated for the second time with METH (METH:METH). These data suggest that astrocytes remain reactive up to 30 days post-METH exposure. In addition, these data indicate that astrocyte reactivity does not reflect acute, METH-induced DA terminal toxicity, whereas microglial reactivity does.

Keywords: astrocyte, dopamine, methamphetamine, microglia, toxicity.

J. Neurochem. (2013) **125**, 566–574.

Methamphetamine (METH) is a highly abused psychostimulant, and repeated high-dose administration of METH results in persistent damage to the dopamine (DA) system. This damage consists of decreased dopamine (DA) tissue concentrations (Kogan *et al.* 1976; Wagner *et al.* 1980), DA transporter (DAT) (Fleckenstein *et al.* 1997; McCann *et al.* 1998) and vesicular monoamine transporter-2 levels (Guilarte *et al.* 2003), and tyrosine hydroxylase activity (Kogan *et al.* 1976) in striatum.

Several studies have documented a robust activation of both astrocytes (Bowyer *et al.* 1994; O'Callaghan and Miller 1994; Cappon *et al.* 1997; Guilarte *et al.* 2003) and microglia (Guilarte *et al.* 2003; LaVoie *et al.* 2004; Thomas *et al.* 2004) following exposure of rodents to a neurotoxic regimen of METH. However, these studies examined astrocyte and microglia activation in response to a single neurotoxic regimen of METH. Human METH abusers administer multiple doses of METH. Thus, to more accurately model the repeated binge administration observed in humans, our lab and others (Thomas and Kuhn 2005; Hanson *et al.* 2009) have conducted studies in which animals are treated with a neurotoxic regimen of METH and challenged 7 or 30 days later with a second neurotoxic regimen of METH. These studies have revealed that such animals are resistant to acute DA neuron toxicity upon exposure to the second METH regimen. This experimental paradigm thus allows for the examination of factors associated with METH toxicity in animals matched for acute METH exposure, but differentiated with respect to acute METH-induced DA terminal degeneration. Prior work with this model has reported that animals that are resistant to the acute METH-induced neurotoxicity also do not demonstrate significant microglial activation following the second exposure as do animals

Received January 8, 2013; revised manuscript received February 8, 2013; accepted February 12, 2013.

Address correspondence and reprint requests to Kristen A. Keefe, Dept. of Pharmacology and Toxicology, 30 South 2000 East, Room 105, Salt Lake City, UT 84112, USA. E-mail: k.keefe@utah.edu (or) Danielle M. Friend, Interdepartmental Program in Neuroscience, University of Utah, Salt Lake City, UT, USA. E-mail: da.friend@utah.edu

Abbreviations used: BBB, blood–brain barrier; CNS, central nervous system; DA, dopamine; DAT, dopamine transporter; GLU, glutamate; METH, methamphetamine; PBS, phosphate buffered saline; PND, post-natal day.

experiencing acute toxicity (Thomas and Kuhn 2005), suggesting a possible role of microglial activation in METH-induced DA toxicity. The extent to which resistance to subsequent METH-induced neurotoxicity is also associated with decreased astrocyte reactivity is currently unknown. Therefore, the purpose of this study was to examine both microglia and astrocyte reactivity, using CD11b and glial-fibrillary acidic protein (GFAP) expression respectively, in animals rendered resistant to the acute DA toxicity induced by METH.

Methods

Animals

Male Sprague-Dawley rats (Charles River Laboratories, Raleigh, NC, USA) were housed in wire mesh cages in a temperature-controlled room on a 12:12-h light:dark cycle with free access to food and water. All animal care and experimental procedures were in accordance with both the ARRIVE guidelines and the *Guide for the Care and Use of Laboratory Animals* (8th Ed., National Research Council) and were approved by the Institutional Animal Care and Use Committee at the University of Utah.

METH administration

Because of tissue availability, one cohort of animals was used to examine GFAP expression and another cohort of animals was used to examine CD11b expression. METH and saline injections were conducted as previously described (Friend *et al.* 2013). Briefly, on treatment days [post-natal day (PND)60 and PND90], rats (5–8 per treatment group) were housed in groups of 6 in plastic tub cages (33 cm × 28 cm × 17 cm) with corncob bedding. Animals received injections of (±)-METH-HCl (10 mg free base/kg, s.c.; kindly provided by the National Institute on Drug Abuse) or 0.9% saline (1 mL/kg, s.c.) at 2-h intervals resulting in a total of four injections. Rectal temperatures were monitored using a digital thermometer (BAT-12; Physitemp Instruments, Clifton, NJ, USA) to ensure the presence of METH-induced hyperthermia. Baseline temperatures for each animal were taken 30 min prior to the first injection and 1 h after each subsequent injection. If the body temperature of an animal exceeded 40.5°C, the animal was cooled by transferring it to a cage placed over wet ice until the body temperature fell below 39°C. Approximately, 18 h after the last injection on PND60, animals were returned to wire mesh cages in the colony room and allowed to recover for 30 days. On PND90, animals were again transferred to plastic tub cages and treated with either METH or saline as described above. This treatment regimen resulted in four treatment groups: Saline:Saline, Saline:METH, METH:Saline, and METH:METH based on treatments on PND60:PND90.

Tissue preparation

Animals were sacrificed 48 h after the last injection on PND90 via exposure to CO for 1 min. Following decapitation, brains were rapidly removed and submerged in 4% paraformaldehyde with 0.9% NaCl for 24 h at 4°C, then cryoprotected in 30% sucrose in 0.1 M phosphate buffered saline (PBS) and stored at 4°C. The brains were then sectioned at 30 μm on a freezing microtome (Microm, HM 440E). For each animal, four coronal sections of striatum (+1.6 mm to +0.2 mm relative to bregma) were sectioned and stored at 4°C in 1 mg/mL sodium azide in 0.1 M PBS.

Immunohistochemistry

DAT immunohistochemistry was performed to evaluate METH-induced DA depletions. Briefly, sections were subject to heat-mediated antigen retrieval in 10 mM citrate buffer containing 0.5% Tween-20 (pH 6.0) for 20 min at 37°C. After cooling at 23°C, sections were washed in 0.1 M PBS, incubated for 10 min in 0.1 M PBS containing 3% H_2O_2, and washed again in 0.1 M PBS. Non-specific antibody binding was blocked by incubating tissue in 0.1 M PBS containing 5% milk and 0.2% Triton X-100 for 60 min. Tissue was then incubated overnight at 4°C in a primary antibody solution containing 0.1 M PBS, 2% milk, 0.2% Triton X-100, and rat anti-DAT antibody (Millipore, Billerica, MA, USA; MAB369, 1 : 5000). The following day, tissue was washed in 0.1 M PBS, incubated in a secondary antibody solution containing 0.1 M PBS, 2% non-fat dry milk, 0.2% Triton X-100 and biotinylated goat anti-rat IgG (Vector Labs, Burlingame, CA, USA; BA-4000, 1 : 200). Finally, tissue was incubated in avidin-biotinylated peroxidase complex solution (ABC Elite Kit; Vector Labs, PK-6100) for 30 min and the reaction terminated by washing in 0.1 M PBS. The tissue sections were then incubated in nickel-enhanced diaminobenzidine tetrahydrochloride (Ni-DAB; Vector, SK-4100) for 3–5 min, washed again in 0.1 M PBS, mounted onto slides, dried, dehydrated and coverslipped with VectaMount (Vector Labs, H-5000).

For GFAP and CD11b immunohistochemistry, sections were washed in 0.1 M PBS, and non-specific antibody binding was prevented by incubating tissue for 2 h at 23°C in a blocking solution containing 10% goat serum and 0.3% Triton X-100 in 0.1 M PBS. Sections were then incubated in a primary antibody solution containing 10% goat serum, 0.3% Triton X-100, and either mouse anti-GFAP antibody conjugated to Alexa Fluor 488 (Millipore, MAB3402X, 1 : 1000) or mouse anti-CD11b (Abcam, Cambridge, MA, USA; AB1211, 1 : 50) overnight at 4°C. The following day, sections labeled for GFAP were washed in 0.1 M PBS, mounted on slides, and coverslipped using Pronglong Gold® with diamidino-2-phenylindole (DAPI; Invitrogen, Grand Island, NY, USA). For CD11b immunohistochemistry, sections were also washed in 0.1 M PBS and then incubated for 2 h at 23°C with a goat anti-mouse secondary antibody conjugated to Alexa Fluor 488 (Invitrogen, A11029, 1 : 1000). Sections were then washed in 0.1 M PBS, mounted on slides, and coverslipped using Pronglong Gold® with DAPI.

Image acquisition and analysis

Image analyses were completed by an experimenter blinded to treatment conditions. For DAT immunohistochemistry, images were digitized and densitometric analysis was performed using the NIH ImageJ software (http://imagej.nih.gov/ij/), yielding background-subtracted, average gray values in both DM and DL striatum. Two rostral (+1.6 mm bregma) and two middle (+0.2 mm bregma) striatal sections per rat were analyzed and averaged. Average gray values were then compared across treatment groups. For GFAP and CD11b immunohistochemistry, 3X3 (0.63 mm^2) montages in both DL and DM striatum were captured at 40X (Leica DM 4000B; 488-nm filter cube, Buffalo Grove, IL, USA). Using NIH ImageJ software, images were thesholded to include cell bodies and processes of GFAP- or CD11b-positive cells. The percent area of

the field with GFAP or CD11b signal was recorded, averaged for each animal, and compared across treatment groups. The use of this approach for quantifying astrocyte and microglia reactivity has previously been established as a reliable method for determining changes in astrocyte and microglia reactivity (LaVoie *et al.* 2004).

Statistical analysis

Statistical analysis was performed using a two-factor ANOVA (PND60 treatment × PND90 treatment) followed by *post hoc* analysis via a Student's *t*-test or Tukey's HSD test, as appropriate. Statistical analysis on body temperatures was conducted using a MANOVA with repeated measures (PND60 treatment × PND90 treatment × time) followed by a *t*-test *post hoc* analysis at individual time points to determine main effects of treatments.

Results

Experiment 1

METH-induced hyperthermia in animals sacrificed to examine GFAP expression

For body temperature data collected during treatment of this cohort of animals on PND60 (Fig. 1a), MANOVA revealed main effects of PND60 treatment ($F_{(1,24)} = 210.08$, $p < 0.0001$) and time ($F_{(4,24)} = 21.36$, $p < 0.0001$) and a significant PND60 treatment × time interaction ($F_{(1,24)} = 27.84$, $p < 0.0001$). *Post hoc* analysis revealed that the temperatures of animals receiving METH on PND60 were not different from controls at baseline (0 min, $t = 0.00$, $p = 1.0$), but were significantly greater than those receiving saline at all four time points after the injections of METH began (60 min, $t = 14.76$, $p < 0.0001$; 180 min, $t = 16.40$, $p < 0.0001$; 300 min, $t = 11.23$, $p < 0.0001$; 420 min, $t = 10.45$, $p < 0.0001$). For body temperature data collected during treatment of this cohort of animals on PND90 (Fig. 1b), MANOVA revealed main effects of PND90 treatment ($F_{(1,24)} = 208.36$, $p < 0.0001$) and time ($F_{(4,24)} = 54.79$, $p < 0.0001$) and a significant PND90 treatment × time interaction ($F_{(1,24)} = 44.73$, $p < 0.0001$). *Post hoc* analysis of the PND90 treatment × time interaction again revealed that temperatures of animals acutely receiving METH (i.e., PND 90 treatment) were not different from controls at baseline ($t = -0.86$, $p = 0.40$), but were significantly higher than those of controls at all time points after the administration of METH began (Fig. 1b; 60 min, $t = 12.91$, $p < 0.0001$; 180 min, $t = 13.08$, $p < 0.0001$; 300 min, $t = 10.61$, $p < 0.0001$; 420 min, $t = 11.46$, $p < 0.0001$). Importantly, there was no significant PND60 treatment × PND90 treatment ($F_{(1,24)} = 0.35$, $p = 0.74$) or PND60 treatment × PND90 treatment × time ($F_{(4,21)} = 1.87$, $p = 0.15$) interactions.

METH-induced DA depletions

METH-treated rats showed significant decreases in DAT immunohistochemical staining compared to saline-treated controls (Table 1). Two-factor ANOVAS for the DL and DM striatum revealed significant PND60 treatment × PND90 treatment interactions (DL striatum: $F_{(1,24)} = 29.32$, $p < 0.0001$; DM striatum: $F_{(1,24)} = 27.80$, $p < 0.0001$). *Post hoc* analysis of the interaction revealed that groups of animals treated with the neurotoxic regimen of METH at PND60, PND90, or at both time points (PND60 and PND90) were significantly different from the Saline:Saline group (Tukey's HSD test, *p*-values < 0.002; Table 1). Furthermore, DAT staining in the Saline:METH group was significantly less than that in the METH:Saline and METH:METH groups (*p*-values < 0.01), which were not different from each other ($p = 0.89$). Thus, as previously shown, rats receiving a second neurotoxic regimen of METH were resistant to further acute neurotoxicity.

Effect of METH on astrocyte reactivity

Rats treated with METH showed significant increases in GFAP immunohistochemical staining compared to saline-treated controls (Fig. 2). Two-factor ANOVAS on data for the DL and DM striatum revealed main effects of PND60 treatment (DL striatum: $F_{(1,27)} = 4.80$, $p < 0.05$; DM striatum: $F_{(1,27)} = 6.83$, $p < 0.05$) and PND90 treatment (DL striatum: $F_{(1,27)} = 9.83$, $p < 0.01$; DM striatum: $F_{(1,27)} = 32.19$, $p < 0.0001$), as well as significant PND60 treatment × PND90 treatment interactions (DL striatum: $F_{(1,108)} = 6.48$, $p < 0.02$; DM striatum: $F_{(1,108)} = 5.11$, $p < 0.05$). *Post hoc* analysis of the significant interactions revealed that all treatment groups, including those that had received the neurotoxic regimen of METH 32 days prior to sacrifice (i.e., METH:Saline group), showed significantly greater levels of GFAP immunohistochemical staining than did the Saline:Saline controls (Tukey's HSD test, *p*-values < 0.05); however, these groups that had received METH (METH:Saline, Saline:METH, METH:METH) were not significantly different (*p*-values > 0.05) from each other with respect to GFAP staining.

Experiment 2

METH-induced hyperthermia in rats sacrificed to examine CD11b expression

For body temperature data collected during treatment of this cohort of animals on PND60 (Fig. 1c), MANOVA revealed a main effect of PND60 treatment ($F_{(1,24)} = 183.33$, $p < 0.0001$) and time ($F_{(4,21)} = 51.99$, $p < 0.0001$) and a significant PND60 treatment × time interaction ($F_{(1,21)} = 31.85$, $p < 0.0001$). *Post hoc* analysis of the interaction revealed that the baseline temperatures of rats treated with saline on PND60 were slightly, but significantly ($t = -2.7$, $p < 0.05$), lower than the temperatures of rats in the METH group. However, the temperatures of animals receiving METH were significantly greater than those of animals receiving saline at all four time points after the injections of METH began (Fig. 1c; 60 min, $t = -16.70$, $p < 0.0001$;

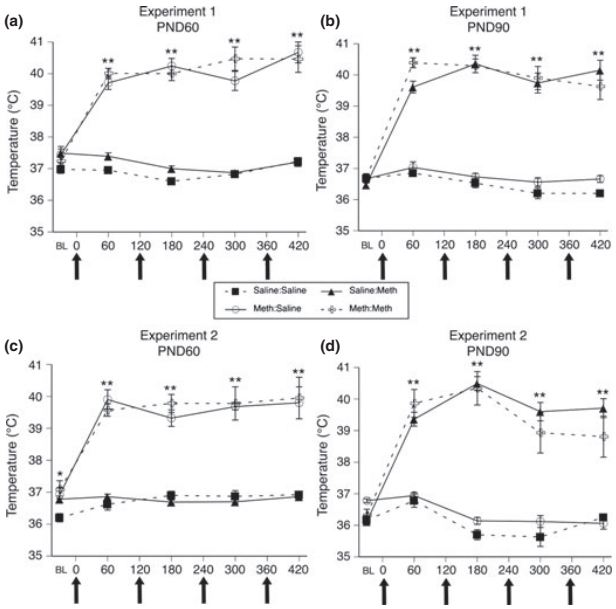

Fig. 1 Body temperatures (mean ± SEM; $n = 5$–8) of animals that received systemic injections of saline (4 × 1 mL/kg, s.c. at 2-h intervals) or (±)-METH (4 × 10 mg/kg, s.c. at 2-h intervals). Treatment group designations indicate post-natal day (PND) 60 treatment:PND90 treatment, resulting in the four treatment groups: Saline:Saline (SS); METH:Saline (MS); Saline:METH (SM); and METH:METH (MM). Temperatures were obtained 30 min prior to the first injection (baseline; BL) and 1 h after each subsequent injection. *X*-axis values represent minutes after the first injection and arrows represent the time of each saline or METH injection. Temperatures of animals sacrificed 48 h after the last injection on PND90 were recorded for experiment 1 on PND60 (a) or PND90 (b) and experiment 2 on PND60 (c) and PND90 (d). *$p < 0.005$ and **$p < 0.01$ Significant effect of METH at this time point.

Table 1 Striatal DAT immunohistochemistry following single or repeated exposure to a neurotoxic regimen of METH

	Experiment 1		Experiment 2	
	DL	DM	DL	DM
Saline:Saline	100 ± 0.73	100 ± 0.90	100 ± 2.18	100 ± 1.77
METH:Saline	72.56 ± 3.57*	62.63 ± 3.45*	65.65 ± 2.68*	65.50 ± 6.59*
Saline:METH	50.40 ± 3.48*·**·***	41.71 ± 4.45*·**·***	28.94 ± 0.95*·**·***	22.76 ± 1.42*·**·***
METH:METH	68.46 ± 4.38*	59.78 ± 5.90*	52.56 ± 3.38*·**	46.42 ± 3.56*·**

Data are mean gray values (± SEM; $n = 5$–8) from densitometric analyses expressed as a percent of the respective Saline:Saline group. Treatment group designations indicate PND60 treatment: PND90 treatment, resulting in four treatment groups: Saline:Saline; METH:Saline; Saline:METH and METH:METH. * indicates ($p < 0.01$) treatment group is significantly different from Saline:Saline. ** indicates ($p < 0.01$) that treatment group is significantly different from METH:Saline. *** indicates ($p < 0.01$) treatment group is significantly different from METH:METH.

180 min, $t = -14.83$, $p < 0.0001$; 300 min, $t = -10.39$, $p < 0.0001$; 420 min, $t = -7.93$, $p < 0.0001$). For body temperature data collected during treatment of this cohort of animals on PND90 (Fig. 1d), MANOVA revealed main effects of PND90 treatment ($F_{(1,24)} = 195.07$, $p < 0.0001$) and time ($F_{(4,24)} = 35.73$, $p < 0.0001$) and a significant PND90 treatment × time interaction ($F_{(1,24)} = 59.30$, $p < 0.0001$). *Post hoc* analysis of the significant interaction revealed that the temperatures of animals receiving METH were significantly greater than those of controls at all four time points after the injections of METH began (Fig. 1d; 60 min, $t = -10.82$, $p < 0.0001$; 180 min, $t = -16.89$, $p < 0.0001$; 300 min, $t = -9.37$, $p < 0.0001$; 420 min, $t = -9.14$, $p < 0.0001$). Importantly, there was no significant PND60 treatment × PND90 treatment interaction ($F_{(1,24)} = 1.7$, $p = 0.21$) or PND60 treatment × PND90 treatment × time interactions ($F_{(4,21)} = 1.32$, $p = 0.29$).

METH-induced DA depletions

As in Experiment 1, administration of METH to this cohort of animals resulted in significant decreases in DAT immunohistochemical staining when compared to that in saline-treated controls (Table 1). Two-factor ANOVAS for DL and DM striatum revealed main effects of PND90 treatment (DL

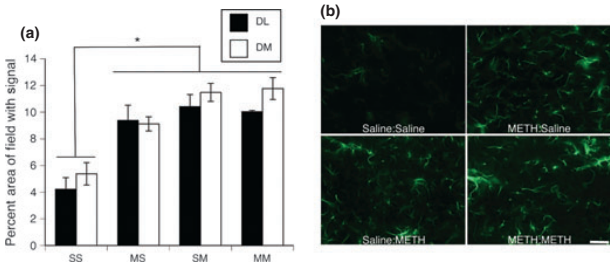

Fig. 2 (a) Quantitative analysis of the effects of single or repeated methamphetamine (METH) administration on glial-fibrillary acidic protein (GFAP) expression in striata of animals killed 48 h after the last injection on post-natal day (PND)90. Data are mean percent area of the total image field with GFAP signal above threshold (± SEM, n = 5–8) in dorsolateral (DL; black bars) and dorsomedial (DM; white bars) striatum. Treatment group designations indicate PND60 treatment:PND90 treatment, resulting in the four treatment groups: Saline:Saline (SS); METH:Saline (MS); Saline:METH (SM); and METH:METH (MM). * All groups significantly different from SS group, $p < 0.05$. (b) Representative images of GFAP immunohistochemical staining 48 h after the last injection on PND90. Scale bar = 50 μm.

striatum: $F_{(1,24)} = 254.58$, $p < 0.0001$; DM striatum: $F_{(1,24)} = 191.10$, $p < 0.0001$) and significant PND60 treatment × PND90 treatment interactions (DL striatum: $F_{(1,24)} = 101.31$, $p < 0.0001$; DM striatum: $F_{(1,24)} = 70.35$, $p < 0.0001$). *Post hoc* analyses of the interactions revealed that all treatment groups were significantly different from all other treatment groups (Tukey's HSD test, p-values < 0.005; Table 1).

Effect of METH on microglia reactivity

Administration of a neurotoxic regimen of METH on PND90 resulted in a significant increase in immunohistochemical staining for CD11b expression only in animals acutely experiencing toxicity (i.e., Saline:METH group; Fig. 3). Two-factor ANOVAS for the DL and DM striatum revealed main effects of PND60 treatment (DL striatum: $F_{(1,24)} = 5.90$, $p < 0.05$; DM striatum: $F_{(1,24)} = 3.02$, $p = 0.095$), main effects of PND90 treatment (DL striatum: $F_{(1,24)} = 23.48$, $p < 0.0001$; DM striatum: $F_{(1,24)} = 19.24$, $p < 0.0002$), and significant PND60 treatment × PND90 treatment interactions (DL striatum: $F_{(1,24)} = 6.76$, $p < 0.02$; DM striatum: $F_{(1,24)} = 4.37$, $p < 0.05$). *Post hoc* analyses of the interactions revealed that CD11b immunohistochemical staining in the Saline:METH group was significantly greater than that in all other treatment groups (Tukey's HSD test, p-values < 0.03; Fig. 3). Conversely, staining was not different between any of the other three groups (i.e., Saline:Saline, METH:Saline, and METH:METH); p-values > 0.2).

Discussion

METH abuse continues to be a significant public health concern, and recent studies report increased incidence of Parkinson's Disease among individuals with a history of amphetamine use (Callaghan *et al.* 2010, 2012). Although it is established that METH exposure results in damage to the DA

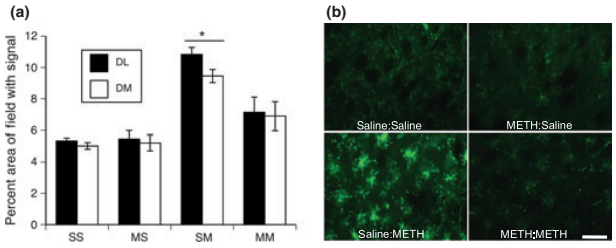

Fig. 3 (a) Quantitative analysis of the effects of single or repeated methamphetamine (METH) exposure on CD11b expression in striata of animals killed 48 h after the last injection on post-natal day (PND)90. Data are mean percent area of the total image field with CD11b signal above threshold (± SEM, n = 5–8) in dorsolateral (DL; black bars) and dorsomedial (DM; white bars) striatum. Treatment group designations indicate PND60 treatment:PND90 treatment, resulting in the four treatment groups: Saline:Saline (SS); METH:Saline (MS); Saline:METH (SM); and METH:METH (MM). * SM group significantly different from all other groups, $p < 0.05$. (b) Representative images of CD11b immunohistochemical staining 48 h after the last injection on PND90. Scale bar = 50 μm.

system, the cascade of events that ultimately results in DA terminal degeneration is not as well understood. Studies using animal models of METH-induced neurotoxicity show robust activation of both astrocytes and microglia (Bowyer *et al.* 1994; O'Callaghan and Miller 1994; Guilarte *et al.* 2003; LaVoie *et al.* 2004; Thomas *et al.* 2004), and recent work demonstrates reactive microglia (Sekine *et al.* 2008; Kitamura *et al.* 2010) and increased density of GFAP-positive astrocytes (Kitamura *et al.* 2010) in brains of human METH abusers. In addition, there is a growing amount of evidence indicating that amphetamine abuse has a high rate of comorbidity among individuals infected with human immunodeficiency virus (HIV) (Harris *et al.* 1993; Crofts *et al.* 1994). Given data suggesting combined effects of HIV and METH, including increased HIV viral load (Ellis *et al.* 2003), synergistic damage to the DA system (Maragos *et al.* 2002), altered glial response (Kaul and Lipton 1999; Zhao *et al.* 2001) and increased cytokine production (Shah *et al.* 2012a,b), studies investigating the role of glial cells in METH-induced neurotoxicity are essential to identifying factors contributing to or mitigating METH-induced damage to DA nerve terminals.

Using an established model (Thomas and Kuhn 2005; Hanson *et al.* 2009) of resistance to acute METH-induced DA terminal injury, this study examined the extent to which animals rendered resistant to further DA depletions are also resistant to astrocyte and microglia reactivity following the second neurotoxic regimen of METH. Consistent with previous work, we demonstrate that exposure to a neurotoxic regimen of METH results in significant astrocyte activation as assessed 48 h after the last injection (i.e., in the Saline:METH group). However, we extend these previous findings by showing that GFAP expression remains elevated compared to controls even 32 days after exposure to a neurotoxic regimen of METH (i.e., in the METH:Saline group). Furthermore, the present findings reveal that the degree of GFAP expression is similar in animals exposed to METH and experiencing acute toxicity (Saline:METH) and those exposed to METH but not experiencing acute toxicity (METH:METH). Also consistent with prior work (Thomas and Kuhn 2005), the present data confirm that activation of microglia mirrors acute DA neuron toxicity, as only animals experiencing acute DA neuron toxicity (i.e., the Saline:METH group) show an increase in CD11b immunohistochemical staining. Thus, these data support the conclusion that activation of microglia, rather than astrocytes, is associated with the acute toxic effects of METH on DA nerve terminals, although we cannot rule out a potential role of persistent astrocyte activation in resistance to acute METH-induced DA terminal toxicity.

Astrocytes have been shown to play important roles in normal brain function, such as neurotransmission and synaptic function, but have also been implicated in several central nervous system (CNS) diseases. GFAP immunohistochemistry is commonly used to assess astrocyte reactivity (Sofroniew and Vinters 2010) and is increased following various CNS pathologies (Hozumi *et al.* 1990; Zhang *et al.* 1999; Borges *et al.* 2003). Herein, we examined GFAP expression in animals that received single or repeated administration of a neurotoxic regimen of METH. In saline-treated control animals (Saline:Saline), GFAP is minimally expressed in striatum. Conversely, in animals treated with METH (METH:Saline, Saline:METH, and METH:METH), GFAP expression is much more dispersed throughout the entire striatum. In these groups, GFAP expression was much more intense and astrocytes took on a more reactive phenotype with thicker processes. To our knowledge, this is the first study to show that GFAP expression remains elevated in METH-exposed rats as far out as 32 days post-treatment. However, these data are consistent with previous work showing elevated GFAP expression in METH-exposed mice 21 days post-treatment (O'Callaghan and Miller 1994) and in primates 30 days post-METH exposure (Harvey *et al.* 2000). It is important to note, however, that in the study examining GFAP expression in mice 21 days following METH exposure (O'Callaghan and Miller 1994), GFAP expression was elevated compared to controls at 21 days, but the expression was decreased compared to GFAP levels in animals examined 2 days after exposure to METH. In the current work, we did not find significant differences in GFAP expression in animals treated with METH 32 days prior and those treated 2 days prior. However, in our work and the work of O'Callaghan and colleagues, the GFAP expression remains elevated for extended periods of time (O'Callaghan and Miller 1994).

It is presently unclear whether persistent astrocytosis in animals previously exposed to a neurotoxic regimen of METH may play a role in the resistance to further DA depletions seen in these animals. For example, astrocytes are key regulators of extracellular glutamate (GLU) via GLU transporters (Anderson and Swanson 2000). Given significant implication of GLU in METH-induced neurotoxicity (Sonsalla *et al.* 1989; Nash and Yamamoto 1992; O'Dell *et al.* 1992; Mark *et al.* 2004; Gross *et al.* 2011; Halpin and Yamamoto 2012; Shah *et al.* 2012b), it is tempting to speculate that changes in transporter expression or activity associated with increased GFAP expression following the first neurotoxic regimen of METH (PND60) may allow for more efficient astrocyte-mediated GLU buffering during the second METH administration (PND90). Astrocytes are also known to be involved in blood–brain barrier (BBB) function (Bowyer and Ali 2006), and changes in BBB during and following METH exposure have been documented (Abbott *et al.* 2006; Ramirez *et al.* 2009; Sharma and Kiyatkin 2009). Therefore, changes in astrocyte reactivity following the initial exposure to METH (PND60) could result in changes in the BBB function, resulting in protection against toxicity when animals are exposed again at PND90. Other possible areas of investigation related to astrocyte activity include protection against oxidative stress via glutathione

production (Chen *et al.* 2001; Shih *et al.* 2003), protection against ammonia toxicity (Halpin and Yamamoto 2012), and regulation of inflammatory responses (Min *et al.* 2006; Okada *et al.* 2006; Shah *et al.* 2012b). Whether such enhanced functions of astrocytes underlie resistance to METH-induced DA terminal remains to be examined.

In this study, elevated GFAP expression was noted in animals exposed to the neurotoxic regimen of METH but not experiencing acute toxicity (i.e., the METH:METH group), suggesting a dissociation between reactive astrogliosis and METH-induced neurotoxicity. However, it remains possible that astrocytes are necessary for acute METH-induced neurotoxicity. The elevated GFAP expression in the METH:METH group likely reflects the persistent GFAP expression arising from the first exposure to the neurotoxic regimen on PND60, as is apparent in the METH:Saline group. In the METH:METH group, there is a lack of further acute activation of astrocytes in response to the second METH regimen on PND90 and a lack of further acute DA neurotoxicity. Thus, the apparent lack of further astrocyte activation and the lack of further toxicity may be linked. Our current understanding of the conditions under which astrocytes become activated, the nature of that activation, and the extent to which they provide detrimental versus beneficial effects in the setting of CNS injury is in its infancy (Sofroniew 2009). Thus, although all of the METH-treated groups show similar levels of GFAP expression, it is thus possible that there are differences in the functions of seemingly similar 'reactive' astrocytes under different METH-exposure conditions and that these differences in function are not reflected in differences in GFAP expression (Sofroniew 2009). It is also possible that the immunhistochemical detection of GFAP used herein may not be sensitive to subtle differences in GFAP expression, as prior work by O'Callaghan and Miller (1994) in mice have suggested some recovery of GFAP expression as assessed by an enzyme-linked immunosorbent assay three weeks after exposure to a similar neurotoxic regimen, whereas such recovery is not apparent in this work. Prior studies of neurotoxicity associated with a single bolus injection of METH in mice show that minocycline pre-treatment prevents the activation of microglia, but does not protect against toxicity or increases in GFAP expression (Sriram *et al.* 2006), suggesting an association between reactive astrocytosis, but not reactive microglia, and METH-induced neurotoxicity. However, that prior study was conducted using a single bolus regimen of METH, and other data suggest notable differences in the nature of the neurotoxicity resulting from a single bolus versus a neurotoxic binge regimen of METH (Zhu *et al.* 2006). Clearly, additional studies are necessary to discern the role of astrocytes in the persistent monoamine neurotoxicity induced by METH and to further define the phenotype of astrocytes under different METH-exposure conditions.

Microglia are the primary antigen-presenting cells in the CNS and also become highly reactive following various CNS insults. Microglia have been shown to migrate to sites of injury and to secrete pro-inflammatory cytokines, as well as a variety of other factors (Hanisch 2002). Reactive microglia have been observed in the brains of both animals (Guilarte *et al.* 2003; LaVoie *et al.* 2004; Thomas *et al.* 2004) exposed to METH and in the brains of human METH abusers (Sekine *et al.* 2008; Kitamura *et al.* 2010). Interestingly, Thomas and colleagues have shown that when animals are pre-treated with a neurotoxic regimen of METH, allowed to recover for 7 days, and treated with a subsequent neurotoxic regimen of METH, they no longer demonstrate significant microglial activation. Similarly, here we show that when the recovery period between METH treatments is extended to 30 days, animals still remain resistant to acute DA-terminal injury and activation of microglia. Activated microglia are often characterized as having retracted, thickened processes with increased cell body size, whereas their 'resting' counterparts demonstrate finely branched processes and ramified morphology and small cell body (Kreutzberg 1996). In control animals and those exposed to METH only at PND60 (METH:Saline), the resting microglia morphology was observed. Similarly, striatal sections from animals resistant to further toxicity also exhibited resting microglia morphology, as reflected in CD11b immunohistochemistry. Conversely, animals exposed to METH on PND90 and experiencing acute toxicity (Saline:METH) exhibited significant thickening of branches and more intense microglia cell body staining. These data are consistent with the findings of Thomas and colleagues (Thomas and Kuhn 2005) and suggest that microglia reactivity remains a specific marker for acute damage to DA terminals following a neurotoxic regimen of METH. However, whether microglial activation contributes to or simply mirrors METH-induced neurotoxicity remains unknown.

Clearly, more direct experiments using pharmacological and genetic manipulations of astrocyte and microglia activation are needed to determine the role of these two cell types in METH-induced DA terminal degeneration. Studies investigating the molecular triggers for the activation of astrocytes and microglia following methamphetamine exposure will lead to a better understanding of the cascade of events that ultimately results in changes in these cells. Finally, more specific markers for the different stages of activation of both astrocytes and microglia are needed to further tease apart the differences in degree of activation and activity of these two cell types following METH exposure.

Acknowledgements

This study was supported by the National Institute of Drug Abuse [Grant DA 013367].

The authors declare no conflicts of interest.

Authorship credit

Contribution to design and interpretation of data: Friend, Keefe; data acquisition and analysis: Friend, Keefe; Drafting article and revising: Friend, Keefe; final approval of the version to be published: Friend, Keefe; the authors thank Dr. Steve O'Dell in Dr. John Marshall's laboratory for assistance with the DAT immunohistochemistry assay.

References

Abbott N. J., Ronnback L. and Hansson E. (2006) Astrocyte-endothelial interactions at the blood-brain barrier. *Nat. Rev. Neurosci.* **7**, 41–53.

Anderson C. M. and Swanson R. A. (2000) Astrocyte glutamate transport: review of properties, regulation, and physiological functions. *Glia* **32**, 1–14.

Borges K., Gearing M., McDermott D. L., Smith A. B., Almonte A. G., Wainer B. H. and Dingledine R. (2003) Neuronal and glial pathological changes during epileptogenesis in the mouse pilocarpine model. *Exp. Neurol.* **182**, 21–34.

Bowyer J. F. and Ali S. (2006) High doses of methamphetamine that cause disruption of the blood-brain barrier in limbic regions produce extensive neuronal degeneration in mouse hippocampus. *Synapse* **60**, 521–532.

Bowyer J. F., Davies D. L., Schmued L., Broening H. W., Newport G. D., Slikker W. Jr. and Holson R. R. (1994) Further studies of the role of hyperthermia in methamphetamine neurotoxicity. *J. Pharmacol. Exp. Ther.* **268**, 1571–1580.

Callaghan R. C., Cunningham J. K., Sajeev G. and Kish S. J. (2010) Incidence of Parkinson's disease among hospital patients with methamphetamine-use disorders. *Mov. Disord.* **25**, 2333–2339.

Callaghan R. C., Cunningham J. K., Sykes J. and Kish S. J. (2012) Increased risk of Parkinson's disease in individuals hospitalized with conditions related to the use of methamphetamine or other amphetamine-type drugs. *Drug Alcohol Depend.* **120**, 35–40.

Cappon G. D., Morford L. L. and Vorhees C. V. (1997) Ontogeny of methamphetamine-induced neurotoxicity and associated hyperthermic response. *Brain Res. Dev. Brain Res.* **103**, 155–162.

Chen Y., Vartiainen N. E., Ying W., Chan P. H., Koistinaho J. and Swanson R. A. (2001) Astrocytes protect neurons from nitric oxide toxicity by a glutathione-dependent mechanism. *J. Neurochem.* **77**, 1601–1610.

Crofts N., Hopper J. L., Milner R., Breschkin A. M., Bowden D. S. and Locarnini S. A. (1994) Blood-borne virus infections among Australian injecting drug users: implications for spread of HIV. *Eur. J. Epidemiol.* **10**, 687–694.

Ellis R. J., Childers M. E., Cherner M., Lazzaretto D., Letendre S. and Grant I. and Group H. I. V. N. R. C. (2003) Increased human immunodeficiency virus loads in active methamphetamine users are explained by reduced effectiveness of antiretroviral therapy. *J. Infect. Dis.* **188**, 1820–1826.

Fleckenstein A. E., Metzger R. R., Wilkins D. G., Gibb J. W. and Hanson G. R. (1997) Rapid and reversible effects of methamphetamine on dopamine transporters. *J. Pharmacol. Exp. Ther.* **282**, 834–838.

Friend D. M., Son J. H., Keefe K. A. and Fricks-Gleason A. N. (2013) Expression and activity of nitric oxide synthase isoforms in methamphetamine-induced striatal dopamine toxicity. *J. Pharmacol. Exp. Ther.* **344**, 511–521.

Gross N. B., Duncker P. C. and Marshall J. F. (2011) Cortical ionotropic glutamate receptor antagonism protects against methamphetamine-induced striatal neurotoxicity. *Neuroscience* **199**, 272–283.

Guilarte T. R., Nihei M. K., McGlothan J. L. and Howard A. S. (2003) Methamphetamine-induced deficits of brain monoaminergic neuronal markers: distal axotomy or neuronal plasticity. *Neuroscience* **122**, 499–513.

Halpin L. E. and Yamamoto B. K. (2012) Peripheral ammonia as a mediator of methamphetamine neurotoxicity. *J. Neurosci.* **32**, 13155–13163.

Hanisch U. K. (2002) Microglia as a source and target of cytokines. *Glia* **40**, 140–155.

Hanson J. E., Birdsall E., Seferian K. S., Crosby M. A., Keefe K. A., Gibb J. W., Hanson G. R. and Fleckenstein A. E. (2009) Methamphetamine-induced dopaminergic deficits and refractoriness to subsequent treatment. *Eur. J. Pharmacol.* **607**, 68–73.

Harris N. V., Thiede H., McGough J. P. and Gordon D. (1993) Risk factors for HIV infection among injection drug users: results of blinded surveys in drug treatment centers, King County, Washington 1988-1991. *J. Acquir. Immune Defic. Syndr.* **6**, 1275–1282.

Harvey D. C., Lacan G., Tanious S. P. and Melega W. P. (2000) Recovery from methamphetamine induced long-term nigrostriatal dopaminergic deficits without substantia nigra cell loss. *Brain Res.* **871**, 259–270.

Hozumi I., Aquino D. A. and Norton W. T. (1990) GFAP mRNA levels following stab wounds in rat brain. *Brain Res.* **534**, 291–294.

Kaul M. and Lipton S. A. (1999) Chemokines and activated macrophages in HIV gp120-induced neuronal apoptosis. *Proc. Natl Acad. Sci. USA* **96**, 8212–8216.

Kitamura O., Takeichi T., Wang E. L., Tokunaga I., Ishigami A. and Kubo S. (2010) Microglial and astrocytic changes in the striatum of methamphetamine abusers. *Leg. Med.* **12**, 57–62.

Kogan F. J., Nichols W. K. and Gibb J. W. (1976) Influence of methamphetamine on nigral and striatal tyrosine hydroxylase activity and on striatal dopamine levels. *Eur. J. Pharmacol.* **36**, 363–371.

Kreutzberg G. W. (1996) Microglia: a sensor for pathological events in the CNS. *Trends Neurosci.* **19**, 312–318.

LaVoie M. J., Card J. P. and Hastings T. G. (2004) Microglial activation precedes dopamine terminal pathology in methamphetamine-induced neurotoxicity. *Exp. Neurol.* **187**, 47–57.

Maragos W. F., Young K. L., Turchan J. T., Guseva M., Pauly J. R., Nath A. and Cass W. A. (2002) Human immunodeficiency virus-1 Tat protein and methamphetamine interact synergistically to impair striatal dopaminergic function. *J. Neurochem.* **83**, 955–963.

Mark K. A., Soghomonian J. J. and Yamamoto B. K. (2004) High-dose methamphetamine acutely activates the striatonigral pathway to increase striatal glutamate and mediate long-term dopamine toxicity. *J. Neurosci.* **24**, 11449–11456.

McCann U. D., Wong D. F., Yokoi F., Villemagne V., Dannals R. F. and Ricaurte G. A. (1998) Reduced striatal dopamine transporter density in abstinent methamphetamine and methcathinone users: evidence from positron emission tomography studies with [11C] WIN-35,428. *J. Neurosci.* **18**, 8417–8422.

Min K. J., Yang M. S., Kim S. U., Jou I. and Joe E. H. (2006) Astrocytes induce hemeoxygenase-1 expression in microglia: a feasible mechanism for preventing excessive brain inflammation. *J. Neurosci.* **26**, 1880–1887.

Nash J. F. and Yamamoto B. K. (1992) Methamphetamine neurotoxicity and striatal glutamate release: comparison to 3,4-methylenedioxymethamphetamine. *Brain Res.* **581**, 237–243.

O'Callaghan J. P. and Miller D. B. (1994) Neurotoxicity profiles of substituted amphetamines in the C57BL/6J mouse. *J. Pharmacol. Exp. Ther.* **270**, 741–751.

O'Dell S. J., Weihmuller F. B. and Marshall J. F. (1992) MK-801 prevents methamphetamine-induced striatal dopamine damage and reduces extracellular dopamine overflow. *Ann. N. Y. Acad. Sci.* **648**, 317–319.

Okada S., Nakamura M., Katoh H. *et al.* (2006) Conditional ablation of Stat3 or Socs3 discloses a dual role for reactive astrocytes after spinal cord injury. *Nat. Med.* **12**, 829–834.

Ramirez S. H., Potula R., Fan S. *et al.* (2009) Methamphetamine disrupts blood-brain barrier function by induction of oxidative stress in brain endothelial cells. *J. Cereb. Blood Flow Metab.* **29**, 1933–1945.

Sekine Y., Ouchi Y., Sugihara G. *et al.* (2008) Methamphetamine causes microglial activation in the brains of human abusers. *J. Neurosci.* **28**, 5756–5761.

Shah A., Silverstein P. S., Kumar S., Singh D. P. and Kumar A. (2012a) Synergistic cooperation between methamphetamine and HIV-1 gsp120 through the P13K/Akt pathway induces IL-6 but not IL-8 expression in astrocytes. *PLoS ONE* **7**, e52060.

Shah A., Silverstein P. S., Singh D. P. and Kumar A. (2012b) Involvement of metabotropic glutamate receptor 5, AKT/PI3K signaling and NF-kappaB pathway in methamphetamine-mediated increase in IL-6 and IL-8 expression in astrocytes. *J. Neuroinflammation* **9**, 52.

Sharma H. S. and Kiyatkin E. A. (2009) Rapid morphological brain abnormalities during acute methamphetamine intoxication in the rat: an experimental study using light and electron microscopy. *J. Chem. Neuroanat.* **37**, 18–32.

Shih A. Y., Johnson D. A., Wong G., Kraft A. D., Jiang L., Erb H., Johnson J. A. and Murphy T. H. (2003) Coordinate regulation of glutathione biosynthesis and release by Nrf2-expressing glia potently protects neurons from oxidative stress. *J. Neurosci.* **23**, 3394–3406.

Sofroniew M. V. (2009) Molecular dissection of reactive astrogliosis and glial scar formation. *Trends Neurosci.* **32**, 638–647.

Sofroniew M. V. and Vinters H. V. (2010) Astrocytes: biology and pathology. *Acta Neuropathol.* **119**, 7–35.

Sonsalla P. K., Nicklas W. J. and Heikkila R. E. (1989) Role for excitatory amino acids in methamphetamine-induced nigrostriatal dopaminergic toxicity. *Science* **243**, 398–400.

Sriram K., Miller D. B. and O'Callaghan J. P. (2006) Minocycline attenuates microglial activation but fails to mitigate striatal dopaminergic neurotoxicity: role of tumor necrosis factor-alpha. *J. Neurochem.* **96**, 706–718.

Thomas D. M. and Kuhn D. M. (2005) Attenuated microglial activation mediates tolerance to the neurotoxic effects of methamphetamine. *J. Neurochem.* **92**, 790–797.

Thomas D. M., Walker P. D., Benjamins J. A., Geddes T. J. and Kuhn D. M. (2004) Methamphetamine neurotoxicity in dopamine nerve endings of the striatum is associated with microglial activation. *J. Pharmacol. Exp. Ther.* **311**, 1–7.

Wagner G. C., Ricaurte G. A., Seiden L. S., Schuster C. R., Miller R. J. and Westley J. (1980) Long-lasting depletions of striatal dopamine and loss of dopamine uptake sites following repeated administration of methamphetamine. *Brain Res.* **181**, 151–160.

Zhang Z. G., Bower L., Zhang R. L., Chen S., Windham J. P. and Chopp M. (1999) Three-dimensional measurement of cerebral microvascular plasma perfusion, glial fibrillary acidic protein and microtubule associated protein-2 immunoreactivity after embolic stroke in rats: a double fluorescent labeled laser-scanning confocal microscopic study. *Brain Res.* **844**, 55–66.

Zhao M. L., Kim M. O., Morgello S. and Lee S. C. (2001) Expression of inducible nitric oxide synthase, interleukin-1 and caspase-1 in HIV-1 encephalitis. *J. Neuroimmunol.* **115**, 182–191.

Zhu J. P., Xu W., Angulo N. and Angulo J. A. (2006) Methamphetamine-induced striatal apoptosis in the mouse brain: comparison of a binge to an acute bolus drug administration. *Neurotoxicology* **27**, 131–136.

CHAPTER 4

PROLIFERATION OF GLIAL CELLS IN STRIATUM FOLLOWING REPEATED METHAMPHETAMINE EXPOSURE

4.1 Abstract

Following brain injury, progenitor cells have the ability to differentiate into neurons and/or glia. Previous work has suggested that a single bolus regimen of methamphetamine (METH) increases the number of proliferating cells in striatum and that some proliferating cells colocalize with beta-III tubulin, suggesting a neuronal fate. However, the identity of these cells has not been clearly elucidated. Also, the extent to which such proliferation is induced simply by exposure to METH or is associated with METH-induced neurotoxicity has not heretofore been examined. Data from our lab and others indicate that rats with partial dopamine (DA) loss resulting from prior exposure to METH are resistant to further decreases in striatal DA when reexposed to METH 30 days later. This experimental paradigm thus allows for examination of factors associated with METH-induced toxicity in animals matched for acute METH exposure, but differentiated with respect to acute METH-induced neurotoxicity. Therefore, this study examined cellular proliferation (BrdU and Ki67) in striata of animals administered saline or a neurotoxic regimen of METH on postnatal days 60 and/or 90 (Saline:Saline, Saline:METH, METH:Saline, METH:METH). Consistent with previous work, we found that animals exposed to METH and acutely experiencing toxicity (Saline:METH) showed an increase in striatal proliferation compared to all other treatment groups. Furthermore, using double-label immunohistochemistry, we determined that a large proportion of the proliferating cells in the Saline:METH treatment group were microglia (CD11b+). Only a small proportion of proliferating cells were astrocytes (GFAP+) or neurons (NeuN+). The results presented herein are consistent with previous reports in that we observe an increase in proliferation following METH exposure. However, we extend the current knowledge by demonstrating that a large proportion of these proliferating cells are also

positive for markers of microglia, suggesting a significant contribution of glial proliferation to the total amount of METH-induced proliferation, and that the increase in proliferation only occurs in animals exposed to METH and experiencing acute toxicity suggesting that microglia reactivity parallels METH-induced neurotoxicity.

4.2 Introduction

Methamphetamine (METH) abuse and the resulting neurotoxicity is a considerable public health concern. METH exposure results in persistent damage to the dopaminergic system in both human METH abusers and in animal models. METH-induced damage to the dopamine (DA) system is reflected in decreased DA tissue content (Kogan et al., 1976; Wagner et al., 1980), dopamine transporter (DAT) binding (Fleckenstein et al., 1997; McCann et al., 1998), tyrosine hydroxylase (TH) immunohistochemical staining (Kogan et al., 1976), and vesicular monoamine transporter activity (Guilarte et al., 2003) in striatum. The importance of elucidating the cascade of events that occurs during and following METH exposure that ultimately results in METH-induced neurotoxicity has only grown due to new evidence indicating that individuals with a history of amphetamine abuse have an increased risk for developing Parkinson's Disease years later (Callaghan et al., 2010; Callaghan et al., 2012).

Multipotent progenitor cells are present in the adult mammalian central nervous system and have the capacity to divide and differentiate into multiple cell types including neurons, astroglia, and oligodendrocytes (for review see De Filippis and Binda, 2012). Recent work has shown cellular proliferation in striatum in response to various CNS injuries including ischemia (Parent et al., 2002), excitotoxicity (Dihne et al., 2001; Collin

et al., 2005), and exposure to neurotoxic drugs including 6-hydroxydopamine (6-OHDA)(Aponso et al., 2008; Wachter et al., 2010) and 1-methyl-4-phenyl-1,2,3,6-tetrahydropyridine (MPTP) (Kay and Blum, 2000; Mao et al., 2001). In particular, increased striatal cellular proliferation has been observed in mice following administration of a bolus injection of a high dose of METH (Tulloch et al., 2011a; Tulloch et al., 2011b; Tulloch et al., 2011c). In these latter studies, at least a portion of the proliferating cells co-localized with beta-III tubulin, suggesting a neuronal phenotype. However, this study did not quantify the degree of co-localization between markers of proliferation and beta-III tublin and did not examine markers for other cells types that may also contribute to the increase in proliferation (Tulloch et al., 2011a). Interestingly, the work by Tulloch and colleagues showed that proliferation peaked at 2 days post-METH treatment, a time point at which it is well established that glial cells are highly reactive (LaVoie et al., 2004; Thomas et al., 2004). Furthermore, as mentioned above, exposure to MPTP or 6-OHDA is associated with increased proliferation in striatum, and immunohistochemical staining identified these proliferating cells as astrocytes and microglia (Kay and Blum, 2000; Mao et al., 2001; Aponso et al., 2008; Wachter et al., 2010). Thus, given the established time course of astrocyte and microglia activation following METH exposure and data indicating significant glial proliferation following exposure to other neurotoxic drugs, the extent to which proliferation following METH exposure is, at least in part, glial-derived requires scrutiny.

While the data noted above (Tulloch et al., 2011a; Tulloch et al., 2011b; Tulloch et al., 2011c) indicate that exposure to METH is associated with proliferation in the striatum, the extent to which the proliferation is a response to METH exposure alone or is

associated with METH-induced neurotoxicity is unknown. Our lab and others (Thomas and Kuhn, 2005; Hanson et al., 2009) have conducted studies in which animals are treated with a neurotoxic regimen of METH and animals are challenged 7 or 30 days later with a second neurotoxic regimen of METH. These studies revealed that such animals are resistant to acute DA neuron toxicity upon exposure to the second METH regimen (Thomas and Kuhn, 2005; Hanson et al., 2009). This experimental paradigm thus allows for the examination of factors associated with METH-induced neurotoxicity in animals matched for acute METH exposure, but differentiated with respect to acute toxicity. In the present study, we therefore used this paradigm to examine proliferation in striata of animals exposed to METH and experiencing acute toxicity (Saline:METH) and in animals exposed to METH but not experiencing acute toxicity (METH:METH). We then determined the identity of proliferating cells using double-label immunohistochemistry with markers of proliferation, including Ki67 (endogenous marker of actively dividing cells, (Bacchi and Gown, 1993)) and BrdU (synthetic analog of thymidine incorporated into newly synthesized DNA (Gratzner, 1982)) with markers for neurons (NeuN), astrocytes (GFAP), and microgla (CD11b). The results presented here are consistent with previous reports in that we observe an increase in proliferation and microglial reactivity following METH exposure. However, we extend the current knowledge by demonstrating that the increase in proliferation only occurs in animals exposed to METH and experiencing acute toxicity, but not in those resistant to such toxicity. Finally, we also show that a large proportion of these proliferating cells are microglia, suggesting a significant contribution of glial proliferation to the total amount of METH-induced proliferation.

4.3 Experimental procedures

4.3.1 Animals

Male Sprague-Dawley rats (Charles River Laboratories, Raleigh, NC) were housed in wire mesh cages in a temperature-controlled room on a 12:12hr light:dark cycle with free access to food and water. All animal care and experimental procedures were in accordance with the *Guide for the Care and Use of Laboratory Animals* (8th Ed., National Research Council) and were approved by the Institutional Animal Care and Use Committee at the University of Utah.

4.3.2 METH and BrdU administration

METH and saline injections were completed as previously described (Friend et al., 2013). On treatment days (PND60 and PND90), rats were housed in groups of 6 in plastic tub cages (33cm x 28cm x 17cm) with corncob bedding. Animals received four injections of (±)-METH-HCl (4 x 10 mg free base/kg, s.c., at 2hr intervals; provided by the National Institute on Drug Abuse) or 0.9% saline (4 x 1 ml/kg, s.c., at 2hr intervals). Rectal temperatures were monitored using a digital thermometer (BAT-12, Physitemp Instruments, Clifton, NJ) to ensure that METH-induced hyperthermia occurred. Baseline temperatures were taken 30 min prior to the first injection and 1hr after each subsequent injection. If the body temperature of an animal exceeded 40.5°C, the animal was transferred to a cage placed over wet ice until the body temperature fell below 39°C. Approximately 18hr after the last injection on PND60, animals were returned to wire mesh cages in the colony room and allowed to recover for 30 days. On PND90, animals were again transferred to plastic tub cages and treated with either METH or saline as described above. This treatment regimen resulted in four treatment groups based on the

animals' PND60:PND90 treatments; Saline:Saline, Saline:METH, METH:Saline, and METH:METH. For BrdU experiments, animals were treated with METH or saline on PND60 and PND90 as described above; however, animals also received an injection of BrdU (100 mg/kg, i.p; Sigma-Aldrich, B5002) dissolved in water 24hr after their last injection on PND90.

4.3.3 Tissue preparation

Animals were sacrificed on PND92 via exposure to CO_2 for 1 min (see Figure 4.1 for experiment time-lines). Following decapitation, brains were rapidly removed and submerged in 4% formaldehyde with 0.9% NaCl for 24hr at 4°C, then cryoprotected in 30% sucrose in 0.1M PBS and stored at 4°C. Brains were then sectioned at 30 μm on a freezing microtome (Microm, HM 440E). For each animal, coronal sections of striatum (+1.6 mm to +0.2 mm relative to bregma) were sectioned and stored at 4°C in 1mg/ml sodium azide in 0.1M PBS, as previously described (Friend and Keefe, 2013).

4.3.4 Immunohistochemistry

To determine METH-induced DA depletions, DAT immunohistochemistry was completed as previously described (Friend and Keefe, 2013). Briefly, sections were subject to heat-mediated antigen retrieval, followed by incubation in 3% H_2O_2, and then washed in PBS. Nonspecific antibody binding was blocked by incubating tissue in 0.1 M PBS containing 5% milk and 0.2% Triton X-100 for 60 min. Sections were then incubated overnight at 4°C in a primary antibody solution (rat anti-DAT antibody (Millipore, MAB369, 1:5000)). The following day, tissue was washed, incubated in a

secondary antibody solution (biotinylated goat anti-rat IgG (Vector Labs, BA-4000, 1:200)), incubated in avidin-biotinylated peroxidase complex solution (ABC Elite Kit, Vector Labs, PK-6100), and washed. The sections were then incubated in nickel-enhanced +3,3'-diaminobenzidine tetrahydrochloride (Ni-DAB; Vector, SK-4100), washed again, mounted onto slides, dried, dehydrated and coverslipped with VectaMount (Vector Labs, H-5000).

For BrdU immunhistochemistry, sections were washed in 2x SSC buffer (0.15 M NaCl with 0.015 M sodium citrate) followed by incubation in 2 N hydrochloric acid for 1hr at room temperature (RT). Sections were then washed in 0.01M sodium borate buffer followed by a wash in 0.1 M PBS. Nonspecific antibody binding was blocked by incubating sections in 5% normal horse serum with 0.02% Triton X-100 in 0.1M PBS for 1hr at RT. Sections were then incubated in a primary antibody solution containing 2% normal horse serum, 0.2% Triton X-100, and sheep anti-BrdU antibody (Novis Biologicals, NB 500-235, 1:5000) in 0.1M PBS overnight at 4°C. The following day, sections were washed and incubated in a secondary antibody solution containing 2% normal horse serum, 0.2% Triton X-100, and donkey anti-sheep IgG conjugated to Alexa Fluor 555 (Invitrogen, A21436, 1:200). Finally, sections were washed in 0.1M PBS, mounted on slides, and coverslipped using Prolong Gold® with DAPI (Invitrogen, 1034067).

For Ki67 immunohistochemistry, sections were initially washed in 0.1M PBS and nonspecific antibody binding was blocked by incubating in 0.1M PBS containing 10% goat serum with 0.2% Triton X-100 for 1hr at RT. Sections were then incubated in primary antibody solution containing 5% goat serum, 0.2% Triton-X 100 and rabbit anti-

Ki67 antibody (Abcam, ab16667, 1:50) overnight at 4°C. The following day, sections were washed in 0.1M PBS and incubated in a secondary antibody solution containing 5% goat serum, 0.2% Triton X-100, and goat anti-rabbit IgG conjugated to Alexa Fluor 555 (Invitrogen, A21428, 1:1000) for 1hr at RT. Finally, sections were washed in 0.1M PBS, mounted on slides, and coverslipped as described above for BrdU. The quantification of proliferation using Ki67 immunohistochemistry was consistent with the quantification of proliferation using BrdU immunohistochemistry. Therefore, because Ki67 immunohistochemistry is more easily combined with other immunohistochemical protocols, we used Ki67 immunohistochemistry for all double-label immunohistochemical analyses.

For double-label immunohistochemisty of Ki67 with GFAP, CD11b, or NeuN, sections were first immunostained for Ki67 as described above. Following immunohistochemical detection of Ki67, immunohistochemistry for GFAP or CD11b was performed, as previously described (Friend and Keefe, 2013). Briefly, sections were washed and blocked for 2hr at RT in blocking solution. Sections were then incubated in primary antibody solution (mouse anti-GFAP antibody conjugated to Alexa Fluor 488, Millipore, MAB3402X, 1:1000 or mouse anti-CD11b, Abcam, AB1211, 1:50). The following day, sections labeled for GFAP were washed, mounted on slides, and coverslipped using Pronglong Gold® with DAPI. For CD11b immunohistochemistry, sections were washed and incubated with the secondary antibody solution (goat anti-mouse IgG conjugated to Alexa Fluor 488, Invitrogen, A11029, 1:1000). Sections were then mounted and coverslipped as described above. For double-label immunohistochemistry of Ki67 and NeuN, following Ki67 immunohistochemical

staining, sections were washed and blocked in a solution containing 10% horse serum and 2% Triton X-100 in 0.1M PBS for 2hr at RT. Sections were then incubated in primary antibody solution containing 5% horse serum and mouse anti-NeuN conjugated to Alexa Fluor 488 (Millipore, MAB377X, 1:600) at RT for 3hr. Sections were then washed, mounted, and coverslipped as described above for BrdU.

4.3.5 Image acquisition and analysis

Image analysis was completed by an experimenter blinded to treatment conditions. For DAT immunohistochemistry, images were digitized and densitometric analysis was performed as previously described, yielding background-subtracted, average gray values in striatum (Friend and Keefe, 2013). Average gray values were then compared across treatment groups. Fluorescent microscopy was used to quantify the total number of proliferating cells (Ki67 and BrdU) in striatum. Montages (3x3 fields; total area 0.63 mm^2) in striatum were captured at 40X (Leica DM 4000B; 555-nm filter cube). Two rostral (+1.6 mm bregma) and two middle (+0.2 mm bregma) striatal sections per animal were imaged and analyzed. The number of cells stained for Ki67 or BrdU were recorded and averaged across sections for each animal and compared across treatment groups. Confocal microscopy was used to visualize fluorescent cells double-labeled with Ki67 and cell type-specific markers (NeuN, GFAP, or CD11b). Two serial sections were imaged and analyzed per label per animal. A Z-stacked image of Ki67 in striatum was captured under 2X zoom with an FV1000 confocal laser-scanning microscope (Olympus) with motorized stage (Prior Scientific) using a 40X, 1.3 NA oil-immersion lens (Plan APO) and 405-nm Diode, 488-nm AR, and 543-nm HENE lasers.

Images were captured at 2-µm intervals through the Z-axis of the section. Cells were examined in each animal for NeuN, GFAP, or CD11b colabeling with Ki67 to determine the percentage of $Ki67^+$ cells that were $Ki67^+/NeuN^+$, $Ki67^+/GFAP^+$, or $Ki67^+/ CD11b^+$ in relation to the total number of $Ki67^+$ cells. The degree of colocalization was then compared across treatment groups.

4.3.6 Statistical analysis

Statistical analysis was performed using a two-factor ANOVA (PND60 treatment x PND90 treatment) followed by *post hoc* analysis using a Tukey's HSD test. Statistical analysis on body temperatures was conducted using a MANOVA with repeated measures (PND60 treatment x PND90 treatment x Time) followed by *post hoc* analysis of significant time x treatment interactions using two-tailed t-tests at each time point.

4.4. Results

4.4.1 METH-induced hyperthermia

4.4.1.1 METH-induced hyperthermia in BrdU cohort

For body temperature data collected during treatment of this cohort of animals on PND60 (Figure 4.2A), MANOVA revealed main effects of PND60 treatment ($F_{(1,21)}$ = 177.51, $p < 0.0001$) and time ($F_{(4,18)} = 144.13$, $p < 0.0001$) and a significant PND60 treatment x time interaction ($F_{(1,18)} = 108.29$, $p<0.0001$). *Post hoc* analysis revealed that the temperatures of animals receiving METH on PND60 were not different from controls at baseline (BL, t = 1.66, $p = 0.11$), but were significantly greater than those receiving saline at all four time points after the injections of METH began (60 min, t = 9.88, $p <$

0.0001; 180 min, t = 13.48, $p < 0.0001$; 300 min, t = 8.92, $p < 0.0001$; 420 min, t = 8.87, $p < 0.0001$). For body temperature data collected during treatment of this cohort of animals on PND90 (Figure 4.2B), MANOVA revealed main effects of PND90 treatment ($F_{(1,21)} = 102.97$, $p < 0.0001$) and time ($F_{(4,18)} = 52.17$, $p < 0.0001$) and a significant PND90 treatment x time interaction ($F_{(1,18)} = 30.82$, $p < 0.0001$). *Post hoc* analysis of the PND90 treatment x time interaction again revealed that temperatures of animals acutely receiving METH on PND90 were not different from controls at baseline (BL, t = -0.69, $p = 0.31$), but were significantly higher than those of controls at all time points after the administration of METH began (60 min, t = 9.84, $p < 0.0001$; 180 min, t = 11.05, $p < 0.0001$; 300 min, t = 7.43, $p < 0.0001$; 420 min, t = 7.94, $p < 0.0001$). Importantly, there were no significant PND60 treatment x PND 90 treatment ($F_{(1,21)} = 0.23$, $p = 0.6300$) or PND60 treatment x PND90 treatment x time ($F_{(4,18)} = 0.3783$, $p = 0.82$) interactions.

4.4.1.2 METH-induced hyperthermia in Ki67 cohort

For body temperature data collected during treatment of this cohort of animals on PND60 (Figure 4.2C), MANOVA revealed main effects of PND60 treatment ($F_{(1,50)} = 332.62$, $p < 0.0001$) and time ($F_{(4,47)} = 64.41$, $p < 0.0001$) and a significant PND60 treatment x time interaction ($F_{(1,47)} = 53.59$, $p < 0.0001$). *Post hoc* analysis revealed that the temperatures of animals receiving METH on PND60 were slightly elevated compared to saline treated animals at baseline (BL, t = 2.06, $p < 0.05$) and were significantly higher than those of animals exposed to saline at all four time points after the injections of METH began (60 min, t = 20.45, $p < 0.0001$; 180 min, t = 19.10, $p < 0.0001$; 300 min, t = 14.05, $p < 0.0001$; 420 min, t = 12.47, $p < 0.0001$). For body temperature data collected

during treatment of this cohort of animals on PND90 (Figure 4.2D), MANOVA revealed main effects of PND90 treatment ($F_{(1,50)} = 381.58$, $p < 0.0001$) and time ($F_{(4,47)} = 87.87$, $p < 0.0001$) and a significant PND90 treatment x time interaction ($F_{(4,47)} = 87.81$, $p < 0.0001$). *Post hoc* analysis of the PND90 treatment x time interaction again revealed that temperatures of animals receiving METH on PND90 were not different from controls at baseline (BL, t = -1.10, $p = 0.52$), but were significantly higher than those of saline treated animals at all time points after the administration of METH began (Figure 2D; 60 min, t = 15.76, $p < 0.0001$; 180 min, t = 18.30, $p < 0.0001$; 300 min, t = 12.58, $p < 0.0001$; 420 min, t = 13.33, $p < 0.0001$). Importantly, there were no significant PND60 treatment x PND 90 treatment ($F_{(1,50)} = 1.57$, $p = 0.22$) or PND60 treatment x PND90 treatment x time ($F_{(4,47)} = 2.23$, $p = 0.08$) interactions.

4.4.2 METH-induced DA depletions

4.4.2.1 METH-induced DA depletions in the BrdU cohort

METH-treated animals showed significant decreases in DAT immunohistochemical staining compared to saline-treated controls (Figure 4.3A). A two-factor ANOVA for striatal DAT revealed no significant main effect of PN60 treatment ($F_{(1,21)} = 0.0111$, $p = 0.9272$); however, the ANOVA revealed a significant effect of PND90 treatment ($F_{(1,21)} = 47.89$, $p < 0.0001$) and a significant PND60 x PND90 treatment interaction ($F_{(1,21)} = 16.34$, $p < 0.001$). *Post hoc* analysis of the interaction revealed that animals treated with the neurotoxic regimen of METH (Saline:METH, METH:Saline, and METH:METH) were significantly different from saline controls (Saline:Saline; Tukey's HSD test, p values <0.05) and that animals treated with METH

only on PND90 (Saline:METH) were different from animals treated with METH only on PND60 (METH:Saline) or animals treated with METH on both PND60 and PND90 (METH:METH; Tukey's HSD test, p values <0.05). DAT staining in the striata of METH:Saline and METH:METH animals were not different from each other ($p = 0.15$). Thus, as previously shown, rats receiving a second neurotoxic regimen of METH were resistant to further acute neurotoxicity.

4.4.2.2 METH-induced DA depletions in the Ki67 cohort

METH-treated animals in this cohort also showed significant decreases in DAT immunohistochemical staining compared to saline-treated controls (Figure 4.3B). A two-factor ANOVA for striatal DAT did not reveal a main effect for PND60 treatment; however, the ANOVA revealed a significant effect of PN90 treatment ($F_{(1,50)}$=123.96, p<0.0001) and a significant PND60 x PND90 treatment interaction ($F_{(1,50)}$=61.95, p<0.0001). *Post hoc* analysis of the interaction revealed that animals treated with the neurotoxic regimen of METH (METH:Saline, Saline:METH, and METH:METH) were significantly different from controls (Saline:Saline; Tukey's HSD test, p values <0.0001; Figure 3B) and that animals treated with METH only on PND90 (Saline:METH) were different from animals treated with METH on PND60 (METH:Saline) and animals treated with METH on both PND60 and PND90 (METH:METH) (Tukey's HSD test, p values <0.001). Furthermore, DAT staining in Saline:METH animals and METH:METH animals were not different from each other ($p = 0.10$). Thus, as previously shown, animals receiving a second neurotoxic regimen of METH were resistant to further acute neurotoxicity.

4.4.3 Proliferation

4.4.3.1 METH-induced proliferation measured via BrdU immunohistochemistry

Animals treated with METH only on PND90 (Saline:METH) showed a significant increase in the number of BrdU-positive cells compared to all other treatment groups (Saline:Saline, METH:Saline, and METH:METH; Figure 4.4A). A two-factor ANOVA of the number of $BrdU^+$ cells revealed significant main effects of PND60 ($F_{(1,21)} = 12.99$, $p < 0.01$) and PND90 treatments ($F_{(1,21)} = 34.39$, $p < 0.0001$), and a significant PND60 x PND90 treatment interaction ($F_{(1,21)} = 8.76$, $p < 0.01$). *Post hoc* analysis of the interaction revealed that animals treated with a neurotoxic regimen only on PND90 (Saline:METH) were significantly different from all other treatment groups (Tukey's HSD test, p values < 0.001). To confirm the accuracy of these measurements, a second experimenter independently performed counts of BrdU-positive cells. The correlation between the two independent investigators' measures was highly significant ($r^2 = 0.4$, $p < 0.0001$, data not shown), indicating accurate measurement of BrdU-positive cells.

4.4.3.2 METH-induced proliferation measured via Ki67 immunohistochemistry

Animals treated with METH on PND90 only (Saline:METH) showed a significant increase in the number of Ki67-positive cells compared to all other treatment groups (Saline:Saline, METH:Saline, and METH:METH; Figure 4.4B). A two-factor ANOVA of the number of Ki67-positive cells revealed that there was no main effect of PND60 treatment ($F_{(1,50)} = 2.61$, $p > 0.11$), but that there was a main effect of PND90 treatment

($F_{(1,50)} = 13.19$, $p < 0.001$) and a significant PND60 treatment x PND90 treatment interaction ($F_{(1,50)} = 5.31$, $p < 0.05$). *Post hoc* analysis of the interaction revealed that animals treated with a neurotoxic regimen of METH only on PND90 (Saline:METH) were significantly different from all other treatment groups (Tukey's HSD test, p values < 0.05).

4.4.3.3 Percentage of proliferating cells that are neurons

Methamphetamine administration did not result in a change in neuronal proliferation 48hr after the last injection on PND90 (Figure 4.5). A two-way ANOVA examining the percentage of Ki67-positive cells double labeled for NeuN revealed no significant main effects of PND60 ($F_{(1,23)} = 0.09$, $p = 0.93$) or PND90 ($F_{(1,23)} = 3.23$, $p = 0.09$) treatment and no significant PND60 treatment x PND90 treatment interaction ($F_{(1,23)} = 0.05$, $p = 0.83$).

4.4.3.4 Percentage of proliferating cells that are astrocytes

Methamphetamine administration resulted in an increase in the degree of astrocyte proliferation 48hr after the last injection on PND90 (Figure 4.6). A two-way ANOVA examining the percentage of Ki67-positive cells double labeled for GFAP revealed a significant main effect of PND90 treatment ($F_{(1,20)} = 2.61$, $p < 0.05$), but no significant main effect of PND60 treatment ($F_{(1,20)} = 0.3586$, $p = 0.56$) and no significant PND60 treatment x PND90 treatment interaction ($F_{(1,20)} = 1.1434$, p=0.25).

4.4.3.5 Percentage of proliferating cells that are microglia

Animals treated METH only on PND90 (Saline:METH) showed increased microglial proliferation 48hr after the last injection on PND90 (Figure 4.7). A two-way ANOVA examining the percentage of Ki67-positive cells double labeled for CD11b revealed main effects of PND60 ($F_{(1,23)} = 5.72$, $p < 0.05$) and PND90 ($F_{(1,23)} = 14.66$, $p < 0.001$) treatments and a significant PND60 treatment x PND90 treatment interaction ($F_{(1,23)} = 4.75$, $p < 0.05$). *Post hoc* analysis of the interaction revealed that animals treated with a neurotoxic regimen of METH only on PND90 (Saline:METH) were significantly different from all other treatment groups (Tukey's HSD test, p values < 0.05).

4.5 Discussion

Methamphetamine use continues to be a significant public health concern. It is well established that abuse results in long-term deficits to the DA system. Notably, recent evidence has shown that individuals with a history of amphetamine abuse, most prominently METH, also show increased incidence of Parkinson's disease several years later (Callaghan et al., 2010; Callaghan et al., 2012), highlighting the clinical relevance of METH-induced neurotoxicity. Thus, clarifying the mechanisms through which METH damages the DA system and how these mechanisms may contribute to the further degeneration resulting in Parkinsonism years later will be essential for the development of therapeutic targets to prevent further degeneration in individuals with a history of METH abuse and addiction, as well as perhaps for individuals with idiopathic Parkinson's disease.

Recent work has documented a significant increase in proliferation in striatum 24-48hrs after exposure to a neurotoxic regimen of METH (Tulloch et al., 2011a; Tulloch et al., 2011b; Tulloch et al., 2011c). Based on double-label immunohistochemical staining, that work suggested that proliferating cells co-localized with beta-III tubulin, a neuron-specific marker (Tulloch et al., 2011a). However, this study did not quantify the degree of co-localization of BrdU and beta-III tubulin, nor did this study examine whether other cell types contributed to total amount of proliferation observed. Given prior data suggesting that glial cells become reactive 24-48hr following exposure to METH and may increased in number (O'Callaghan and Miller, 1994; LaVoie et al., 2004), we wanted to explore the possibility that microglia and astrocytes contribute to the increased proliferation occurring in striatum following exposure to a neurotoxic regimen of METH. To answer this question we used double-label immunohistochemistry with markers of cellular proliferation (Ki67 and BrdU) and cell type-specific markers to identify astrocytes (GFAP), microglia (CD11b), and neurons (NeuN).

Consistent with previous work (Tulloch et al., 2011a; Tulloch et al., 2011b), we found that proliferation is increased in animals following exposure to a neurotoxic regimen of METH. We found similar degrees of proliferation in two separate cohorts of animals using two separate markers of proliferation, BrdU and Ki67. Interestingly, we found that cellular proliferation was only increased in animals that were exposed to METH and experiencing acute toxicity (Saline:METH), whereas animals resistant to further METH-induced DA depletions (METH:METH) did not show increased proliferation compared to saline-treated controls (Saline:Saline).

To determine the identity of proliferating cells we initially performed double-label immunohistochemisty with Ki67 and NeuN (neuron specific marker) to determine the percentage of Ki67 positive cells that were neurons. Here, we found that in saline treated animals, approximately 15% of the Ki67+ cells in striatum also stained for NeuN, a finding that is consistent with quantifications of baseline neuronal proliferation in striatum (Van Kampen et al., 2004). Surprisingly, we did not observe an increase in the percentage of $Ki67^{+}$ cells that colocalized with NeuN in animals exposed to a neurotoxic regimen of METH compared to those exposed to saline. These data are inconsistent with the previous work suggesting that many of the proliferating (*i.e.,* BrdU-positive) cells observed after METH exposure co-localize with beta-III tubulin, a neuron-specific marker (Tulloch et al., 2011c); however, beta-III tubulin is known to label immature neurons, whereas NeuN labels neurons that are fully differentiated (von Bohlen Und Halbach, 2007). Therefore, there remains the possibility that neuronal precursors (beta-III tubulin) are proliferating 48hr after METH exposure, but have not yet fully differentiated into neurons (expressing NeuN).

Next, double-label immunohistochemistry was performed to determine the percentage of Ki67+ cells that also stained for GFAP. Here we found that a small proportion of proliferating cells were, in fact, astrocytes. Here we found a main effect of PND90 treatment, indicating that astrocyte proliferation was increased in animals exposed to METH on PND90 (Saline:METH and METH:METH), compared to animals exposed to saline on PND90 (Saline:Saline and Saline:METH). These data suggest that havn't proliferation of astrocytes may partially contribute to the total number of proliferating cells observed following METH exposure.

Finally, we determined the percentage of proliferating cells that are microglia by performing double-label immunohistochemistry using Ki67 and CD11b, a microglia-specific marker. We found that a large proportion (~40%) of proliferating cells in animals exposed to METH and experiencing acute toxicity (Saline:METH) were microglia, as evidenced by CD11b staining. Interestingly, this increase in the percentage of cells double-labeled for Ki67 and CD11b was only observed in animals treated with METH and acutely experiencing toxicity (Saline:METH); very little colocalization of Ki67 with CD11b occurred in animals exposed to METH but not experiencing acute toxicity (METH:METH). These later data demonstrating the proliferation of microglia only in animals experiencing acute METH-induced toxicity are consistent with previous work. For example, our lab and others have previously shown that animals exposed to METH and experiencing acute toxicity (Saline:METH) have highly reactive microglia throughout striatum, whereas animals exposed to METH but resistant to METH-induced neurotoxicity (METH:METH) do not show microglial activation (Thomas and Kuhn, 2005; Friend and Keefe, 2013). Furthermore, irradiated mice given bone marrow transplants from mice expressing eGFP and then later exposed to METH do not show any evidence of eGFP-expressing microglia in striatum (Thomas et al., 2008). However, a typical activated microglia response is still observed in these animals after exposure to METH. Taken together with the present findings, the data suggest that the microglial response to METH exposure, at least in part, reflects proliferation of resident striatal microglia. Additionally these data also indicate that the microglial response following a neurotoxic regimen of METH parallels toxicity in that increased cd11b expression and microglia proliferation only occurs in animals exposed to METH and experiencing acute

toxicity (Saline:METH) but not in animals exposed to METH and not experiencing acute toxicity (METH:METH).

Although the present findings demonstrate that astrocytes, neurons to a lesser degree, and microglia make up a large proportion of the proliferating cells observed in striatum following exposure to a neurotoxic regimen of METH, there still remains a subpopulation of proliferating cells that are unaccounted for. The possibility remains that a portion of the proliferating cells are neuronal precursors that at 48hr after METH exposure do not yet express NeuN (Kempermann et al., 2003; von Bohlen Und Halbach, 2007; Liu et al., 2008), but that are beta-III tubulin-positive (Tulloch et al., 2011a). Additionally, glial/oligodendrocyte precursors are known to enter the cell cycle and to proliferate following various CNS injuries (Levine, 1994; Keirstead et al., 1998; Redwine and Armstrong, 1998; Levine and Reynolds, 1999; Nielsen et al., 2006) These precursors are positive for the chondroitin sulfate proteoglycan NG2 and give rise to both astrocytes and oligdendrocytes (Levine et al., 2001; Trotter et al., 2010). To our knowledge, changes in proliferation of NG2-positive cells has yet to be examined in the context of a neurotoxic regimen of METH, and thus deserves attention in this context. Future work will be aimed at determining whether neuronal precursors and/or oligodendrocyte progenitors also contribute to METH-induced striatal cellular proliferation.

4.6 Conclusions

These studies demonstrate a significant increase in the number of proliferating cells in striatum 48hr following a neurotoxic regimen of METH. Importantly, the increase in proliferation is only seen in animals exposed to METH and experiencing

toxicity, not in those resistant to such toxicity. Using double-label immunohistochemistry, we show that a large portion of these proliferating cells are microglia, whereas only a small number of cells co-express markers for astrocytes (GFAP) or differentiated neurons (NeuN). These data are consistent with previous work from our lab and others demonstrating that glial cells are highly reactive 24-48hr after exposure to a neurotoxic regimen of METH and that animals resistant to METH-induced DA depletions as result of prior exposure to the drug do not show reactive microglial phenotypes. Taken together, these data provide further support for a link between microglial proliferation and METH-induced neurotoxicity in the striatum.

4.7 References

Aponso PM, Faull RL and Connor B (2008) Increased progenitor cell proliferation and astrogenesis in the partial progressive 6-hydroxydopamine model of Parkinson's disease. *Neuroscience* **151**:1142-1153.

Bacchi CE and Gown AM (1993) Detection of cell proliferation in tissue sections. *Braz J Med Biol Res* **26**:677-687.

Callaghan RC, Cunningham JK, Sajeev G and Kish SJ (2010) Incidence of Parkinson's disease among hospital patients with methamphetamine-use disorders. *Mov Disord* **25**:2333-2339.

Callaghan RC, Cunningham JK, Sykes J and Kish SJ (2012) Increased risk of Parkinson's disease in individuals hospitalized with conditions related to the use of methamphetamine or other amphetamine-type drugs. *Drug Alcohol Depend* **120**:35-40.

Collin T, Arvidsson A, Kokaia Z and Lindvall O (2005) Quantitative analysis of the generation of different striatal neuronal subtypes in the adult brain following excitotoxic injury. *Exp Neurol* **195**:71-80.

De Filippis L and Binda E (2012) Concise review: self-renewal in the central nervous system: neural stem cells from embryo to adult. *Stem Cells Transl Med* **1**:298-308.

Dihne M, Block F, Korr H and Topper R (2001) Time course of glial proliferation and glial apoptosis following excitotoxic CNS injury. *Brain Res* **902**:178-189.

Fleckenstein AE, Metzger RR, Gibb JW and Hanson GR (1997) A rapid and reversible change in dopamine transporters induced by methamphetamine. *Eur J Pharmacol* **323**:R9-10.

Friend DM and Keefe KA (2013) Glial Reactivity in Resistance to Methamphetamine-Induced Neurotoxicity. *J Neurochem*.

Friend DM, Son JH, Keefe KA and Fricks-Gleason AN (2013) Expression and activity of nitric oxide synthase isoforms in methamphetamine-induced striatal dopamine toxicity. *J Pharmacol Exp Ther* **344**:511-521.

Gratzner HG (1982) Monoclonal antibody to 5-bromo- and 5-iododeoxyuridine: A new reagent for detection of DNA replication. *Science* **218**:474-475.

Guilarte TR, Nihei MK, McGlothan JL and Howard AS (2003) Methamphetamine-induced deficits of brain monoaminergic neuronal markers: distal axotomy or neuronal plasticity. *Neuroscience* **122**:499-513.

Hanson JE, Birdsall E, Seferian KS, Crosby MA, Keefe KA, Gibb JW, Hanson GR and Fleckenstein AE (2009) Methamphetamine-induced dopaminergic deficits and refractoriness to subsequent treatment. *Eur J Pharmacol* **607**:68-73.

Kay JN and Blum M (2000) Differential response of ventral midbrain and striatal progenitor cells to lesions of the nigrostriatal dopaminergic projection. *Dev Neurosci* **22**:56-67.

Keirstead HS, Levine JM and Blakemore WF (1998) Response of the oligodendrocyte progenitor cell population (defined by NG2 labelling) to demyelination of the adult spinal cord. *Glia* **22**:161-170.

Kempermann G, Gast D, Kronenberg G, Yamaguchi M and Gage FH (2003) Early determination and long-term persistence of adult-generated new neurons in the hippocampus of mice. *Development* **130**:391-399.

Kogan FJ, Nichols WK and Gibb JW (1976) Influence of methamphetamine on nigral and striatal tyrosine hydroxylase activity and on striatal dopamine levels. *Eur J Pharmacol* **36**:363-371.

LaVoie MJ, Card JP and Hastings TG (2004) Microglial activation precedes dopamine terminal pathology in methamphetamine-induced neurotoxicity. *Exp Neurol* **187**:47-57.

Levine JM (1994) Increased expression of the NG2 chondroitin-sulfate proteoglycan after brain injury. *J Neurosci* **14**:4716-4730.

Levine JM and Reynolds R (1999) Activation and proliferation of endogenous oligodendrocyte precursor cells during ethidium bromide-induced demyelination. *Exp Neurol* **160**:333-347.

Levine JM, Reynolds R and Fawcett JW (2001) The oligodendrocyte precursor cell in health and disease. *Trends Neurosci* **24**:39-47.

Liu YW, Curtis MA, Gibbons HM, Mee EW, Bergin PS, Teoh HH, Connor B, Dragunow M and Faull RL (2008) Doublecortin expression in the normal and epileptic adult human brain. *Eur J Neurosci* **28**:2254-2265.

Mao L, Lau YS, Petroske E and Wang JQ (2001) Profound astrogenesis in the striatum of adult mice following nigrostriatal dopaminergic lesion by repeated MPTP administration. *Brain Res Dev Brain Res* **131**:57-65.

McCann UD, Wong DF, Yokoi F, Villemagne V, Dannals RF and Ricaurte GA (1998) Reduced striatal dopamine transporter density in abstinent methamphetamine and methcathinone users: evidence from positron emission tomography studies with [11C]WIN-35,428. *J Neurosci* **18**:8417-8422.

Nielsen HH, Ladeby R, Drojdahl N, Peterson AC and Finsen B (2006) Axonal degeneration stimulates the formation of NG2+ cells and oligodendrocytes in the mouse. *Glia* **54**:105-115.

O'Callaghan JP and Miller DB (1994) Neurotoxicity profiles of substituted amphetamines in the C57BL/6J mouse. *J Pharmacol Exp Ther* **270**:741-751.

Parent JM, Vexler ZS, Gong C, Derugin N and Ferriero DM (2002) Rat forebrain neurogenesis and striatal neuron replacement after focal stroke. *Ann Neurol* **52**:802-813.

Redwine JM and Armstrong RC (1998) In vivo proliferation of oligodendrocyte progenitors expressing PDGFalphaR during early remyelination. *J Neurobiol* **37**:413-428.

Thomas DM, Francescutti-Verbeem DM and Kuhn DM (2008) Methamphetamine-induced neurotoxicity and microglial activation are not mediated by fractalkine receptor signaling. *J Neurochem* **106**:696-705.

Thomas DM and Kuhn DM (2005) Attenuated microglial activation mediates tolerance to the neurotoxic effects of methamphetamine. *J Neurochem* **92**:790-797.

Thomas DM, Walker PD, Benjamins JA, Geddes TJ and Kuhn DM (2004) Methamphetamine neurotoxicity in dopamine nerve endings of the striatum is associated with microglial activation. *J Pharmacol Exp Ther* **311**:1-7.

Trotter J, Karram K and Nishiyama A (2010) NG2 cells: Properties, progeny and origin. *Brain Res Rev* **63**:72-82.

Tulloch I, Afanador L, Mexhitaj I, Ghazaryan N, Garzagongora AG and Angulo JA (2011a) A single high dose of methamphetamine induces apoptotic and necrotic striatal cell loss lasting up to 3 months in mice. *Neuroscience* **193**:162-169.

Tulloch I, Ghazaryan N, Mexhitaj I, Ordonez D and Angulo JA (2011b) Role of neurokinin-1 and dopamine receptors on the striatal methamphetamine-induced proliferation of new cells in mice. *Brain Res* **1399**:33-39.

Tulloch IK, Afanador L, Zhu J and Angulo JA (2011c) Methamphetamine induces striatal cell death followed by the generation of new cells and a second round of cell death in mice. *Curr Neuropharmacol* **9**:79-83.

Van Kampen JM, Hagg T and Robertson HA (2004) Induction of neurogenesis in the adult rat subventricular zone and neostriatum following dopamine D3 receptor stimulation. *Eur J Neurosci* **19**:2377-2387.

von Bohlen Und Halbach O (2007) Immunohistological markers for staging neurogenesis in adult hippocampus. *Cell Tissue Res* **329**:409-420.

Wachter B, Schurger S, Rolinger J, von Ameln-Mayerhofer A, Berg D, Wagner HJ and Kueppers E (2010) Effect of 6-hydroxydopamine (6-OHDA) on proliferation of glial cells in the rat cortex and striatum: evidence for de-differentiation of resident astrocytes. *Cell Tissue Res* **342**:147-160.

Wagner GC, Ricaurte GA, Seiden LS, Schuster CR, Miller RJ and Westley J (1980) Long-lasting depletions of striatal dopamine and loss of dopamine uptake sites following repeated administration of methamphetamine. *Brain Res* **181**:151-160.

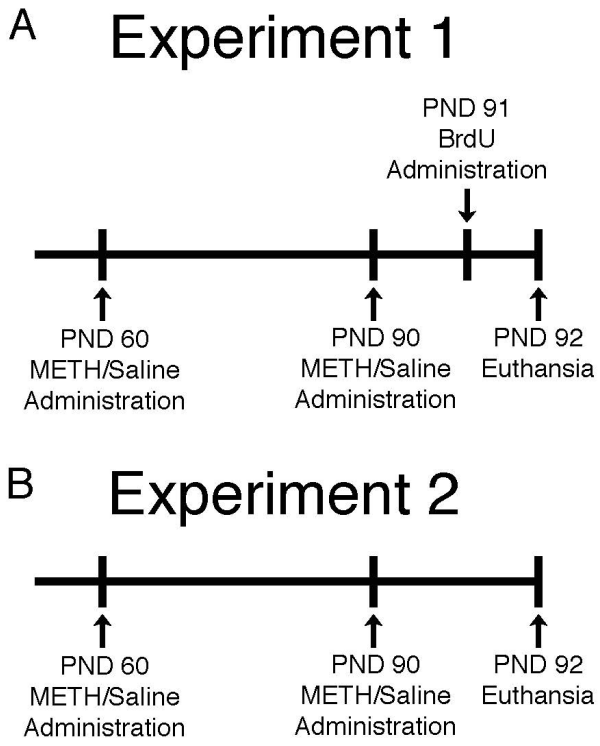

Figure 4.1**.** Experimental time lines. (A) Experimental time line for BrdU experiments. Animals were treated with METH or saline on PND60, allowed to recover for 30 days and treated again with METH or saline on PND90. BrdU injections were given 24 hr after the final METH or saline injection on PND90. Animals were sacrificed 24 hr following injection with BrdU. (B) Experimental time line for Ki67 experiments. Animals were treated with METH or saline on PND60, allowed to recover for 30 days and treated again with METH or Saline on PND90. Animals were sacrificed 48 hr after the final METH or saline injection on PND90.

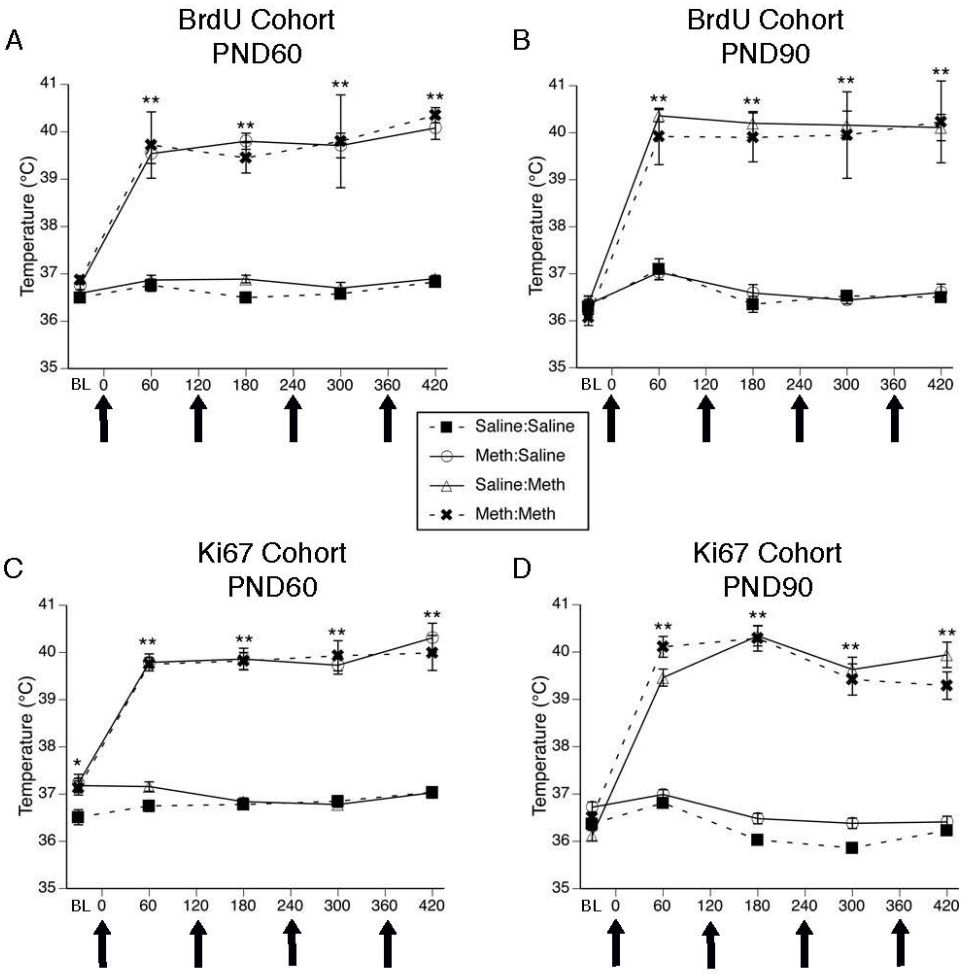

Figure 4.2. Body temperatures (mean ± SEM; n = 4-17/group) of animals that received systemic injections of saline (4 x 1 mL/kg, s.c. at 2-hr intervals) or (±)-METH (4 x 10 mg/kg, s.c. at 2-hr intervals). Treatment group designations indicate PND60:PND90 treatment, resulting in the four treatment groups: Saline:Saline; METH:Saline; Saline:METH; and METH:METH. Temperatures were obtained 30 min prior to the first injection (baseline; BL) and 1 hr after each subsequent injection. X-axis values represent minutes after the first injection and arrows represent the time of each saline or METH injection. (A & B) Body temperatures of animals used for BrdU experiments treated with either METH or saline on PND60 (A) or PND90 (B). (C & D) Body temperatures of animals used for Ki67 experiments treated with either METH or saline on PND60 (C) or PND90 (D). * $p < 0.05$; ** $p < 0.01$, Significantly different from saline.

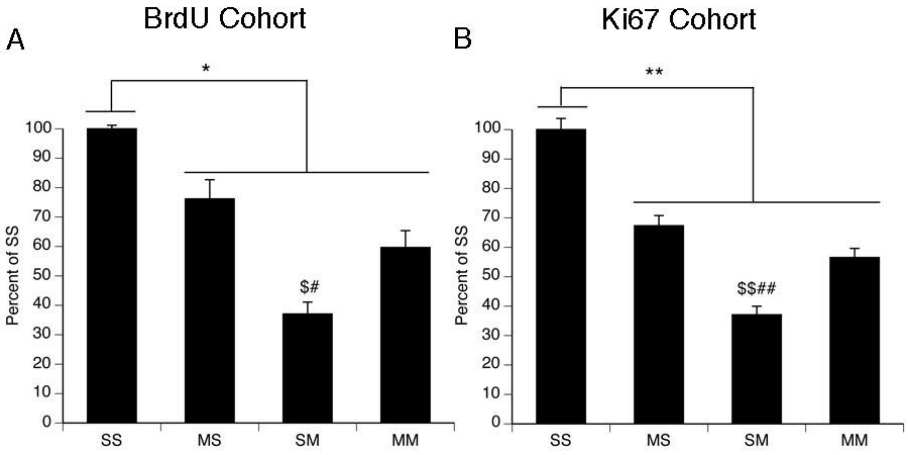

Figure 4.3. Striatal DAT immunohistochemical staining following single or repeated exposure to a neurotoxic regimen of METH. Data are mean gray values from densitometric analyses expressed as a percent of the respective Saline:Saline group (mean ± SEM; n=4-17/group). Treatment group designations indicate PND60:PND90 treatment, resulting in the four treatment groups: Saline:Saline (SS); METH:Saline (MS); Saline:METH (SM); and METH:METH (MM). (A) METH-Induced DA depletions of animals used for BrdU experiments. (B) METH-Induced DA depletions of animals used for Ki67 experiments. * $p < 0.05$; ** $p < 0.01$, significantly different from Saline:Saline. \$ $p < 0.05$, \$\$ $p < 0.01$, significantly different from METH:Saline.

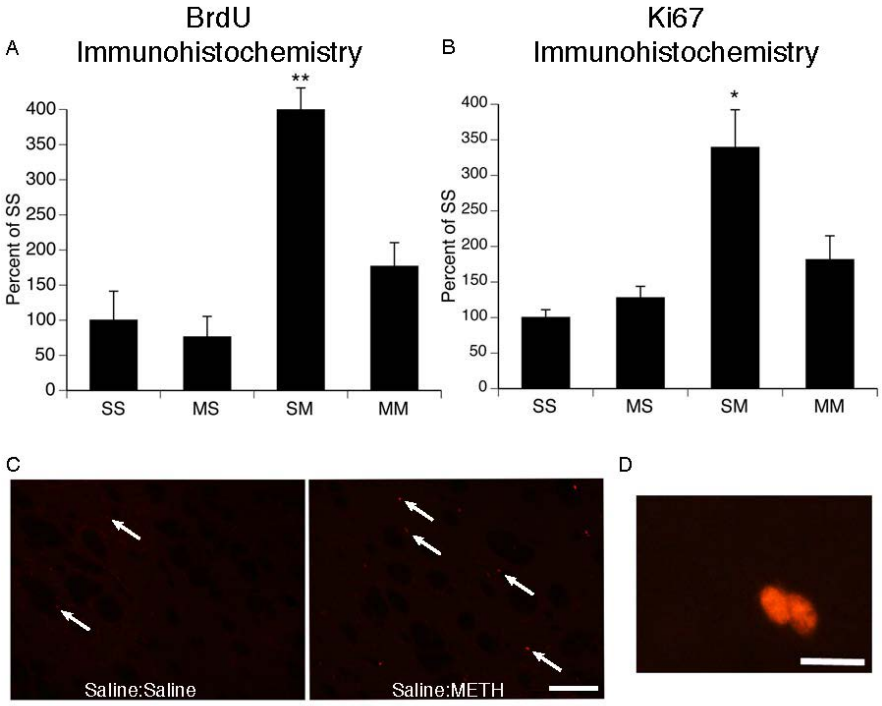

Figure 4.4. Cell proliferation in striatum following single or repeated exposure to a neurotoxic regimen of METH. Data are the average number of BrdU (A)- or Ki67 (B)-positive cells counted in four striatal sections from each animal expressed as a percent of the respective Saline:Saline group (mean ± SEM; n=10-17/group). Treatment group designations indicate PND60:PND90 treatment, resulting in the four treatment groups: Saline:Saline (SS); METH:Saline (MS); Saline:METH (SM); and METH:METH (MM). (C) Representative images of Ki67 immunohistochemistry in a Saline:Saline animal and a Saline:METH animal. Scale bar = 50µm. (D) Representative image of Ki67-positive dividing cells, often seen in Saline:METH animals. Scale bar = 10µm. * $p < 0.05$, ** $p < 0.01$, significantly different from all other groups.

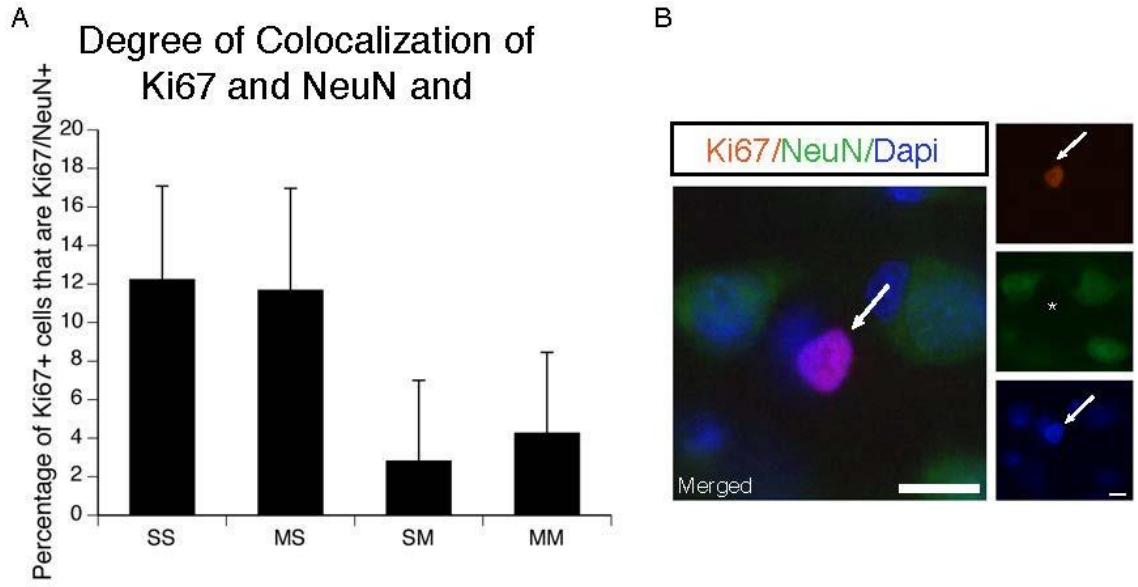

Figure 5. Co-localization of Ki67 and NeuN following single or repeated exposure to a neurotoxic regimen of METH. (A) Data are the percentage of Ki67-positive cells also positive for NeuN staining (mean ± SEM; n=5-8/group). Treatment group designations indicate PND60:PND90 treatment, resulting in the four treatment groups: Saline:Saline (SS); METH:Saline (MS); Saline:METH (SM); and METH:METH (MM). There were no significant main effects or interactions. (B) Representative image from a Saline:METH animal. Scale bar = 10μm.

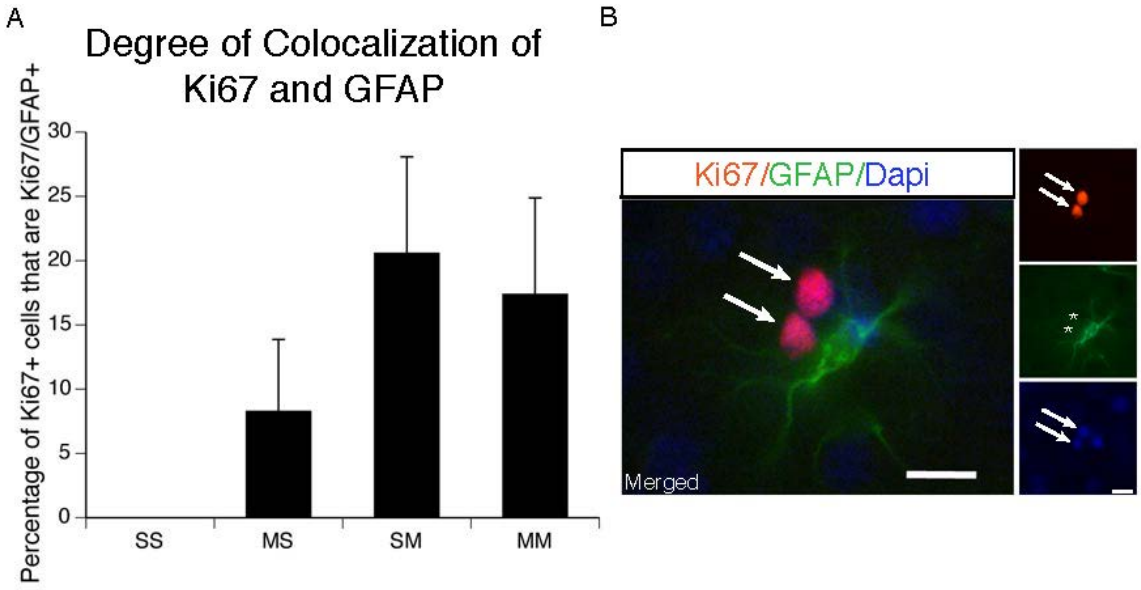

Figure 4.6. Co-localization of Ki67 and GFAP following single or repeated exposure to a neurotoxic regimen of METH. (A) Data are the percentage of Ki67-positive cells also positive for GFAP staining (mean ± SEM; n=5-8/group). Treatment group designations indicate PND60:PND90 treatment, resulting in the four treatment groups: Saline:Saline (SS); METH:Saline (MS); Saline:METH (SM); and METH:METH (MM). * $p< 0.05$, ** $p<0.01$significantly different from all other treatment groups. (B) Representative image from a Saline:METH animal. Scale bar = 10µm.

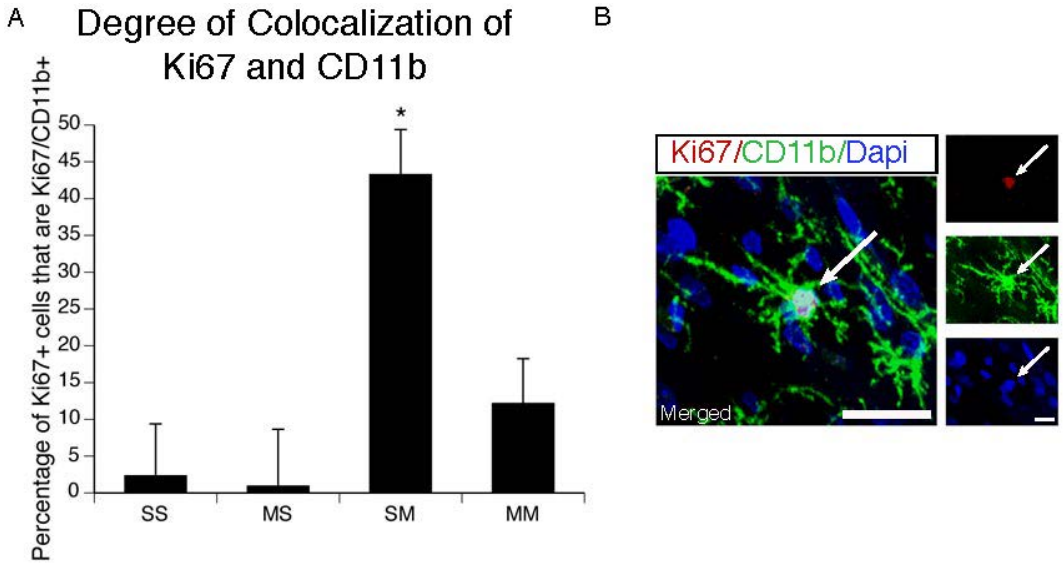

Figure 4.7. Co-localization of Ki67 and CD11b following single or repeated exposure to a neurotoxic regimen of METH. (A) Data are the percentage of Ki67-positive cells also positive for CD11b staining (mean ± SEM; n=5-8/group). Treatment group designations indicate PND60:PND90 treatment, resulting in the four treatment groups: Saline:Saline (SS); METH:Saline (MS); Saline:METH (SM); and METH:METH (MM). * $p < 0.05$, significantly different from all other groups. (B) Representative image from a Saline:METH animal. Scale bar = 10µm.

CHAPTER 5

DISCUSSION

Exposure to methamphetamine (METH) results in significant damage to the dopaminergic system, particularly in the caudate-putamen of human METH abusers and in the striatum of animals (Kogan et al., 1976; Sekine et al., 2001; Volkow et al., 2001; McCann et al., 2008 and others). Several factors have been implicated in such toxicity, including increased extracellular and cytosolic dopamine (DA) (e.g. O'Dell et al., 1991; Albers and Sonsalla, 1995; LaVoie and Hastings, 1999; Gross et al., 2011b), increased extracellular glutamate (GLU) (Nash and Yamamoto, 1992; Mark et al., 2004), the production of reactive oxygen (Wagner et al., 1986; Fukami et al., 2004) and nitrogen species (Ali and Itzhak, 1998; Imam et al., 1999; Itzhak et al., 2000 and others), and the activation of glial cells (LaVoie et al., 2004; Thomas and Kuhn, 2005).

The goal of this dissertation was to further explore the role of nitric oxide (NO) and activated glial cells in METH-induced neurotoxicity. To determine if these factors are sufficient for METH-induced monoamine toxicity, we used a model of resistance to such toxicity, in which animals are treated with a binge regimen of METH, but do not show acute monoamine toxicity. In this regard, animals were treated with either saline or a neurotoxic regimen of METH on PND60. Animals were allowed to recover for 30 days and then challenged with saline or a binge regimen of METH at PND90. This treatment regimen results in four treatment groups based on the animals' PND60:PND90 treatments (Saline:Saline, Saline:METH, METH:Saline, and METH:METH). Previous studies using this treatment regimen have shown that animals with partial DA loss induced by the initial exposure to binge regimen of METH on PND60 fail to exhibit further

depletions of DA, DAT or VMAT-2 when exposed to the second neurotoxic regimen on PND90 (METH:METH) (Thomas and Kuhn, 2005; Hanson et al., 2009). This paradigm thus allows for the examination of factors associated with METH-induced monoamine toxicity in animals matched for acute METH exposure, but differentiated with respect to acute METH-induced DA terminal degeneration. The extent to which this resistance to subsequent METH-induced neurotoxicity is associated with decreased NO production or glial activation was unknown. Therefore, using this treatment regimen, we first wanted to determine whether animals rendered resistant to acute METH-induced DA depletions (METH:METH) demonstrated decreased NO production compared to animals experiencing acute toxicity (saline:METH). Furthermore, we also wanted to determine the isoform of NOS responsible for METH-induced NO production. Second, we wanted to determine whether animals resistant to acute METH-induced DA depletions (METH:METH) demonstrate similar glial activation compared to animals acutely experiencing toxicity (saline:METH). The following discussion describes the results of these studies, has well as the future implications for this work.

In the initial set of experiments pertaining to NO production in METH-induced neurotoxicity (Chapter 2), we first examined the production of NO by performing immunohistochemistry for protein nitration. Here we found that all animals exposed to METH on PND90 (saline:METH and METH:METH), whether or not they were experiencing acute toxicity, had significant increases in protein nitration compared to controls (saline:saline) or animals treated with METH 30 days prior (METH:saline), suggesting that exposure to the binge regimen of METH increases production of NO, but that such NO production during METH exposure is not sufficient for METH-induced DA

terminal degeneration. Next, to elucidate the isoform of NOS responsible for METH–induced NO production, we examined expression of all three isofroms of NOS in response to exposure to the binge regimen of METH. Here we found that neither the expression of nNOS nor eNOS changed in striata of animals exposed to METH. Furthermore, consistent with previous work (Deng and Cadet, 1999), we did not observe any induction of iNOS following the binge regimen of METH. However, given that nNOS and eNOS are constitutively expressed and can increase production of NO without a change in the expression of either isoform, we also wanted to determine if the increase in NO during METH exposure resulted from an increase in NOS activity. To do this, we used NADPH diaphorase histochemical staining, an indirect measure of NOS activity (Dawson et al., 1991; Hope et al., 1991). During analysis of these data, we restricted our quantification of the staining to include only cell bodies and processes of nNOS-expressing striatal interneurons, thereby excluding eNOS as a contributor to the observed changes in NADPH diaphorase histochemical staining. Paralleling the results obtained from examination of protein nitration, we found that animals exposed to the binge regimen of METH at PND90 had a significant increase in nNOS activity whether the animal was experiencing acute toxicity or not (saline:METH and METH:METH). Taken together, these data suggest that there is a disassociation between the production of NO and METH-induced neurotoxicity, indicating that NO is not sufficient for METH-induced DA nerve terminal degeneration. Additionally, these data indicate that the METH-induced increase in NO production likely results from increased activity of nNOS (Friend et al., 2013).

Although the results of the work detailed in Chapter 2 indicate that METH-induced NO production likely results from an increase in nNOS activity and that this NO does not appear to be sufficient for METH-induced DA terminal degeneration, future studies could strengthen and clarify these findings. For example, future experiments using double-label immunohistochemistry with markers for nNOS and markers for specific cell types will lead to a clear identification of the particular cell types contributing to METH-induced NO production. Furthermore, studies using shRNA knockdown of nNOS in these specific cell types while controlling for METH-induced hyperthermia will provide more conclusive results regarding the lack of a role for NO in METH-induced neurotoxicity. Finally, identifying the mechanism initiating the increased NO following a neurotoxic regimen of METH will lead to more specific ways in which this process can be inhibited in this context.

In the second set of experiments (Chapter 3), we examined astrocyte and microglial activation in the context of the resistance paradigm. Here we found that microglia were reactive only in animals exposed to METH on PND90 and experiencing acute toxicity (saline:METH), but not in those exposed to METH and resistant to such toxicity (METH:METH)(Friend and Keefe, 2013). These findings are consistent with previous work demonstrating that animals resistant to DA nerve terminal degeneration do not show an activated microglia phenotype (Thomas and Kuhn, 2005). Next, we examined the response of astroyctes to the binge regimen of METH using GFAP immunohistochemistry. Here we found that all animals exposed to METH (METH:saline, Saline:METH, and METH:METH) showed an equivalent increase in GFAP staining compared to controls (Saline:Saline) (Friend and Keefe, 2013). These

data are novel in that they are the first to document increased GFAP levels as far out as 32 days post-METH treatment; however, they are consistent with previous work showing increased expression of GFAP compared to controls at 21 days post-METH treatment (O'Callaghan and Miller, 1994).

Finally, in addition to examining markers for activated glia, we also examined striatal proliferation using the same treatment regimen (Chapter 4). We found that animals exposed to METH at PND90 and experiencing acute toxicity (Saline:METH) show an increase in proliferation compared to all other treatment groups (Saline:Saline, METH:saline, and METH:METH). Additionally, when we performed double-label immunohistochemistry with markers of proliferation (Ki67) combined with markers for neurons (NeuN), astrocytes (GFAP), and microglia (OX-42), we found that microglia make up a large proportion of the proliferating cells (approximately 40 percent) in animals experiencing acute toxicity (Saline:METH). Only a small proportion of the proliferating cells were positive for GFAP or NeuN, and those porportions did not vary as a function of acute METH-induced neurotoxicity. Altogether, these data indicate that microglial activation appears to parallel METH-induced neurotoxicity, as we only observed activated microglia in animals exposed to METH and experiencing acute toxicity (Saline:METH). Additionally, microglia show significant proliferation in animals exposed to METH and experiencing toxicity (saline:METH), further suggesting that activated microglia are only observed under conditions during which degeneration of DA nerve terminals occurs. Conversely, the activation of astrocytes does not parallel acute METH-induced neurotoxicity, as we observed an increase in GFAP expression

even in animals exposed to METH 30 days prior (METH:Saline). Thus activation of astrocytes is not likely to be necessary for acute METH-induced neurotoxicity.

Although these data provide significant insight into the activation of glial cells in the context of METH-induced neurotoxicity, whether activated glia are a cause or consequence of METH-induced neurotoxicity remains unknown. Future work is still needed in order to clearly answer this question. For example, the signals initiating glial activation following METH exposure are currently unknown. Determining the exact cascade of events that results in METH-induced glial activation could lead to more specific ways in which activation of these cell types can be inhibited. Future work should also examine specific manipulations of both microglial and astrocyte activation, possibly using conditional knockout animals, in order to determine whether activated glia are neuroprotective or contribute to neurotoxicity in the context of METH-induced DA nerve terminal degeneration.

Another factor associated with METH-induced neurotoxicity that deserves further exploration is extracellular DA and the subsequent activation of D1-type DA receptors. It is well established that METH exposure results in a significant increase in extracellular DA (O'Dell et al., 1991; O'Dell et al., 1993; Gross et al., 2011b). Additionally, it appears that increased extracellular DA may result in neurotoxicity via activation of D1-type DA receptors. For example, D1-type DA receptor antagonists systemically co-administered with METH partially protect against METH-induced neurotoxicity (Broening et al., 2005). Similarly, intrastriatal infusion of D1-type DA receptor antagonist during METH exposure also was reported to protect against METH-induced neurotoxicity (Gross et al., 2011); however, that protection may at least partially have resulted from mitigation of

METH-induced hyperthermia, a factor also tightly associated with METH-induced neurotoxicity (Ali et al., 1994). More recently however, animals with a deletion of the D1-type DA receptor gene were also reported to be protected against METH-induced neurotoxicity—an effect that appears to not solely depend upon attenuation of METH-induced hyperthermia (Ares-Santos et al., 2012). Thus, due to the inconclusive, yet promising results in the literature during the course of this dissertation work regarding a role for D1-type DA receptor activation in METH-induced neurotoxicity, we wanted to further examine whether blockade of D1-type DA receptors in striatum during METH exposure protects against METH-induced DA nerve terminal degeneration when METH-induced hyperthermia is maintained. To answer this question, we conducted preliminary studies in which we infused the D1-type DA receptor antagonist SCH23390 (R-(+)-8-chloro-2,3,4,5-tetrahydro-3-methyl-5-phenyl-1H-3-benzazepine-7-ol) directly into the striata of animals just prior to and during administration of the binge regimen of METH. The ambient temperature in the rats' environment was manipulated to maintain METH-induced hyperthermia.

One week prior to METH or saline treatment, male Sprague-Dawley rats (Charles River Laboratories, Raleigh, NC) were anesthetized with ketamine/xylazine (90/10 mg/kg, i.p.) and placed in a stereotaxic apparatus. Guide cannulae were implanted bilaterally to end just dorsal to dorsal striatum. The guides were secured with skull screws and dental acrylic and dummy cannulae were inserted. Subsequent infusions were made through 33-gauge infusion cannulae extending 3.8 mm beyond the guides.

On PND60, 30 min prior to saline or METH injections, intrastriatal infusions of either saline (0.1 µl/1 min, 0.9% saline) or SCH23390 (2 µg/µl in 0.9% saline, at 0.1

μl/min) were started. Infusions continued until 1 hr after the last injection of either saline or METH, therefore producing a total elapsed time of infusion of 7.5 hr.

METH and saline injections were conducted as previously described in Chapters 2-4. Rectal temperatures were monitored using a digital thermometer (BAT-12, Physitemp Instruments, Clifton, NJ) to ensure the presence of METH-induced hyperthermia. Baseline temperatures for each animal were taken 30 min prior to the first injection and 1 hr after each subsequent injection. If the body temperature of an animal exceeded 40.5°C, the animal was cooled by transferring it to a cage placed over wet ice until the body temperature fell below 39°C. Conversely, cages of SCH23390 infused, METH-treated animals were placed on a heating pad with a heating lamp in order to maintain METH-induced hyperthermia (39°C-40.4°C). Approximately 18hr after the last injection, animals were returned to their home cages in the colony room. Animals were then sacrificed 7 days after the last METH or saline injection and the brains processed as described in Chapters 2-4 for immunohistochemical detection of DAT to assess METH-induced DA neurotoxicity.

For body temperature data collected during METH or saline treatment (Figure 5.1), MANOVA revealed a significant main effects of infusion ($F_{(1,20)}$= 8.98, p<0.01), a significant main effect of treatment ($F_{(1,20)}$= 250.9, p<0.0001) and a significant effect of time ($F_{(4,17)}$= 26.8, p<0.0001). Furthermore, there was also a significant treatment x time interaction ($F_{(4,17)}$= 13.7, p<0.0001). *Post hoc* analysis revealed that the temperatures of animals receiving METH were not different from controls at baseline (0 min, t=1.29, p=0.2), but were significantly greater than those receiving saline at all four time points after the injections of METH began (60 min, t=5.03, p<0.0001; 180 min, t=5.30,

$p<0.0001$; 300 min, t=8.52, $p<0.0001$; 420 min, t=5.90, $p<0.0001$). Importantly, there was no time x infusion interaction ($F_{(4,17)}$ =0.6, $p>0.7$) or an infusion x treatment x time interaction ($F_{(4,17)}$= 0.7, $p>0.6$), indicating the maintenance of METH-induced hyperthermia in the rats receiving intrastriatal infusions of SCH23390.

METH-treated rats showed significant decreases in DAT immunohistochemical staining compared to saline-treated controls. Striatal placement of infusion cannulae in striatum is shown in Figure 5.2. However SCH23390 infusions appeared to result in partial protection against such toxicity (Figure 5.3). A two-factor ANOVA of the average gray value of DAT immunohistochemical signal in striatum revealed significant main effects of infusion ($F_{(1,20)}$ =4.6, $p<0.05$) and treatment ($F_{(1,20)}$ =40.4, $p<0.0001$), and a significant infusion x treatment interaction ($F_{(1,20)}$ =4.5, $p<0.05$). *Post hoc* analysis of the interaction revealed that animals treated with a neurotoxic regimen of METH (saline:METH and SCH:METH) had significantly lower DAT immunohistochemical signal compared to saline-treated controls (saline:saline and SCH:saline)(Tukey's HSD test, p values <0.05; Figure 5.3). Importantly, animals infused with saline and treated with METH (saline:METH) showed significantly lower DAT immunohistochemical signal in striatum compared to all other treatment groups (saline:saline, SCH:saline, and SCH:METH)(Tukey's HSD test, p values <0.05; Figure 5.3).

Here we found that animals infused with the D1-DA receptor antagonist SCH23390 into the striata bilaterally showed a significant degree of protection following METH exposure compared to their counterparts treated with METH and infused with saline. Together, these data indicate that the neuroprotection observed in animals infused

with SCH23390 during METH injections resulted from the blockade of D1-type DA receptors in the striatum, and not from disruption of METH-induced hyperthermia.

Interestingly, D1-type DA receptors are located postsynaptic to DA nerve terminals that undergo degeneration following METH exposure (Levey et al., 1993). Therefore, although unexplored in the current study, one possible way in which D1 DA receptor activation may play a causal role in damage to DA terminals is through altered basal ganglia output secondary to METH-induced DA release and activation of D1 DA receptors, ultimately leading to excessive corticostriatal excitation and GLU-mediated excitotoxicity to DA nerve terminals. As reviewed in the Introduction, the striatum receives significant GLU inputs from corticostriatal projections (Gerfen, 1989; Bellomo et al., 1998). Further, corticostriatal activity can be regulated by nigrothalamic and thalamocortical projections, as GABA release from D1 DA receptor-containing, striatonigral neurons activates GABA-A receptors in the SNpr and decreases thalamic neuron firing (Deniau and Chevalier, 1985; Nicholson et al., 1995; Timmerman and Westerink, 1997). Nigrothalamic activity can then influence glutamatergic thalamocortical and corticostriatal projections (Kaneko and Mizuno, 1988). Studies have shown that METH-induced GLU release is associated with GABA release in the SNpr and decreased GABA release in the thalamus (Mark et al., 2004) and that GABA-A receptor antagonism in the SNpr can reduce METH-induced GABA release in the thalamus, as well as GLU release and DA nerve terminal degeneration in the striatum (Mark et al., 2004). These data suggest that striatonigral neuron activation is important for METH-induced GLU release. Other work has also shown that intrastriatal infusions of D1-type DA receptor antagonists prevent apomorphine-induced cortical immediate-

early gene expression and sensorimotor responsiveness (Steiner and Kitai, 2000), further implicating activation of D1-type DA receptors in striatum in influencing corticostriatal activity. Lastly, recent evidence has shown that NMDA-type GLU receptor antagonist applied epidurally to the cortex reduces both METH-induced c-*fos* gene expression and DA nerve terminal degeneration in striatum (Gross et al., 2011a). Taken together, these data suggest that METH may increase GLU release and ultimately DA neuron toxicity via the activation of D1 DA receptors on striatonigral efferent neurons.

Given that increased extracellular DA, subsequent activation of D1-type DA receptors, and altered output of the basal ganglia have been suggested to play such an important role in the induction of METH-induced neurotoxicity, future work exploring this pathway in the context of such toxicity may provide novel therapeutic targets for human METH abusers. For example, studies using approaches to block activation of the striatonigral neurons, such as Designer Receptors Exclusively Activated by a Designer Drug (DREDD) expression, may prove fruitful in further defining a critical role of striatonigral neuron activation in METH-induced DA terminal injury. Clarification of this role will then point to potential therapeutic targets for preventing METH-induced toxicity to DA neurons.

5.1 References

Albers DS and Sonsalla PK (1995) Methamphetamine-induced hyperthermia and dopaminergic neurotoxicity in mice: pharmacological profile of protective and nonprotective agents. *J Pharmacol Exp Ther* **275**:1104-1114.

Ali SF and Itzhak Y (1998) Effects of 7-nitroindazole, an NOS inhibitor on methamphetamine-induced dopaminergic and serotonergic neurotoxicity in mice. *Ann N Y Acad Sci* **844**:122-130.

Ali SF, Newport GD, Holson RR, Slikker W, Jr. and Bowyer JF (1994) Low environmental temperatures or pharmacologic agents that produce hypothermia decrease methamphetamine neurotoxicity in mice. *Brain Res* **658**:33-38.

Ares-Santos S, Granado N, Oliva I, O'Shea E, Martin ED, Colado MI and Moratalla R (2012) Dopamine D(1) receptor deletion strongly reduces neurotoxic effects of methamphetamine. *Neurobiol Dis* **45**:810-820.

Bellomo M, Giuffrida R, Palmeri A and Sapienza S (1998) Excitatory amino acids as neurotransmitters of corticostriatal projections: immunocytochemical evidence in the rat. *Arch Ital Biol* **136**:215-223.

Broening HW, Morford LL and Vorhees CV (2005) Interactions of dopamine D1 and D2 receptor antagonists with D-methamphetamine-induced hyperthermia and striatal dopamine and serotonin reductions. *Synapse* **56**:84-93.

Dawson TM, Bredt DS, Fotuhi M, Hwang PM and Snyder SH (1991) Nitric oxide synthase and neuronal NADPH diaphorase are identical in brain and peripheral tissues. *Proc Natl Acad Sci U S A* **88**:7797-7801.

Deng X and Cadet JL (1999) Methamphetamine administration causes overexpression of nNOS in the mouse striatum. *Brain Res* **851**:254-257.

Deniau JM and Chevalier G (1985) Disinhibition as a basic process in the expression of striatal functions. II. The striato-nigral influence on thalamocortical cells of the ventromedial thalamic nucleus. *Brain Res* **334**:227-233.

Friend DM and Keefe KA (2013) Glial Reactivity in Resistance to Methamphetamine-Induced Neurotoxicity. *J Neurochem*.

Friend DM, Son JH, Keefe KA and Fricks-Gleason AN (2013) Expression and activity of nitric oxide synthase isoforms in methamphetamine-induced striatal dopamine toxicity. *J Pharmacol Exp Ther* **344**:511-521.

Fukami G, Hashimoto K, Koike K, Okamura N, Shimizu E and Iyo M (2004) Effect of antioxidant N-acetyl-L-cysteine on behavioral changes and neurotoxicity in rats after administration of methamphetamine. *Brain Res* **1016**:90-95.

Gerfen CR (1989) The neostriatal mosaic: striatal patch-matrix organization is related to cortical lamination. *Science* **246**:385-388.

Gross NB, Duncker PC and Marshall JF (2011a) Cortical ionotropic glutamate receptor antagonism protects against methamphetamine-induced striatal neurotoxicity. *Neuroscience* **199**:272-283.

Gross NB, Duncker PC and Marshall JF (2011b) Striatal dopamine D1 and D2 receptors: Widespread influences on methamphetamine-induced dopamine and serotonin neurotoxicity. *Synapse* **65**:1144-1155.

Hanson JE, Birdsall E, Seferian KS, Crosby MA, Keefe KA, Gibb JW, Hanson GR and Fleckenstein AE (2009) Methamphetamine-induced dopaminergic deficits and refractoriness to subsequent treatment. *Eur J Pharmacol* **607**:68-73.

Hope BT, Michael GJ, Knigge KM and Vincent SR (1991) Neuronal NADPH diaphorase is a nitric oxide synthase. *Proc Natl Acad Sci U S A* **88**:2811-2814.

Imam SZ, Crow JP, Newport GD, Islam F, Slikker W, Jr. and Ali SF (1999) Methamphetamine generates peroxynitrite and produces dopaminergic neurotoxicity in mice: protective effects of peroxynitrite decomposition catalyst. *Brain Res* **837**:15-21.

Itzhak Y, Martin JL and Ail SF (2000) nNOS inhibitors attenuate methamphetamine-induced dopaminergic neurotoxicity but not hyperthermia in mice. *Neuroreport* **11**:2943-2946.

Kaneko T and Mizuno N (1988) Immunohistochemical study of glutaminase-containing neurons in the cerebral cortex and thalamus of the rat. *J Comp Neurol* **267**:590-602.

Kogan FJ, Nichols WK and Gibb JW (1976) Influence of methamphetamine on nigral and striatal tyrosine hydroxylase activity and on striatal dopamine levels. *Eur J Pharmacol* **36**:363-371.

LaVoie MJ, Card JP and Hastings TG (2004) Microglial activation precedes dopamine terminal pathology in methamphetamine-induced neurotoxicity. *Exp Neurol* **187**:47-57.

LaVoie MJ and Hastings TG (1999) Dopamine quinone formation and protein modification associated with the striatal neurotoxicity of methamphetamine: evidence against a role for extracellular dopamine. *J Neurosci* **19**:1484-1491.

Levey AI, Hersch SM, Rye DB, Sunahara RK, Niznik HB, Kitt CA, Price DL, Maggio R, Brann MR and Ciliax BJ (1993) Localization of D1 and D2 dopamine receptors in brain with subtype-specific antibodies. *Proc Natl Acad Sci U S A* **90**:8861-8865.

Mark KA, Soghomonian JJ and Yamamoto BK (2004) High-dose methamphetamine acutely activates the striatonigral pathway to increase striatal glutamate and mediate long-term dopamine toxicity. *J Neurosci* **24**:11449-11456.

McCann UD, Kuwabara H, Kumar A, Palermo M, Abbey R, Brasic J, Ye W, Alexander M, Dannals RF, Wong DF and Ricaurte GA (2008) Persistent cognitive and dopamine transporter deficits in abstinent methamphetamine users. *Synapse* **62**:91-100.

Nash JF and Yamamoto BK (1992) Methamphetamine neurotoxicity and striatal glutamate release: comparison to 3,4-methylenedioxymethamphetamine. *Brain Res* **581**:237-243.

Nicholson LF, Faull RL, Waldvogel HJ and Dragunow M (1995) GABA and GABAA receptor changes in the substantia nigra of the rat following quinolinic acid lesions in the striatum closely resemble Huntington's disease. *Neuroscience* **66**:507-521.

O'Callaghan JP and Miller DB (1994) Neurotoxicity profiles of substituted amphetamines in the C57BL/6J mouse. *J Pharmacol Exp Ther* **270**:741-751.

O'Dell SJ, Weihmuller FB and Marshall JF (1991) Multiple methamphetamine injections induce marked increases in extracellular striatal dopamine which correlate with subsequent neurotoxicity. *Brain Res* **564**:256-260.

O'Dell SJ, Weihmuller FB and Marshall JF (1993) Methamphetamine-induced dopamine overflow and injury to striatal dopamine terminals: attenuation by dopamine D1 or D2 antagonists. *J Neurochem* **60**:1792-1799.

Sekine Y, Iyo M, Ouchi Y, Matsunaga T, Tsukada H, Okada H, Yoshikawa E, Futatsubashi M, Takei N and Mori N (2001) Methamphetamine-related psychiatric symptoms and reduced brain dopamine transporters studied with PET. *Am J Psychiatry* **158**:1206-1214.

Steiner H and Kitai ST (2000) Regulation of rat cortex function by D1 dopamine receptors in the striatum. *J Neurosci* **20**:5449-5460.

Thomas DM and Kuhn DM (2005) Attenuated microglial activation mediates tolerance to the neurotoxic effects of methamphetamine. *J Neurochem* **92**:790-797.

Timmerman W and Westerink BH (1997) Electrical stimulation of the substantia nigra reticulata: detection of neuronal extracellular GABA in the ventromedial thalamus and its regulatory mechanism using microdialysis in awake rats. *Synapse* **26**:62-71.

Volkow ND, Chang L, Wang GJ, Fowler JS, Franceschi D, Sedler M, Gatley SJ, Miller E, Hitzemann R, Ding YS and Logan J (2001) Loss of dopamine transporters in

methamphetamine abusers recovers with protracted abstinence. *J Neurosci* **21**:9414-9418.

Wagner GC, Carelli RM and Jarvis MF (1986) Ascorbic acid reduces the dopamine depletion induced by methamphetamine and the 1-methyl-4-phenyl pyridinium ion. *Neuropharmacology* **25**:559-561.

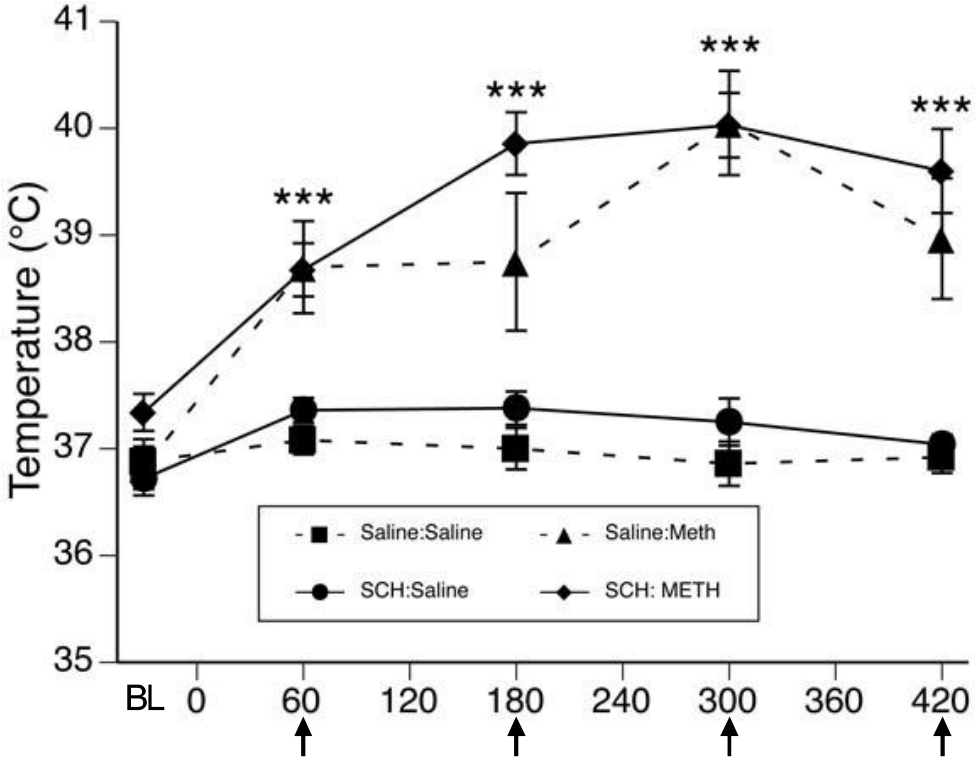

Figure 5.1. Body temperatures (mean±SEM; n=4-8) of animals that received systemic injections of saline (4 x 1 mL/kg, s.c. at 2-hr intervals) or (±)-METH (4 x 10 mg/kg, s.c. at 2-hr intervals) and intrastriatal infusions of either saline or SCH222390. Treatment group designations indicate infusion:treatment, resulting in the four treatment groups: Saline:Saline (S:S); SCH:Saline (SCH:S); Saline:METH (S:M); and SCH:METH (SCH:M). Temperatures were obtained 30 min prior to the first injection (baseline; BL) and 1 hr after each subsequent injection. X-axis values represent minutes after the first injection and arrows represent the time of each saline or METH injection. ***p<0.0001 significant effect of METH at this time point.

Figure 5.2. Diagram indicating location of infusion sites in striatum with the black dots representing tips of the cannulae. Numbers represent mm from Bregma.

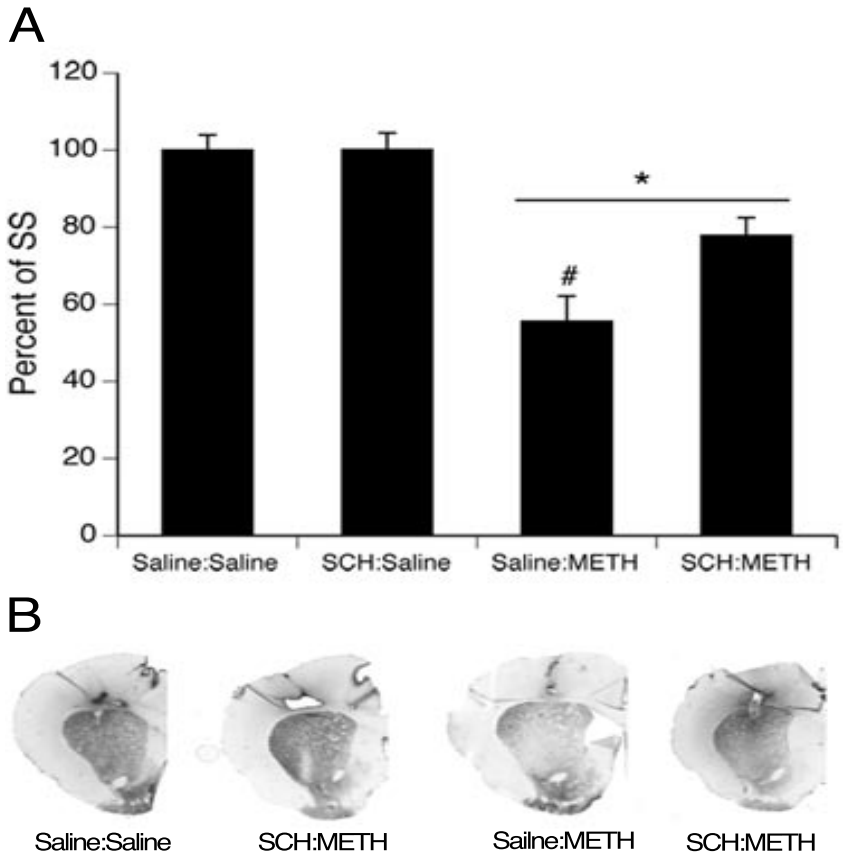

Figure 5.3. Striatal DAT immunohistochemical signal in animals that received systemic injections of saline (4 x 1 mL/kg, s.c. at 2-hr intervals) or (±)-METH (4 x 10 mg/kg, s.c. at 2-hr intervals) and intrastriatal infusions of either saline or SCH222390. Treatment group designations indicate infusion:treatment, resulting in the four treatment groups: Saline:Saline (S:S); SCH:Saline (SCH:S); Saline:METH (S:M); and SCH:METH (SCH:M). * indicates significant differences from saline:saline and SCH:saline, $p<0.05$; # indicates significant difference from SCH:METH, $p<0.05$. (B) Representative images of DAT autoradiography.